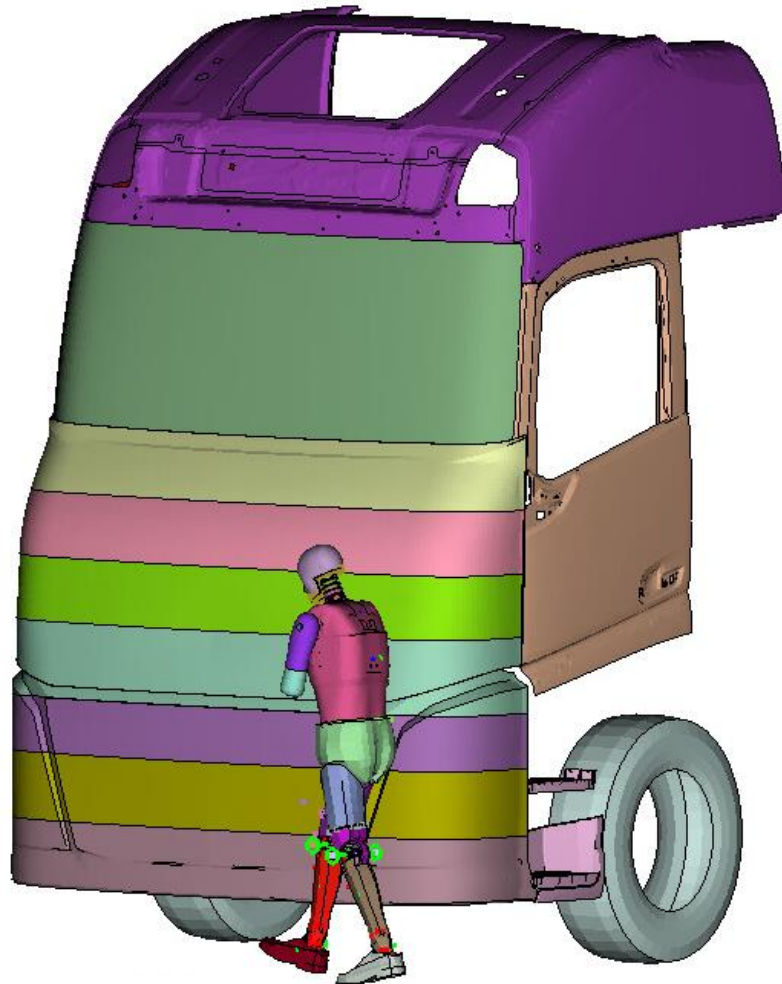




CHALMERS
UNIVERSITY OF TECHNOLOGY



VRU-to-Truck Collision Compatibility

Master's thesis in Automotive Engineering

Jieer Cao, Zhetong Mo

MASTER'S THESIS IN AUTOMOTIVE ENGINEERING

VRU-to-Truck Collision Compatibility

Jieer Cao, Zhetong Mo

Department of Applied Mechanics
Division of Vehicle Safety
CHALMERS UNIVERSITY OF TECHNOLOGY
Göteborg, Sweden 2017

VRU-to-Truck Collision Compatibility
Jieer Cao, Zhetong Mo

© Jieer Cao, Zhetong Mo, 2017-09-01

Master's Thesis 2017:78
ISSN 1652-8557
Department of Applied Mechanics
Division of Vehicle Safety
Chalmers University of Technology
SE-412 96 Göteborg
Sweden
Telephone: + 46 (0)31-772 1000

Cover:

The original collision scenario between the simplified truck with elongation in the front and a walking 50th percentile male dummy model.

Department of Applied Mechanics
Göteborg, Sweden 2017-09-01

VRU-to-Truck Collision Compatibility
Master's thesis in Automotive Engineering
Jieer Cao, Zhetong Mo
Department of Applied Mechanics
Division of Vehicle Safety
Chalmers University of Technology

Abstract

Pedestrian safety is an important concern for truck collision compatibility development. Numerical crash simulation is widely used for truck design today and some numerical pedestrian dummy and human models are available for injury prediction in pedestrian collision simulations. A study of the collision between pedestrian and new truck front with an ideal spring system based on MADYMO has been carried out by Volvo Truck. The result shows that with this spring system, the number of pedestrian sustaining MAIS2+ injuries can be reduced potentially by up to 20%.

One of this thesis work's objectives is to compare the results between the MADYMO Ellipsoid 50th percentile male human model simulations previously done, with LS-DYNA 50th percentile male Autoliv IA pedestrian dummy model simulations. The other target is to develop a honeycomb structure to replace this simplified spring system for future industry market.

The same collision scenarios as previous MADYMO study, including the truck model and different postures of pedestrian model, were constructed and simulated in LS-DYNA. The result shows that in primary impact, the deformable neck of IA model is potential to cause more severe head and neck injury than that of Ellipsoid model. Instead, the deformable arm of IA model has positive effect on reducing head injury in truck collisions.

After that, six finite element (FE) plastic honeycomb structure models were developed to replace the spring system. The material of this honeycomb is Zytel® ST811HS NC010 and the thickness and length for different honeycombs were selected by FE bench test simulations aiming for similar yield force levels as in the spring systems. The result shows that this honeycomb structure performs well since 90% of the injury values' absolute difference in low impact speed (truck speed, 24km/h) collisions and 81% in high impact speed (truck speed, 40km/h) collisions compared to reference value in spring system collisions are smaller than 20%. The stiffness of honeycomb becomes larger in high impact speed collision is the potential reason for worse performance in high speed collisions.

In the future, injury caused by secondary impact needs to be further studied. The rigid truck front surface may also need to be evolved to be deformable for future design.

Key words: Pedestrian, Truck frontal collision, Finite Element Analysis, IA pedestrian dummy model, Spring system, Honeycomb

Contents

Abstract	I
Contents	III
Preface.....	VII
Notations	VIII
1 Introduction.....	1
1.1 Road safety accidents data	1
1.2 Work of pedestrian protection.....	2
1.2.1 Truck active safety	2
1.2.2 Truck passive safety.....	2
1.3 Crash test dummy.....	2
1.3.1 Physical crash test dummy	2
1.3.2 Virtual crash test dummy model	2
1.3.3 IA dummy FE model	3
1.3.4 Ellipsoid pedestrian MB model	4
1.4 Dummy injury criteria.....	6
1.4.1 Head injury criteria.	6
1.4.2 Neck injury criterion	6
1.4.3 Thoracic injury criteria	7
1.4.4 Abdomen injury criteria	9
1.4.5 Pelvis injury criteria.....	9
1.4.6 Leg injury criteria	10
1.5 Aim of the project	10
2 Previous MADYMO study	11
2.1 Global coordinate system	11
2.2 Pedestrian model	11
2.3 Truck models.....	12
2.4 Collision scenarios	14
3 Method	15
3.1 FE truck model construction	15
3.1.1 Truck front FE modelling	15
3.1.2 Verification of FE truck model	16
3.2 FE pedestrian dummy model modification	17
3.3 Collision scenarios construction.....	19
3.4 Comparison of MADYMO and LS-DYNA results.....	19

3.5	The development of honeycomb structure	20
3.5.1	The material of honeycomb	20
3.5.2	The size of honeycomb	21
3.5.3	Honeycomb A for each contact parts	23
3.5.4	Verification of selected thickness	23
4	Result	26
4.1	FMH verification	26
4.1.1	Head contact force	26
4.1.2	Head injury, HIC ₃₆	26
4.2	Comparison of results of MADYMO human model and LS-DYNA dummy model 27	27
4.2.1	HIC ₃₆	27
4.2.2	Torso acceleration	29
4.2.3	Neck resultant force	32
4.2.4	Neck resultant moment	35
4.3	Comparison of results of reference FH truck and studied truck	37
4.3.1	Stand posture with the impact speed of 24kph	38
4.3.2	‘Stand’ posture with the impact speed of 40kph	39
4.3.3	‘Walk’ posture with the impact speed of 24kph	41
4.3.4	‘Walk’ posture with the impact speed of 40kph	42
4.3.5	‘Walk 180’ posture with the impact speed of 24kph	43
4.3.6	‘Walk 180’ posture with the impact speed of 40kph	44
4.4	Comparison of results of Truck A and trucks with honeycomb.	45
4.4.1	Head injury	45
4.4.2	Neck injury	46
4.4.3	Torso injury	47
4.4.4	Motion of pedestrian and impact condition for Truck B.	48
5	Discussion	49
5.1	MADYMO and LS-DYNA pedestrian model injury results	49
5.1.1	Secondary impact	49
5.1.2	Primary impact	49
5.2	The performance of mass-spring system	53
5.3	The performance of honeycomb structure	54
5.3.1	Primary impact	54
5.3.2	Secondary impact	58
5.4	Limitation of the work	62
5.4.1	Lack of pedestrian models in different sizes	62

5.4.2	Lack of collision scenarios.....	62
5.4.3	Lack of secondary impact analysis	63
5.4.4	Difficulty to create the same impact scenarios	63
6	Conclusion	64
6.1	The similarities and difference between MADYMO and LSDYNA pedestrian model	64
6.2	The performance of mass-spring system.....	64
6.3	The performance of honeycomb B	64
7	Future work	65
7.1	Validation of spring system.....	65
7.2	Honeycomb and truck front surface development	65
	References	66
	Appendix	69
Appendix A	Contact between pedestrian and truck	69
Appendix B	Material card in FE model	69
Appendix C	Modification of IA pedestrian dummy model	71
	Head flesh material substitution.....	71
	Head accelerometer.....	71
	Dummy self-contact.....	71
	Robustness	72
Appendix D	Contact card in FE model	72
Appendix E	Injury data.....	76
Appendix F	Pedestrian motion in collisions of Truck A and trucks with honeycombs	80
	24kph collisions	80
	40kph collisions	83

Preface

The main work in this thesis work was carried out at the department of Vehicle Structures & Passive Safety, Volvo GTT, Sweden, from September 2016 to June 2017. This work is a part of a research project concerning pedestrian protection in truck accidents. The finite element pedestrian dummy model used in this project is provided by Autoliv.

This thesis work is under the supervision of Stefan Thorn and Fredrik Jenefeldt from Volvo GTT and Professor Karin Brolin from Chalmers. We would like to appreciate Björn Cognell and Göran Peterson from Volvo GTT for their supervision on FEM work. We would also like to thank Urban Elfsberg (Volvo GTT) for his suggestion on materials and Christer Lundgren from Autoliv for his help within pedestrian model.

Göteborg, 2017-09-01

Jieer Cao, Zhetong Mo

Notations

Roman upper case letters

N_{ij}	An injury criteria for assessing neck injury based on resultant force and moment. ‘i’ represents the axial load (tension or compression) and ‘j’ represents the sagittal plane bending moment (flexion or extension).
N_{TE}	Neck injury when load in tension and bending moment in extension.
N_{TF}	Neck injury when load in tension and bending moment in flexion.
N_{CE}	Neck injury when load in compression and bending moment in extension.
N_{CF}	Neck injury when load in compression and bending moment in flexion.
F_Z	Axial load.
F_{int}	The normalized critical intercept value of load according to the specific dummy corresponding to F_Z .
M_y	Bending moment.
M_{int}	The normalized critical intercept value for moment according to the specific dummy corresponding to M_y .
C	The instantaneous normalized compression.
D	The compression length.
D_0	The original length.
V	Velocity.
Age	Age of the test dummy (in years).
$RIBY$	Max absolute value of rib acceleration on struck side in lateral direction.
$T12Y$	Max absolute value of the twelfth thoracic vertebrae acceleration in the lateral direction.
M	Mass.
M_{std}	Standard mass of 50th percentile male, 75 kg.
F_p	The pubic force.
F_1	The measured compressive axial force(kN) in the superior-inferior direction.
M_1	The resultant moment of the medial-lateral and the anterior-posterior moments.
F_C	The normalized critical intercept value of load according to the specific dummy corresponding to F_1 .
M_C	The normalized critical intercept value for moment according to the specific dummy corresponding to M_1 .

Roman lower case letters

t_1	The beginning time (in seconds) of any arbitrary time interval of this acceleration curve.
t_2	The end time (in seconds) of any arbitrary time interval of this acceleration curve.
a_{head}	The acceleration at the center of gravity of head.
p	The possibility.

g Gravitational acceleration.

Definitions and abbreviations

VRU	Vulnerable road user, including pedestrians, cyclists, moped drivers, etc.
HGV	Heavy goods vehicle, gross vehicle weight above 3.5 metric tons.
ATD	Anthropomorphic test device.
FE	Finite element.
MB	Multi-body.
HIC	Head injury criterion.
SNPRM	Supplemental Notice for Proposed Rulemaking.
FMVSS	Federal motor vehicle safety standard.
TTI	Thoracic trauma index.
PMHS	Post mortem human subjects.
VC	Viscous criterion.
TI	Tibia index.
AIS	The Abbreviated Injury Scale, an anatomical-based coding system created by the Association for the Advancement of Automotive Medicine to classify and describe the severity of injuries.
FH Reference	The reference MADYMO FH truck described in Section 2.1.2.
Truck A	The FE reference truck with spring system but without face 2.
Truck 1	The truck with one honeycomb for ‘Lid mid 1’ and 6 springs for other parts.
Truck 2	The truck with one honeycomb for ‘Lid lower 1’ and 6 springs for other parts.
Truck 3	The truck with one honeycomb for ‘Grille upper 1’ and 6 springs for other parts.
Truck 4	The truck with one honeycomb for ‘Grille lower 1’ and 6 springs for other parts.
Truck 5	The truck with one honeycomb for ‘Bumper upper 1’ and 6 springs for other parts.
Truck B	The truck with 5 honeycombs for ‘Lid mid 1’, ‘Lid lower 1’, ‘Grille upper 1’, ‘Grille lower 1’ and ‘Bumper upper 1’, and remain 2 springs for ‘Lid upper 1’ and ‘Bumper lower 1’.
TorsoUp	Upper torso 3ms clip acceleration
TorsoLow	Lower torso 3ms clip acceleration
NeckUpFRES	Upper neck resultant force.
NeckLowFRES	Lower neck resultant force.
NeckUpMRES	Upper neck resultant moment.
NeckLowMRES	Lower neck resultant moment.

1 Introduction

1.1 Road safety accidents data

Nowadays, safety of vulnerable road user (VRU) has become a significant concern. According to statistics from EU commission (European Commission, 2016a), as seen in Figure 1.1, from 2005 to 2014, although the pedestrian fatality number decreases in Europe, the percentage of pedestrians in all road fatalities goes up to around 21%. Therefore, the protection of pedestrians needs to be further developed.



Figure 1.1 The fatality number of pedestrian and percentage of all road fatalities in Europe from 2005 to 2014, data from EU commission (European Commission, 2016a).

In heavy goods vehicle (HGV) safety performance aspect, according to Traffic Safety Basic Facts 2016 report of Heavy Goods Vehicles and Buses (2016), 4896 people died in road accidents involving HGVs in 2014 and 17% of them are pedestrians. Almqvist and Heinig (2013) also found that VRUs are involved in 15% to 25% of the heavy truck accidents causing seriously injury or fatality in Europe, 2013. In addition, the study of Mesina and Margaritis (2005) indicated that in urban area, in 52% of the HGV to pedestrian collisions, the first impact zone is the front part of the truck. Hence, pedestrians' injury caused in pedestrians-to-truck front collision needs to be further reduced.

Mesina and Margaritis (2005) also reported that the main motion of truck in these heavy truck-to-pedestrian accidents in France, Netherland and UK from 1958 to 2003 was going straight forward, occupying around 75%. In fatal heavy truck accidents involving pedestrians and cyclists, overrun cases account for over 75% (Almqvist and Heinig, 2013). However, non- overrun situations were more frequent, which made up of 64% pedestrian-to-truck collisions (Mesina and Margaritis, 2005). Puthan et al. (2016) estimated that impact velocities in overrun cases causing Abbreviated Injury Scale(AIS)3+, were mostly in the 1-10km/h (36%) and the 21-40 km/h (50%) intervals according to German In-Depth Accident Database(GIDAS) from 1999 to 2015 June. Non-overrun situations in 31-40km/h and 61-70km/h intervals accounted for 61% of

the AIS3+ cases (Puthan et al., 2016). Hence, these truck velocity intervals when truck moving straight forward may need to be further studied to improve VRU's safety.

1.2 Work of pedestrian protection

Nowadays, both active safety and passive safety research work has been carried out and well developed to improve pedestrian protection in pedestrian-to-truck collisions.

1.2.1 Truck active safety

In 90% of all truck collision cases, human error of driver is a contributing factor to accidents (Almqvist and Heinig, 2013). Therefore, some active safety technologies, such as visibility support, driver awareness support, etc. have been developed to avoid accident or reduce pedestrians' injury (Almqvist and Heinig, 2013). Electronic speed limiting is also helpful to reduce the possibility of accidents and pedestrian detection is one of the useful functions to protect pedestrian (Gandhi and Trivedi, 2007). These active safety technologies are helping reduce crash risk in the real world.

1.2.2 Truck passive safety

Researcher and industry try to improve pedestrian safety in different aspects. For example, protection airbag was studied to be applied in trucks front structure to reduce VRUs' injury (Gandhi and Trivedi, 2007). Chawla et al. (2000) concerned the structure improvement and studied truck's bumper height, bumper offset and grille inclination to reduce head and upper body injury of pedestrian based on MADYMO. Feist et al. (2009) found by numerical calculation simulations that the head injury caused by the secondary impact with ground is a big issue in VRU-to-truck collision. In the meantime, some pedestrian crash test dummies and pedestrian numerical models have been developed to predict pedestrian's injury, which could help optimize vehicle's structure in terms of pedestrian safety. This part will be further introduced in Section 1.3. Volvo Group have also carried out some projects studying e.g. truck frontal energy absorption structure to improve pedestrian safety. One of them, a truck with spring system in its front structure, will be further introduced in Chapter 2.

1.3 Crash test dummy

1.3.1 Physical crash test dummy

Today, crash test dummy plays an important role in vehicle tests. The crash test dummy is a full-scale anthropomorphic test device (ATD), simulating the dimensions, weight proportions and stiffness of articulation of the human body (Crash test dummy, 2016). It is able to reflect the dynamic behavior of the human body and collect expected data such as velocity of impact, impact force, impact deflection, torque, acceleration rates, etc. in the meantime for certain load conditions or crash scenarios (Crash test dummy, 2016). For example, Hybrid III dummies (Backaitis and Mertz, 1993) are developed for front impact scenarios while WorldSID dummies (Moss et al. 2000) and EuroSID-1 dummies (Neilson et al. 1985) are implemented in side impact tests. For pedestrian concern, pedestrian dummies, such as POLAR dummy (Akiyama et al, 2001) and IA dummy (Elmasoudi, 2015), also have been developed for crash tests.

1.3.2 Virtual crash test dummy model

With the development of crash safety numerical simulation work, finite element (FE) and multi-body (MB) dummy models have been developed for the request of predicting injury. In automotive industry, LS-DYNA (LSTC, 2014), a non-linear FE program

capable of simulating complex real world problems, is widely used. Many FE pedestrian dummy models are written into LS-DYNA's non-linear structure codes. MADYMO (Automotive, TNO, 2015a) is a simulation program combining the capabilities of MB and FE. It also provides accurate MB pedestrian models such as Facet pedestrian models and Ellipsoid pedestrian models for customers (Automotive, TNO, 2015b).

Generally, FE and MB dummy models are built to include detailed descriptions of the dummy geometry and internal parts, such as the ribs, internal dampers, foam pads and joints (Kirkpatrick et al, 1993). Therefore, the models are sensitive to the modification of dummy geometry and material properties. Also, they are designed to be able to run in a reasonable duration of time as realistic dummy model on an engineering work simulation in a typical application, which is important for data accuracy (Kirkpatrick et al, 1993). These models need to be validated in component level, sub-system model and full dummy level by comparing the simulated data with corresponding experimental data in certain load conditions like drop test, pendulum tests, sled test, etc.

The way to construct FE dummy models and MB dummy models is different. The detailed FE models are constructed mainly through geometry modeling and material modeling. The physical geometry is replicated down to small elements with different material properties. The connections between body parts are realized by constraints and contacts between elements. These FE models are written into different non-linear structure codes such as LS-DYNA, ABAQUS, etc. for industry and research use. Because of the detailed modeling way, FE dummy models are expected to provide high accuracy level of the dummy behavior prediction. The deformable ability could also provide a more accurate interaction between dummy and vehicles than MB dummy. However, it generally results in high CPU costs compared to MB dummy models (Himmetoglu et al, 2007).

MB dummy model is considered as an efficient tool for extensive design optimization study (Himmetoglu et al, 2007). For MB models, the head and vertebrae are modeled as rigid bodies while the soft tissues (intervertebral discs, facet joints, ligaments, muscles) are modeled as massless spring-damper elements (Himmetoglu et al, 2007). As a result, multi-body models are capable of producing reasonable kinematic responses. Due to the simplified nature, MB models' biofidelic responses are often expected to be less accurate (Verhoeve et al, 2001).

1.3.3 IA dummy FE model

A50th percentile male side impact dummy model so called IA dummy model provided by Autoliv (Elmasoudi, 2015) as seen in Figure 1.2, is used for truck-to-pedestrian collision in this study. This model is developed based on IA dummy (Figure 1.2) by Autoliv. The upper body of IA dummy, including head, neck and thorax, is from EuroSID II dummy (Wismans et al, 2001), while the lower body, including pelvis and legs, is mainly from Hybrid III dummy (Mohan et al, 2010). The knees in the legs of Hybrid III dummy were replaced by an in-house designed knee to prevent the axial rotation of the leg during the impact (Beillas et al, 2011). The lumbar spine also has been substituted with a spring that can allow extension, bending and torsion, thus providing more realistic motion (Fernando and Jardinier, 2002).

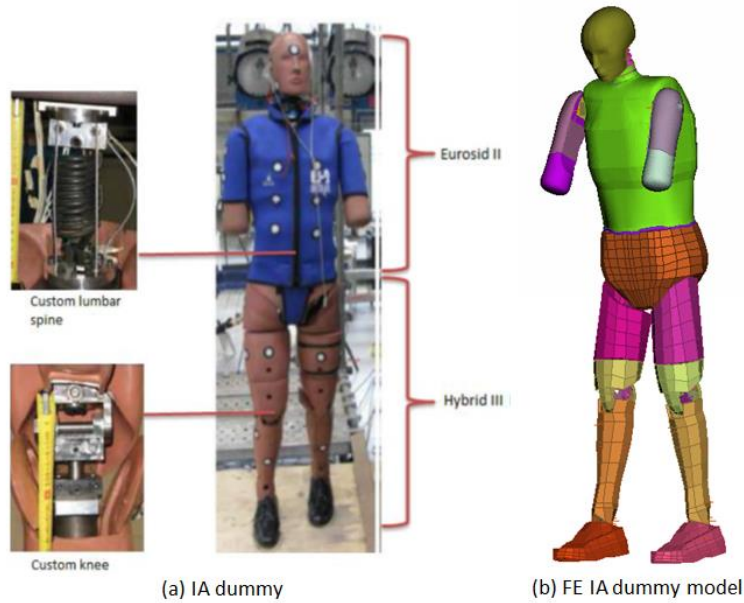


Figure 1.2 IA pedestrian dummy (Elmasoudi, 2015) and FE model.

The model has been validated by crash test and corresponding numerical simulation on LS-DYNA (Elmasoudi, 2015). It is able to collect the acceleration data of head, upper spine, lower spine, left arm, clavicle and 3 ribs as seen the positions in Figure 1.3. It is also capable of getting force and moment of upper neck, lower neck, lumbar, T12 of spine, clavicles and back by load cell beam elements, see Figure 1.3.

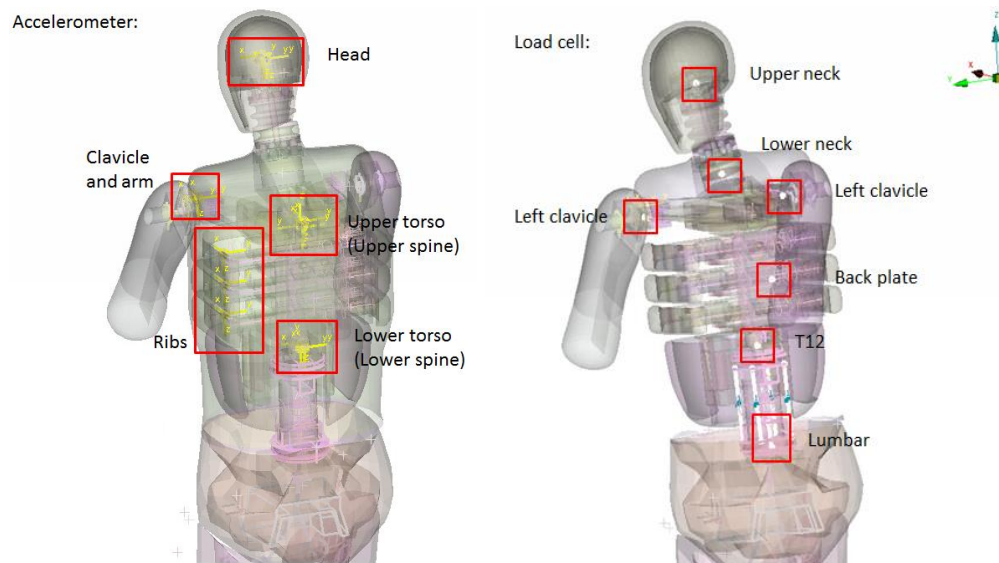


Figure 1.3 The data collection positions of FE IA pedestrian dummy model.

1.3.4 Ellipsoid pedestrian MB model

MADYMO released Ellipsoid pedestrian MB family models of five body sizes (Automotive, TNO, 2015b) as seen in Figure 1.4.

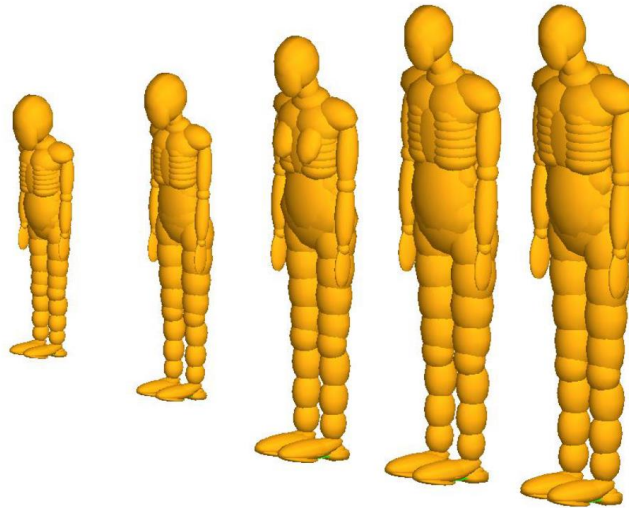


Figure 1.4 Ellipsoid pedestrian MB models (the 3-year-old child, 6-year-old child, 5th percentile female, 50th percentile male and 95th percentile male model from left to right (Automotive, TNO, 2015)).

The anthropometry of the 50th percentile male pedestrian model was first constructed based on the database of the RAMSIS (RAMSIS, 1997). The Western European population aged 18-70 years in 1984 has been used to define the geometry. The 3-year-old child, 6-year-old child, 5th percentile female and 95th percentile male model were scaled from this 50th percentile model.

This pedestrian model consists of 52 rigid bodies and its outer surface is constructed by 64 ellipsoids and 2 planes. It has been validated by blunt impact tests and car-to-pedestrian impact tests (Automotive, TNO, 2015b). After validation, the model could accurately predict the global kinematics. It is able to record the force, moment and acceleration data of body parts. For instance, the force and moment data of upper and lower neck and legs, the acceleration data of head, upper torso and lower torso (pelvis), as seen in Figure 1.5 and 1.6.

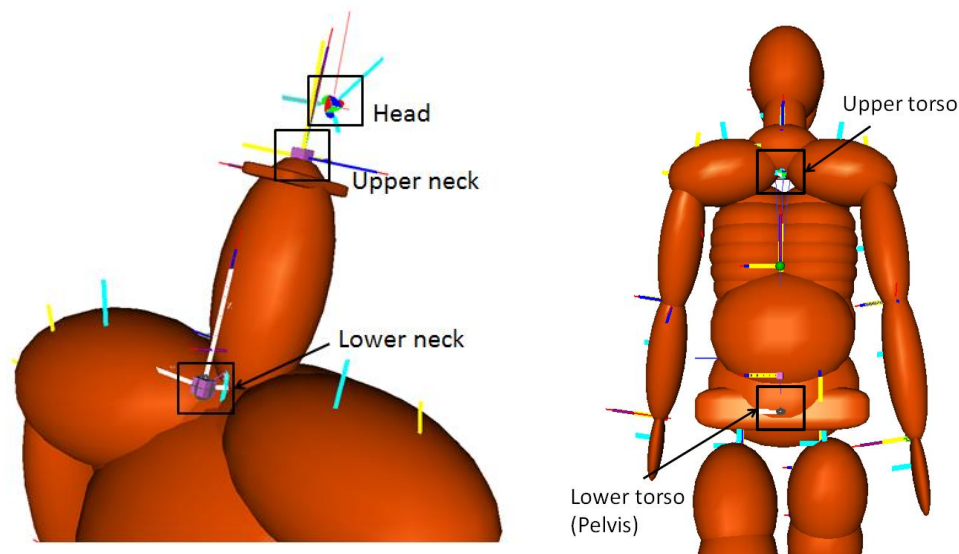


Figure 1.5 Data collection positions of 50th percentile male Ellipsoid pedestrian model's upper body.

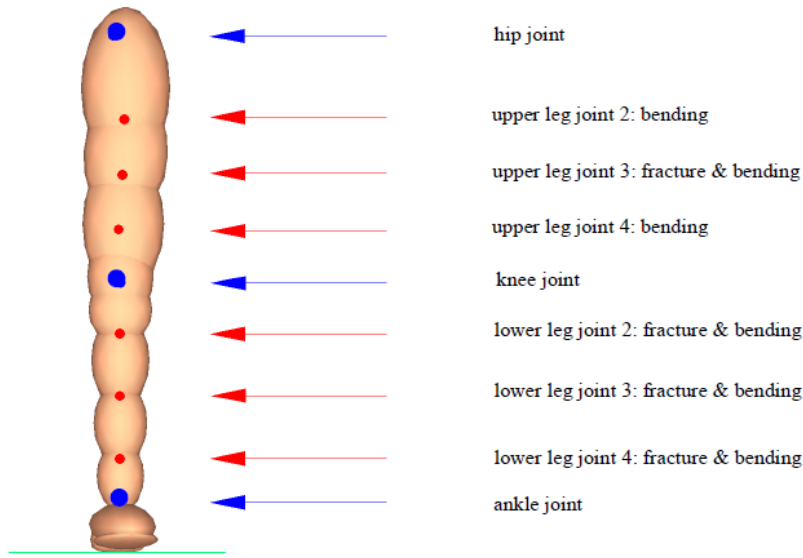


Figure 1.6 Structure and data collection positions of 50th percentile male Ellipsoid pedestrian model's leg (Automotive, TNO, 2015b).

1.4 Dummy injury criteria

To evaluate the injury level of different dummy body parts, a number of injury criteria have been developed in the past.

1.4.1 Head injury criteria.

Head Injury Criterion (HIC) is a widely used injury criteria for measuring head injury caused by an impact, based on head acceleration and time duration of impact. The current HIC is first proposed by Versace (1971) and it was then proposed by NHTSA in FMVSS No. 208.

HIC is computed according to the following expression:

$$HIC = \left\{ \left[\frac{1}{t_2 - t_1} \int_{t_1}^{t_2} a_{head}(t) dt \right]^{2.5} (t_2 - t_1) \right\}_{max} \quad (1.1)$$

Where $a_{head}(t)$ is the acceleration at the center of gravity of head measured in standard gravity acceleration, g (Versace, 1971). t_1 and t_2 are the beginning time and end time (in seconds) of any arbitrary time interval of this acceleration curve (Versace, 1971).

The common time duration between t_1 and t_2 is either 36ms or 15ms, corresponding HIC criteria HIC_{36} , HIC_{15} respectively. For adult, the limit value of HIC_{36} is 1000 while HIC_{15} uses 700 as limit value (Eppinger et al. 1999).

1.4.2 Neck injury criterion

1.4.2.1 N_{ij}

N_{ij} is an injury criteria for assessing neck injury, based on resultant neck force and moment and is used by NHTSA's since 1996 (Klinich et al. 1996). 'i' represents the axial load (tension or compression) and 'j' represents the sagittal plane bending moment (flexion or extension) (Eppinger et al. 1999). Therefore, four injury mechanisms, N_{TE} , N_{TF} , N_{CE} , and N_{CF} are used to represent different axial load and sagittal plane bending moment. N_{ij} is calculated according to equation (1.2):

$$N_{ij} = \frac{F_z}{F_{int}} + \frac{M_y}{M_{int}} \quad (1.2)$$

Where:

F_z = axial load ;

F_{int} = the normalized critical intercept value of load according to the specific dummy corresponding to F_z ;

M_y = bending moment

M_{int} = the normalized critical intercept value for moment according to the specific dummy corresponding to M_y .

The threshold value of N_{ij} for all dummy sizes in Supplemental Notice for Proposed Rulemaking (SNPRM) is 1 (Eppinger et al. 1999).

1.4.2.2 Neck forces and moments

Besides N_{ij} , independent evaluation of neck forces and moments are also supported by to evaluate neck injury of dummy and used in alternative sled test in FMVSS 208 (Eppinger et al. 1999). The values of dummy should be limited in the grey box shown in Figure 1.7.

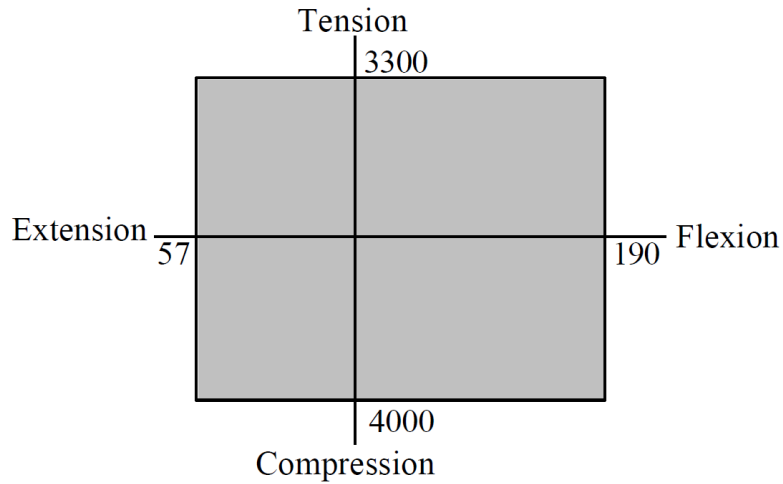


Figure 1.7 The sled test alternative neck injury criteria in FMVSS 208 in 1999 (Eppinger et al. 1999).

1.4.3 Thoracic injury criteria

1.4.3.1 Thoracic trauma index

The Thoracic trauma index (TTI) is a side impact injury criterion based on acceleration. It uses the data from post mortem human subjects (PMHS) sled tests which are numerous side impacts (Eppinger et al 1984., Morgan et al., 1986). Federal motor vehicle safety standard (FMVSS) 214 applied this injury criterion and then this criterion has been accepted for measuring trauma in side impact scenarios. The TTI value is defined as the equation (1.3) (Morgan et al., 1986):

$$TTI = 1.4Age + 0.5(RIBY + T12Y) \frac{M}{M_{std}} \quad (1.3)$$

Where:

Age = Age of the test subject (in years)

$RIBY$ = Max absolute value of rib acceleration on struck side in lateral direction

$T12Y$ = Max absolute value of the twelfth thoracic vertebrae acceleration in the lateral direction

M = Subject mass

M_{std} = Standard mass of 50th percentile male, 75 kg

Based on PMHS side impact experiments, the TTI criteria are summarized in Table 1.1.

Table 1.1 TTI criteria for the thorax from PMHS side impact experiments (Morgan et al., 1986; Forbes 2005)

Injury level	25% probability	50% probability
TTI (G's)		
$AIS \geq 3$	110	130
$AIS \geq 4$	150	168
$AIS \geq 5$	223	265

1.4.3.2 Viscous criterion

The viscous criterion (VC) was proposed by Lau and Viano (1986) and defined as the equation (1.4).

$$VC(t) = V(t)C(t) \quad (1.4)$$

Where:

$C(t) = \frac{D(t)}{D_0}$, the instantaneous normalized compression, $D(t)$ is the compression length, D_0 is the original length.

$V(t) = \frac{d[D(t)]}{dt}$, the velocity of deformation

It is the soft tissue injury potential calculated by rate sensitive torso compression. A series of compression experiments have been done (Viano et al. 1989b) to propose the VC_{max} values for side impact scenario as seen in Table 1.2. Specifically, the threshold value used in ECE R95 side impact crash test is 1m/s (Forbes, 2005).

Table 1.2 Viscous Criteria Results for the Thorax (Forbes, 2005)

Injury level	25% probability	50% probability
Lateral VC_{max} (m/s)		
$AIS \geq 3$	*	1.00
$AIS \geq 4$	1.47	1.65
*Data not provided		

1.4.3.3 3ms clip acceleration

3ms clip acceleration (A_c) is one of the available thoracic injury criteria. It is the 3ms clip value of the spine resultant acceleration and is used to assess AIS level. The chest acceleration limit of A_c for 50th percentile male is 60, and the corresponding threshold values for the other dummy sizes are scaled from the 50th percentile male (Eppinger, 1999).

AIS injury probability level is evaluated based on the following expressions (Eppinger, 1999):

$$p(AIS2+) = \frac{1}{1+e^{1.2324-0.0576*A_c}} \quad (1.5)$$

$$p(AIS3+) = \frac{1}{1+e^{3.1493-0.0630*A_c}} \quad (1.6)$$

$$p(AIS4+) = \frac{1}{1+e^{4.3425-0.0630*A_c}} \quad (1.7)$$

$$p(AIS5+) = \frac{1}{1+e^{8.7652-0.0659*A_c}} \quad (1.8)$$

1.4.4 Abdomen injury criteria

Acceleration, deflection, rate of deflection, force, and VC are five main criteria to assess abdominal injury level. For EuroSID II dummy model, since the deflection of abdomen cannot be measured, force or acceleration are two main concerned injury criteria (Kuppa, 2004). Kuppa (2004) proposed the injury risk equation (1.9) and (1.10) to predict the abdominal injury based on abdomen force. Some threshold points are also listed in Table 1.3.

$$p(AIS3+) = \frac{1}{1+e^{6.4044-0.002133*F}} \quad (1.9)$$

$$p(AIS4+) = \frac{1}{1+e^{9.282-0.002133*F}} \quad (1.10)$$

Where F is the total applied force on the cadaver abdomen or total force in the abdomen in 'N'.

Table 1.3 Point values of ES-2 abdominal force corresponding to 25% and 50% probability of AIS 3+ and AIS 4+ abdominal injury (Kuppa, 2004).

Injury predictor	25% prob. of injury		50% prob. of injury	
Maximum total abdominal force in ES-2	AIS 3+	AIS 4+	AIS 3+	AIS 4+
	2300 N	3800 N	2800 N	4400 N

1.4.5 Pelvis injury criteria

Maximum pelvic force is one of the criteria to evaluate pelvis injury, especially for side impact dummy model. For EuroSID II dummy model, the pubic symphysis force of pelvis can be measured by load cell to calculate AIS injury probability according to the following equations 1.11 and 1.12 and the threshold points are also listed in Table 1.4 (Kuppa, 2004).

$$p(AIS2+) = \frac{1}{1+e^{6.403-0.00163*F_p}} \quad (1.11)$$

$$p(AIS3+) = \frac{1}{1+e^{7.5969-0.0011*F_p}} \quad (1.12)$$

Where F_p is the pubic force.

Table 1.4 Point values of ES-2re pubic symphysis force corresponding to 25% and 50% probability of AIS 2+ and AIS 3+ pelvic injury (Kuppa, 2004).

Injury predictor	25% prob. of injury		50% prob. of injury	
Maximum public symphysis force in ES-2	AIS 2+	AIS 3+	AIS 2+	AIS 3+
	3250 N	6000 N	4000 N	7000 N

1.4.6 Leg injury criteria

The *tibia index* (TI) is widely used for assessing leg injury. It was first proposed by Mertz (Mertz, 1993) as an injury tolerance criterion for the leg of Hybrid III dummy. TI combines bending moment and axial compressive loads on the leg and currently it is calculated according to equation (1.13).

$$TI = \frac{F_1}{F_C} \cdot \frac{M_1}{M_C} \cdot 1.3 \quad (1.13)$$

Where F_1 is the measured compressive axial force (kN) in the superior-inferior direction. M_1 is the resultant moment of the medial-lateral and the anterior-posterior moments. For Hybrid III 50% male dummy model, the value of M_C and F_C is 225Nm and 35.9kN respectively (Eppinger, 1999).

1.5 Aim of the project

This thesis work is based on a MADYMO study conducted by Volvo Truck. In previous study, a new truck front with spring system was developed to improve pedestrian safety.

One of the main aims of this master thesis work are to compare the results between the MADYMO Ellipsoid 50th percentile male human model simulations previously done, with LS-DYNA 50th percentile male Autoliv IA pedestrian dummy model simulations. The other main aim is to find out a suitable physical honeycomb structure to replace the spring system (see Section 3.1.1) located in the truck front while maintaining the truck front's performance of reducing pedestrian injury.

2 Previous MADYMO study

This project is based on previous pedestrian to truck collision MADYMO study conducted by Volvo Group. The aim of this MADYMO study is to develop a truck equipped with a spring system in its front structure in order to define optimal truck front properties for an improved pedestrian protection. Collisions between four pedestrian models and two truck models, FH truck (reference truck) and truck with spring system (studied truck), are simulated. The simulation result shows that with this simplified and ideal spring system, the number of pedestrian sustaining MAIS2+ injuries can be reduced potentially by up to 20%. The main simulation method is described below.

2.1 Global coordinate system

In MADYMO study, the global coordinate system is shown in Figure 2.1. X-coordinate is from truck front to rear, Y-coordinate from truck left to right and Z-coordinate upwards.

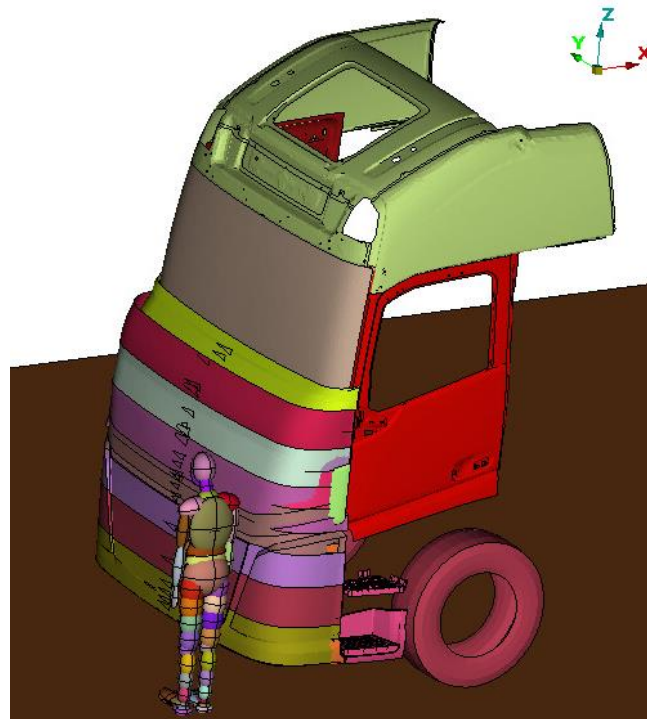


Figure 2.1 Global coordinate system.

2.2 Pedestrian model

In this MADYMO study, the 6-year old child, the 5th percentile female, the 50th percentile male and the 95th percentile male Ellipsoid pedestrian models described in Section 1.2.4 were used in simulations. Each size model is modified into 2 postures, 'Walk' and 'Stand' postures, as seen the example of the 50th percentile male model in Figure 2.2.

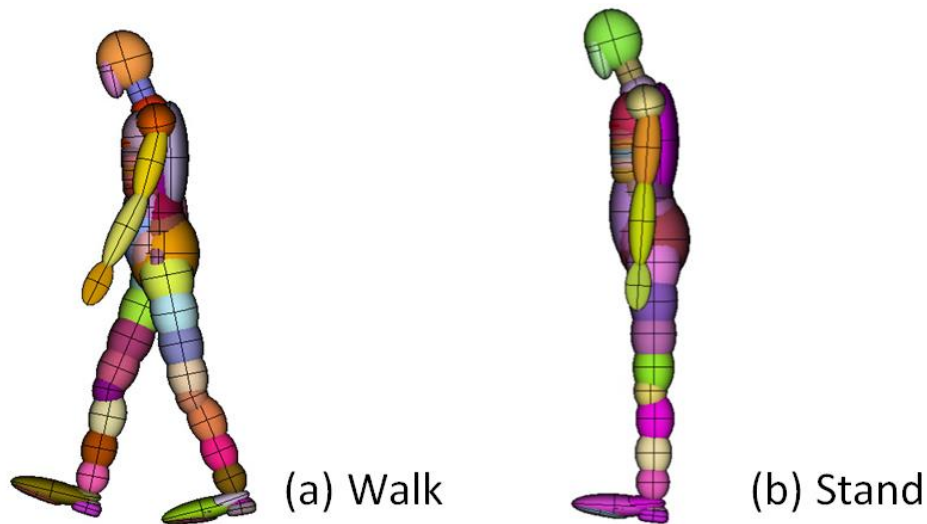


Figure 2.2 Two postures of 50th percentile male Ellipsoid pedestrian model.

The modification of each model's joints for two postures can be referred in Table 2.1.

Table 2.1 Positions of inner joints for Walk and Stand postures.

Posture	Left shoulder	Right shoulder	Left hip	Right hip	Left knee	Right knee	Left ankle	Right ankle
Walk	-0.2	0.3	0.2	-0.4	0.2	0.2	-0.1	0
Stand	0	0	0	0	0	0	0	0

2.3 Truck models

The reference FH truck model is a simplified rigid body truck exterior model, as seen in Figure 2.2(a). The studied truck model is a rigid body truck exterior model with a 300mm front nose elongation, as seen in Figure 2.2(b).

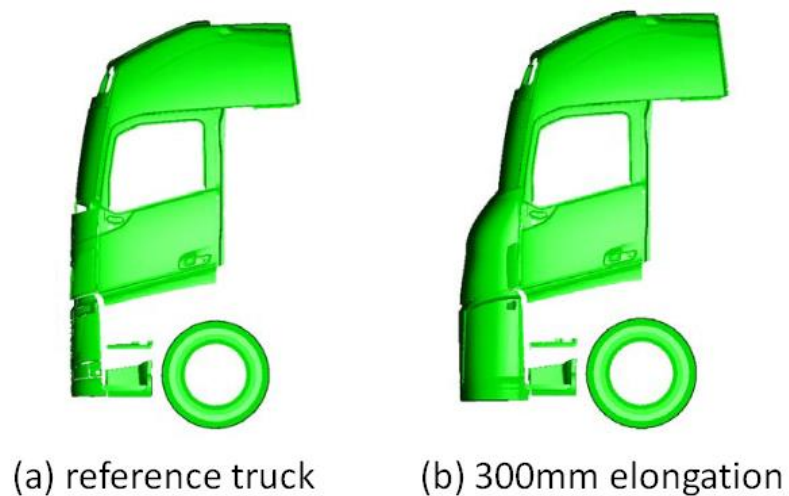


Figure 2.2 Reference truck and studied truck exterior.

The front face of the studied truck is divided into seven parts by height from low to high, as seen in Table 2.2 and the face 1 in Figure 2.3. Face 1 is the studied truck front face, consisting of ‘Bumper lower 1’, ‘Bumper upper 1’, ‘Grille lower 1’, ‘Grille upper 1’, ‘Lid lower 1’, ‘Lid middle 1’ and ‘Lid upper 1’, without gap between every part from low to high along positive Z direction. Because of the limitation of MADYMO model, in order to get the contact force between each dummy body part and truck front surface, the twin 7 parts are first created by copying original parts, named by changing ‘1’ to ‘2’. For example, the part copied from ‘Lid upper 1’ is named as ‘Lid upper 2’. Then, to fit the position of contact body part of models in different sizes during crashing, ‘Grille upper 2’, ‘Lid lower 2’ and ‘Lid middle 2’ are shifted up by 150mm along Z direction, as seen the face 2 in Figure 2.3. The contact between dummy body parts and truck front is listed in Table 9.1, Appendix A.

Table 2.2 *The character of 7 front surface contact parts of studied truck.*

Parts (Position from low to high)	Mass [kg]	Height of the part (Z direction) [mm]
Bumper lower 1	0.1285	275.6
Bumper upper 1	0.1285	275.4
Grille lower 1	0.1285	225.85
Grille upper 1	0.2845	309
Lid lower 1	0.2845	259.5
Lid middle 1	0.2845	274.1
Lid upper 1	0.2845	259.2

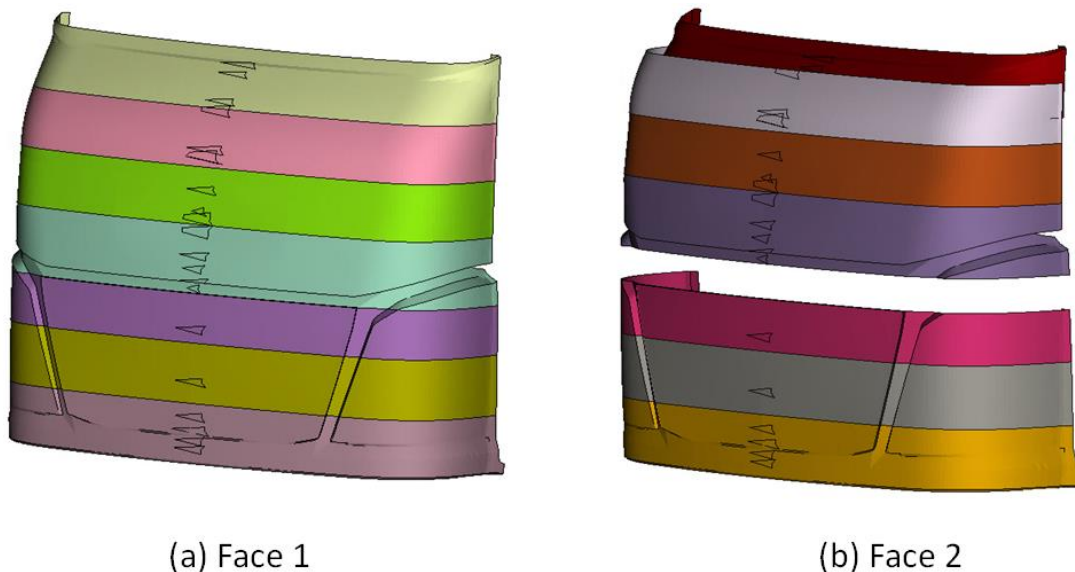


Figure 2.3 *The two faces of studied truck’s front structure.*

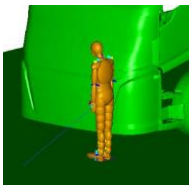
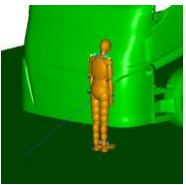
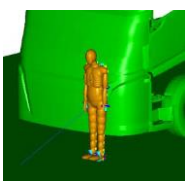
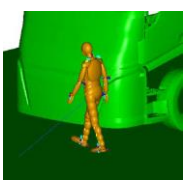
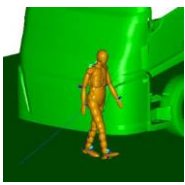
All 14 parts in face 1 and face 2 are set to have the spring and damper characteristics and the twin parts share the same characteristics.

2.4 Collision scenarios

By rotating ‘Walk’ and ‘Stand’ models along center Z axle in different degrees, five different impact positions can be got as seen the example of 50th percentile male model in Table 2.6. ‘Walk180’ is defined as rotating the ‘Walk’ model by 180 degrees along Z direction. ‘Stand 90’ and ‘Stand 270’ are defined as rotating the ‘Stand’ model by 90 degrees and 270 degrees respectively along Z direction.

The truck goes straight forward within velocity of 24km/h (6.67m/s) and 40km/h (11m/s) respectively in all scenarios. The human model’s moving speed is set to be 1.7m/s along +Y direction in all scenarios. Therefore, total 10 collision scenarios between 50th percentile male model and truck are shown in Table 2.3. Same impact scenarios were used both for the reference truck model and for the elongated truck front model.

Table 2.3 Impact scenarios between 50th percentile male model and truck in MADYMO study.

Case number	1	2	3	4	5	6	7	8	9	10
Impact speed, km/h	40	24	40	24	40	24	40	24	40	24
Impact direction	 Stand		 Stand90		 Stand270		 Walk		 Walk180	

3 Method

In the first stage, the LS-DYNA truck model with same front face geometrical properties and spring and damper characteristics as in the previous MADYMO elongated truck front model is constructed. After getting different pedestrian postures, the same collision scenarios as previous MADYMO study referred in Section 2.4 is simulated in LS-DYNA. The LS-DYNA results are compared with MADYMO simulation results to identify possible differences between the MADYMO based 50% male human body model and the LS-DYNA based IA ATD model.

In the second stage, a FE honeycomb structure is developed to replace the spring system. To verify it, the collisions between ‘Walk’ pedestrian and new trucks with honeycomb structure are simulated and the result is compared with previous results from FE truck with spring system.

3.1 FE truck model construction

3.1.1 Truck front FE modelling

In this study, the global coordinate system is the same as that in MADYMO study, as shown in Figure 2.1. The studied truck in FE study has the same geometry as that in MADYMO study, as seen in Figure 3.1. The materials of the FE truck body parts are also rigid and the front structure also consists of 2 faces with 14 contact parts. The mass of these contact parts are same as that in the MADYMO truck model, see Table 2.2.



Figure 3.1 The geometry of the FE truck model.

To construct spring system, 14 rigid supporters with large mass for each contact parts were built, as seen in Figure 3.2. The spring and damper elements were created between every part and its corresponding supporter along X direction. An example of the material cards of the springs of ‘Lid mid 1’ and ‘Lid mid 2’ are shown in Appendix B. The damper’s material card is also shown in Appendix B. The length of the spring and

damper is set to be 350mm, which is the same as that in MB truck's spring. Every spring and damper element has the same load and unload property as that in MB model.

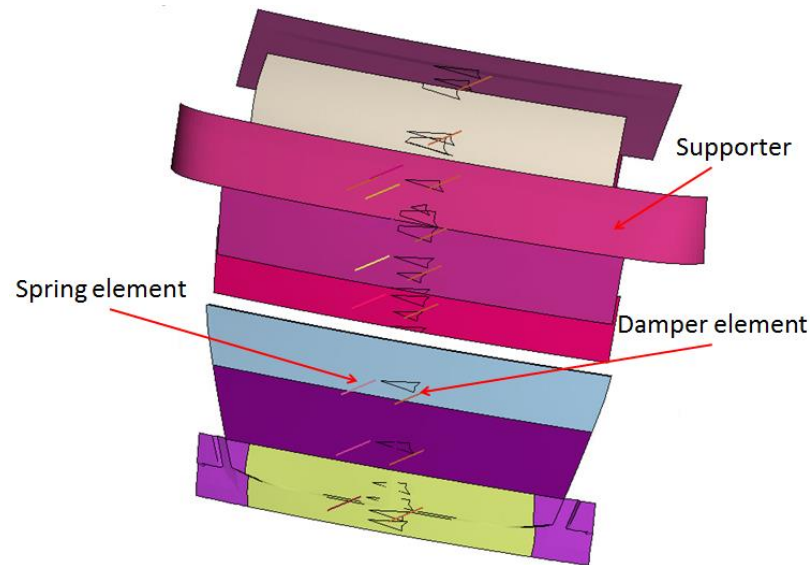


Figure 3.2 Supporters, damper and spring elements of FE studied truck.

There is no contact between each component of truck model. Since the total mass of truck model in MADYMO study is infinitive, the density of these 14 supporters was set to be a random high value. As a result, the total mass of these supporters is 6.4×10^6 kg, which can be considered as infinitive mass.

3.1.2 Verification of FE truck model

The LS-DYNA front surface and spring system's performance is verified vs. MADYMO by free motion headform (FMH). FMH is intended for upper interior head impact tests. It was constructed and calibrated in terms of mass, acceleration, force, etc. based on lab experiments. LS-DYNA and MADYMO both provide FMH models, which are 'LSTC FMH (Version LSTC.FMH.091201 V2.0)' and 'MADYMO FMVSS201Headform' respectively as seen in Figure 3.3.

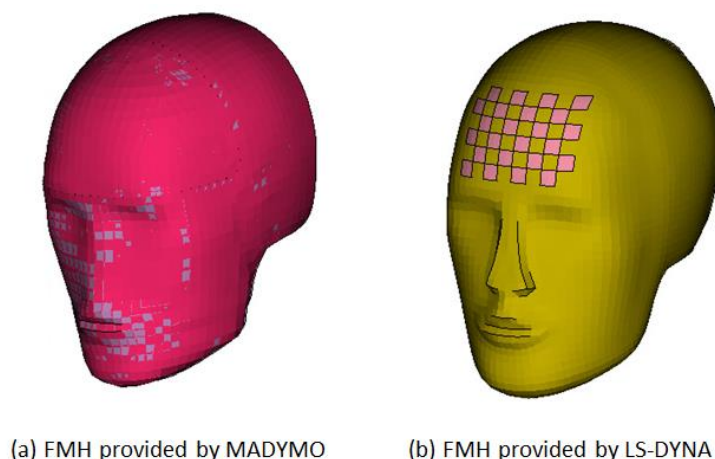


Figure 3.3 Verification of truck system with FMH.

The FMH model is located in same position in both MADYMO and LS-DYNA simulation. It impacts on the 'lid lower 2' part at 24km/h and 40km/h respectively, see Figure 3.4 below. HIC_{36} and contact force are two main criteria for comparison.

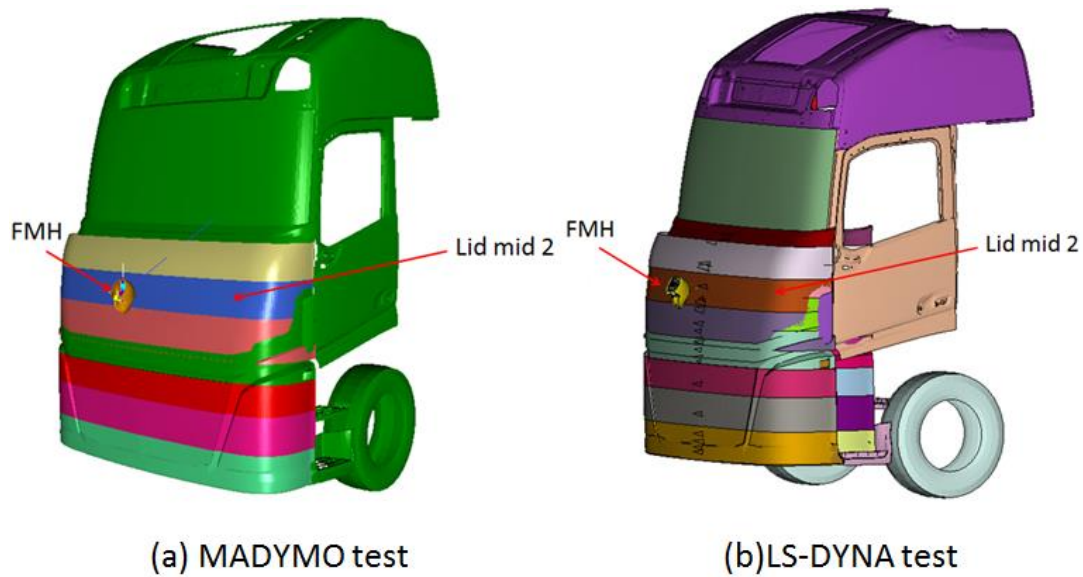


Figure 3.4 Verification of FE truck model with FMH in MADYMO and LS-DYNA.

3.2 FE pedestrian dummy model modification

The FE pedestrian dummy model used in this study is IA dummy model as referred in Section 1.3.3. Some modification based on this dummy model to suit simulation, see Appendix C.

Also, in this study, IA model has the same ‘Walk’ and ‘Stand’ posture as that in MADYMO study by rotating corresponding body parts according to Table 2.3. IA dummy model with corresponding MADYMO model are shown in Figure 3.5 and Figure 3.6.



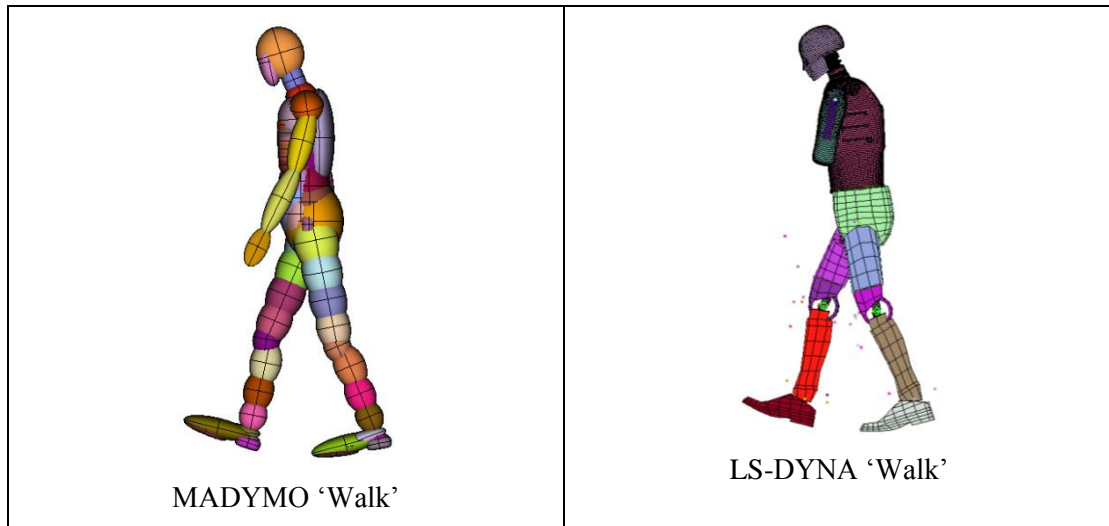


Figure 3.5 The 'Walk' posture of IA pedestrian dummy model.

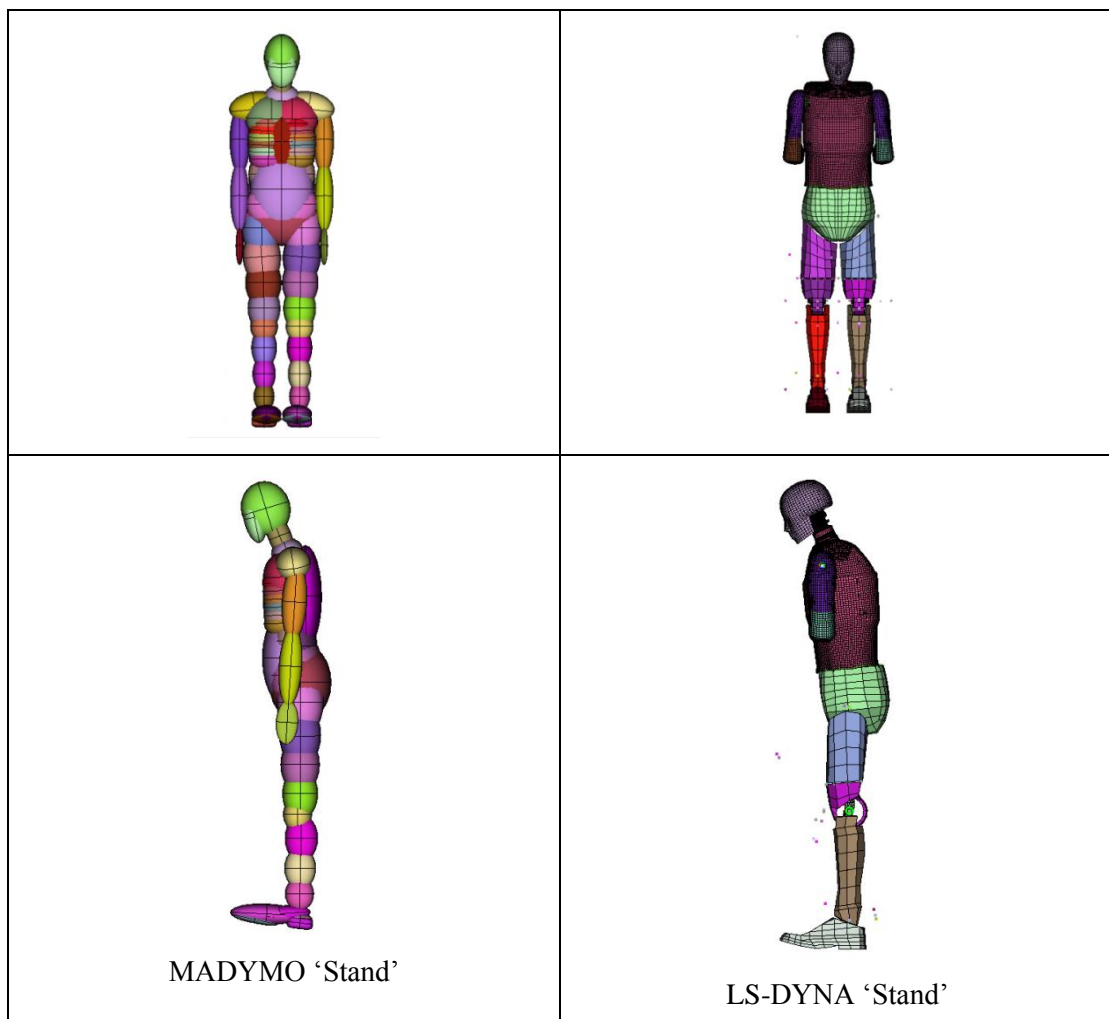


Figure 3.6 The 'Stand' posture of IA pedestrian dummy FE model.

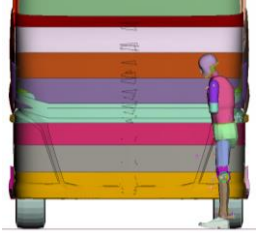
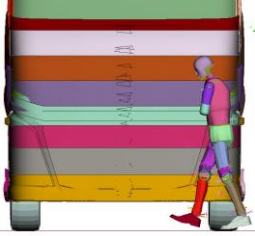

3.3 Collision scenarios construction

Since the IA pedestrian dummy model is only validated in side impact, the ‘Stand90’ and ‘Stand 270’ front impacts were not carried out with this model. Therefore, only ‘Walk’, ‘Walk 180’ and ‘Stand’ postures are simulated in this study. The positions of dummy are set to be same as that in the MADYMO simulation.

By setting initial velocity in LS-DYNA, the FE truck has same velocity as MB truck, 24km/h and 40km/h along -X direction respectively, and the FE dummy is also set to have same speed as MB dummy, 1.7m/s along +Y direction. The movement of truck, 14 contact parts are restrained to be only in X direction.

A rigid surface without any degree of freedom is built to be road. The gravity acceleration, 9.82m/s^2 , is set by adding ‘load body’. The contact card ‘Automatic_Surface_to_Surface’ is used in the contact between pedestrian and truck, pedestrian and road, shoes and road, as seen in Appendix D. The friction coefficient between pedestrian and truck as well as between pedestrian body and road is 0.3. The friction coefficient between shoes and road is larger, 0.58. The contacts relationship between pedestrian body parts and corresponding truck front contact parts are set to be the same as in MADYMO study, as seen in Table 2.3.

Table 3.1 Collision scenarios between FE studied truck and IA pedestrian model.

Case number	1	2	3	4	5	6
Impact speed, km/h	24	40	24	40	24	40
Impact direction	 stand		 walk		 Walk180	

3.4 Comparison of MADYMO and LS-DYNA results

For comparison, the injury data should be able to be collected in both IA and Ellipsoid pedestrian models. Therefore, according to Section 1.3.3 and 1.3.4, HIC_{36} , maximum upper/lower neck resultant force and moment, and upper/lower torso 3ms clip acceleration are selected for comparison. However, the IA pedestrian model gets the torso lower acceleration at lower spine while the Ellipsoid pedestrian model gets it at pelvis. Therefore, to compare lower torso acceleration, an accelerometer is constructed at pelvis’ inertia center of IA pedestrian model, see Figure 3.7.

The injury values in primary and secondary impact may be compared separately for detailed comparison. The primary impact in pedestrian-to-truck collision in this case refers to the impact between pedestrian and truck front surface, while secondary impact referring the impact between pedestrian and ground.

Besides these injury parameters, the track of the pedestrian motion, the impact duration, the time to get maximum value of the injury criteria, etc. may be compared.

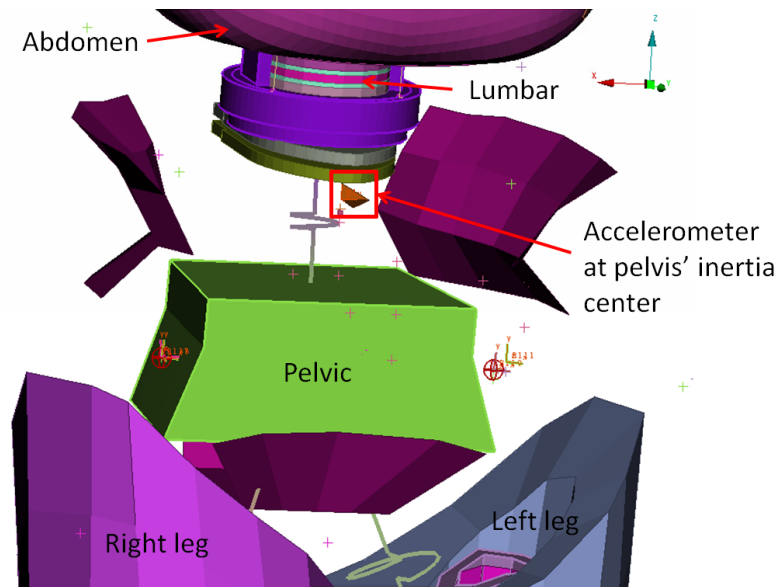


Figure 3.7 The accelerometer at pelvis' inertia center of IA pedestrian dummy FE model.

3.5 The development of honeycomb structure

To meet the demand of energy absorbing and ventilation of front surface, honeycomb structure is selected to replace the ideal spring system. However, the bumper lower part's spring doesn't have yield stage in its load curve and it has high stiffness and strength, which is difficult for honeycomb to replace. Hence, bumper lower part's spring will not be replaced by honeycomb structure.

3.5.1 The material of honeycomb

According to the requirements of being able to work in outside environment, suitable for injection modeling production, not splintering or cracking easily, not rather bending or buckling to absorb energy, and low stiffness, Zytel® ST811HS NC010, a kind of PA6-I plastic material provided by DuPont Engineering Polymers, is selected to be the material for this honeycomb structure product. This material has good chemical resistance performance and is easy to be recycled. The main mechanical property of this material is shown in Table 3.2 and the stress-to-strain curve at 23°C is shown in Figure 3.8. MAT24 material card is used for modeling this material as seen in Appendix B in LS-DYNA.

Table 3.2 Mechanical property of Zytel® ST811HS NC010.

Property	Value	Property	Value
Density, kg/m ³	1040	Young's modulus, MPa	400
Nominal strain at break	0.5	Poisson's ratio	0.35
Yield stress, MPa	19.7		

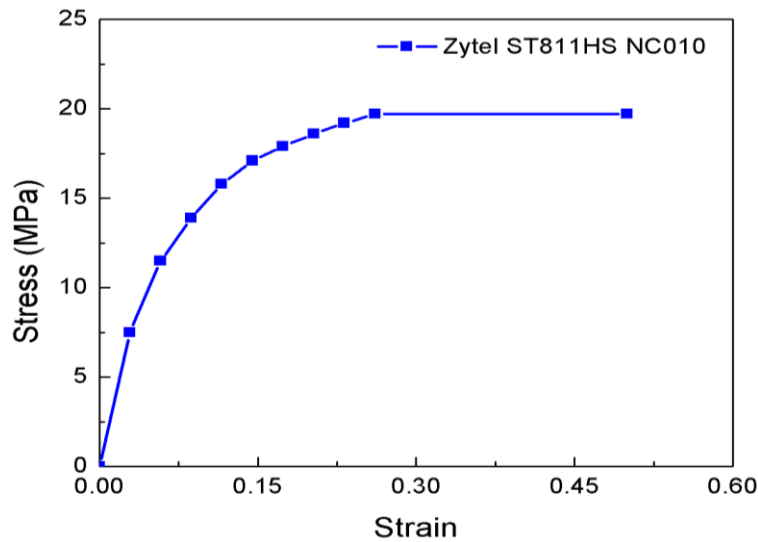


Figure 3.8 The stress-to-strain curve of Zytel® ST811HS NC010 at 23°C.

3.5.2 The size of honeycomb

According to Table 2.2, the minimum height of all 7 parts is around 226mm. Therefore, the height (along Z direction) of honeycomb structure is selected to be around 200mm to fit all 7 parts well. Based on these two requirements, 2 models are first considered as seen in Figure 3.9.

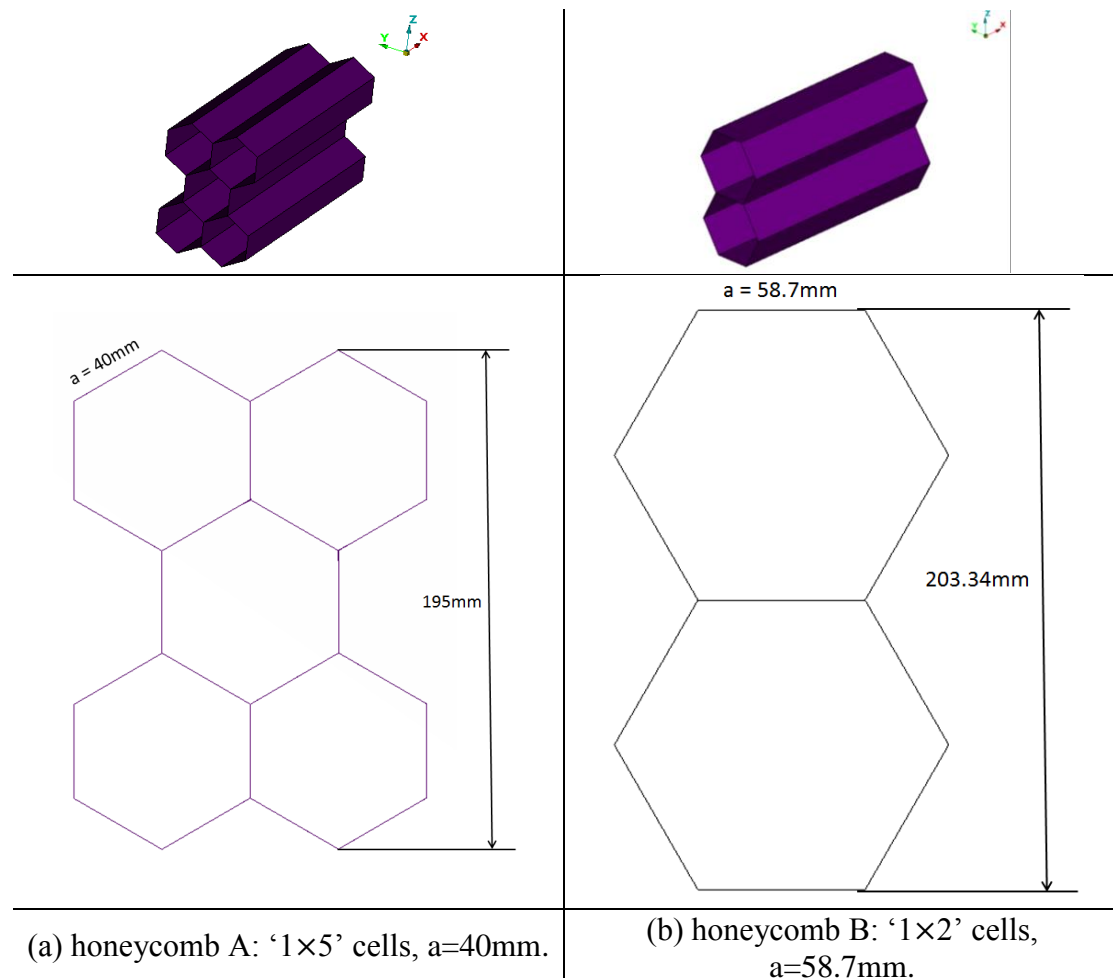


Figure 3.9 Honeycomb A and Honeycomb B structures.

To select the suitable one, the selection principle is to meet the demand of yield force within corresponding bottom out deformation for each part. Therefore, the first peak resistance force is selected as the selection principle parameter for force level. In addition, because of the limitation of injection modeling production, the thickness of honeycomb structure should not be smaller than 1mm.

Bench tests are conducted for selection as seen in Figure 3.10. The rigid plate 1 moves along +X direction at 0.35m/s. The rigid plate 2 is constrained in all freedom degree. The initial length of honeycomb A and B is set to be the largest length among 7 springs. The tested thickness is 1mm and 1.5mm. The resistance force are collected by 3 cross section plates in YZ coordinate from front to rear along X direction.

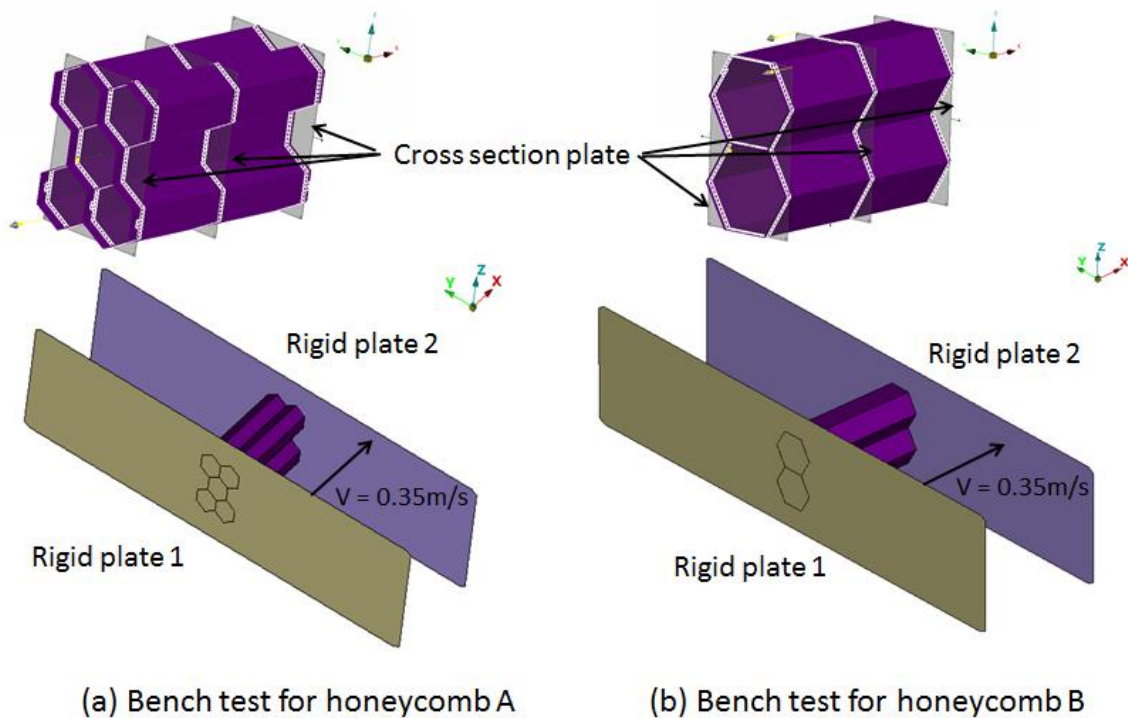


Figure 3.10 Bench test for 2 honeycomb structure.

The Figure 3.11 shows that the normalized peak resistance force of honeycomb A with thickness 1mm is already higher than 1. If the length of other honeycombs is reduced for other parts, with 1mm thickness, the resistance force may be higher than demanded. Hence, honeycomb A is not suitable for this study.

Honeycomb B's normalized resistance force has variation between 0.5 and 0.8 when thickness is between 1mm and 1.5mm. This is possible for all 7 parts to get feasible thickness. Therefore, honeycomb B is finally selected to replace the spring system.

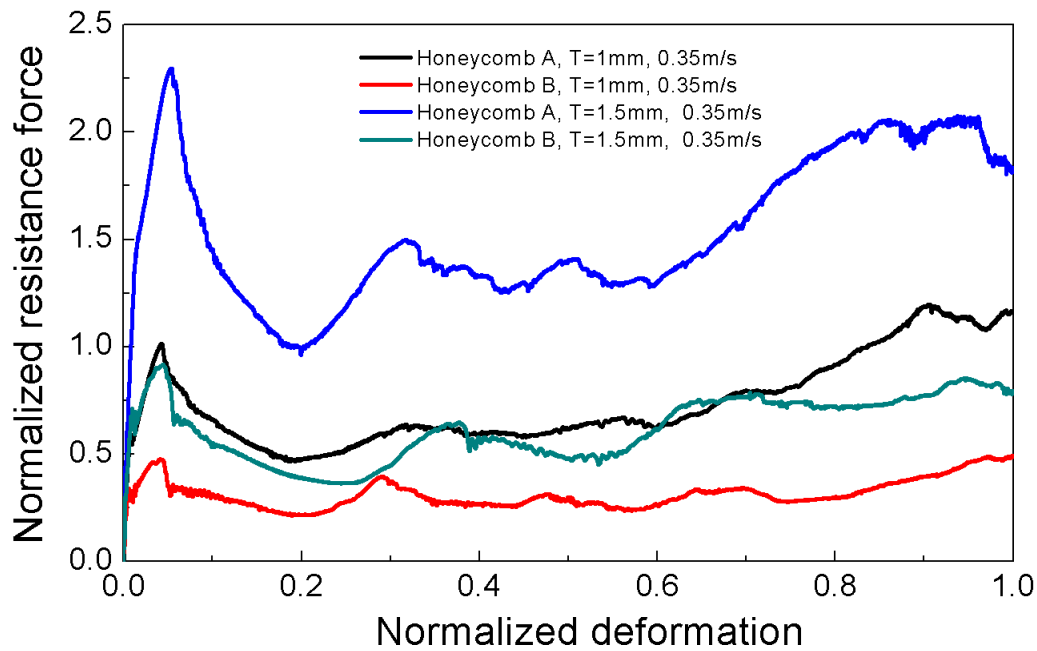


Figure 3.11 Normalized resistance force of different honeycomb structures.

3.5.3 Honeycomb A for each contact parts

Honeycomb structures for each contact part (lower bumper excluded) have been constructed with corresponding bottom out length as for the spring system. To define the thickness for every honeycomb, bench tests described in Section 3.5.2 are conducted. Table 3.3 shows the defined thickness for each contact part.

Table 3.3 Defined thickness of honeycomb A for each contact part.

Parts	Lid upper	Lid mid	Lid lower	Grille upper	Grille lower	Bumper upper
Thickness, mm	1.35	1.5	1.55	1.55	1.4	1.3

3.5.4 Verification of selected thickness

A new reference truck based on studied truck, called truck A, is constructed for verification as seen in Figure 3.12. The face 2 of studied truck has been deleted while face 1 remains. The contact between pedestrian and truck front 7 parts is the same as the contact between pedestrian body parts and contact parts in Section 3.3. Other settings are also same as in Section 3.3. ‘Walk’ posture scenarios with truck velocity at 24km/h and 40km/h, so called 2 reference scenarios, are simulated.

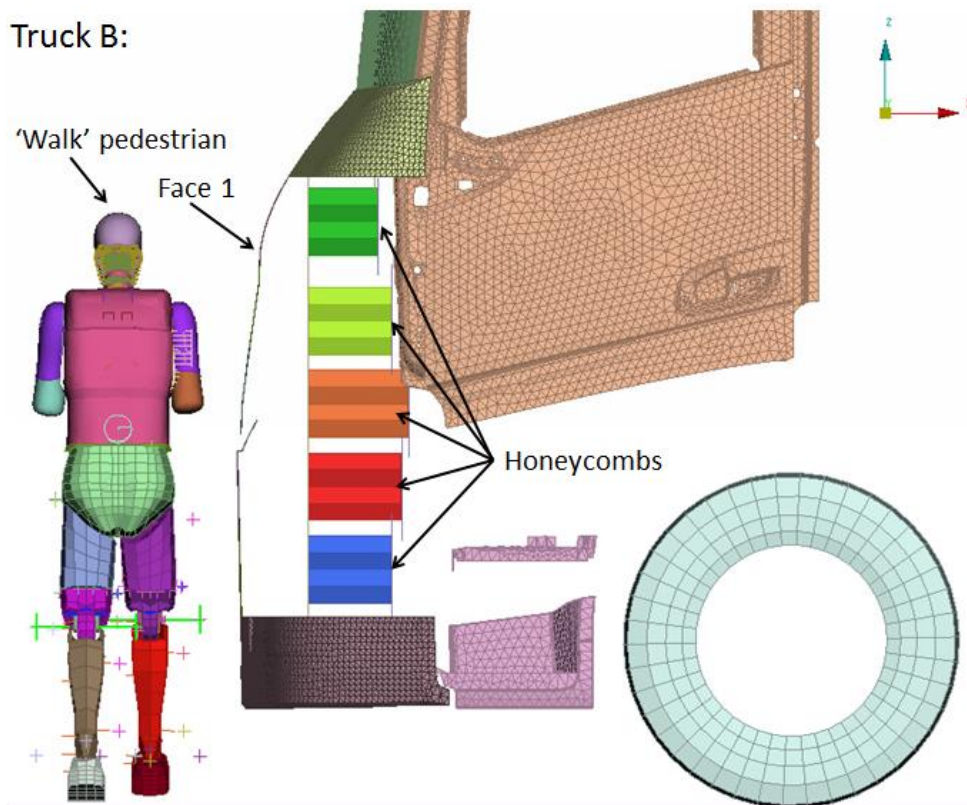


Figure 3.13 The 'Truck B' with 5 honeycombs and 'Walk' pedestrian.

The injury parameters selected in Section 3.4 except pelvis acceleration replaced by lower spine acceleration are compared between the simulations of Truck A and other trucks in reference scenarios. Other factors such as motion of pedestrian will also be compared.

4 Result

4.1 FMH verification

4.1.1 Head contact force

The normalized contact force between FMH and ‘Lid mid 2’ of 24km/h and 40km/h’s scenarios in MADYMO simulation and LS-DYNA simulation are show in Figure 4.1. The time to begin impact is different since the initial positions of FMH are same in two speed condition. The impact in 24km/h scenario happens later than that in 40km/h scenario. The time durations of impact and the contact force level in LS-DYNA and corresponding MADYMO simulations are similar.

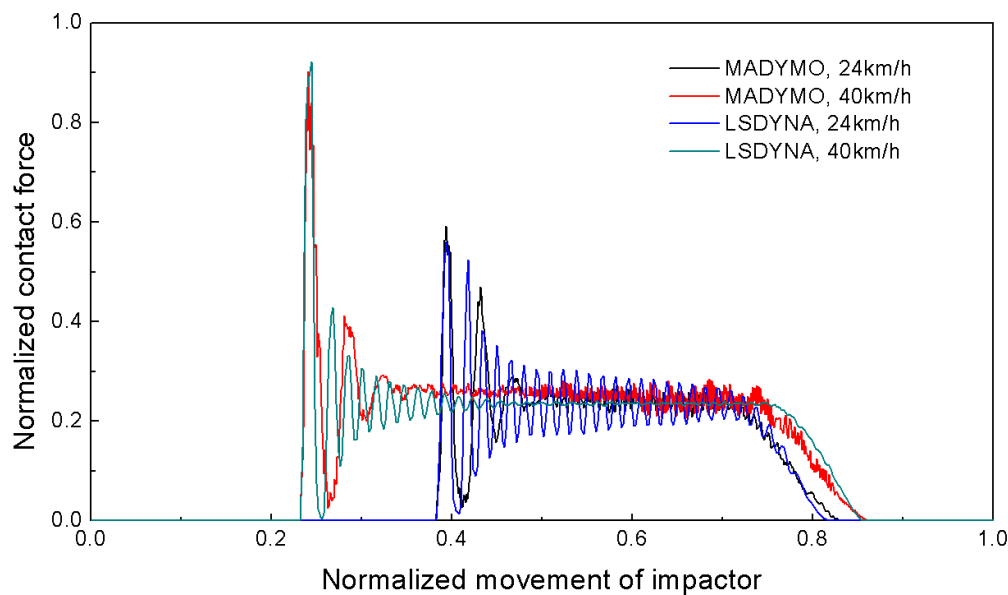


Figure 4.1 FMH results comparison.

4.1.2 Head injury, HIC₃₆

The HIC₃₆ values of 4 simulations are shown in Table 4.1.

Table 4.1 HIC₃₆ value of FMH verification

Truck velocity	Software	HIC ₃₆	Time interval
24km/h	MADYMO	226.7	from 19.3 to 38.0ms
	LS-DYNA	218.5	from 19.2 to 38.5ms
40km/h	MADYMO	377.6	from 11.7 to 39.4ms
	LS-DYNA	366.3	from 11.6 to 40.4ms

At 24km/h, the HIC₃₆ value in LS-DYNA study is 3.6% smaller than the value in MADYMO study.

$$(218.5 - 226.7) / 226.7 \approx -3.6\%$$

At 40km/h, the HIC₃₆ value in LS-DYNA study is 3% smaller than the value in MADYMO study.

$$(366.3 - 377.6) \div 377.6 \approx -3\%$$

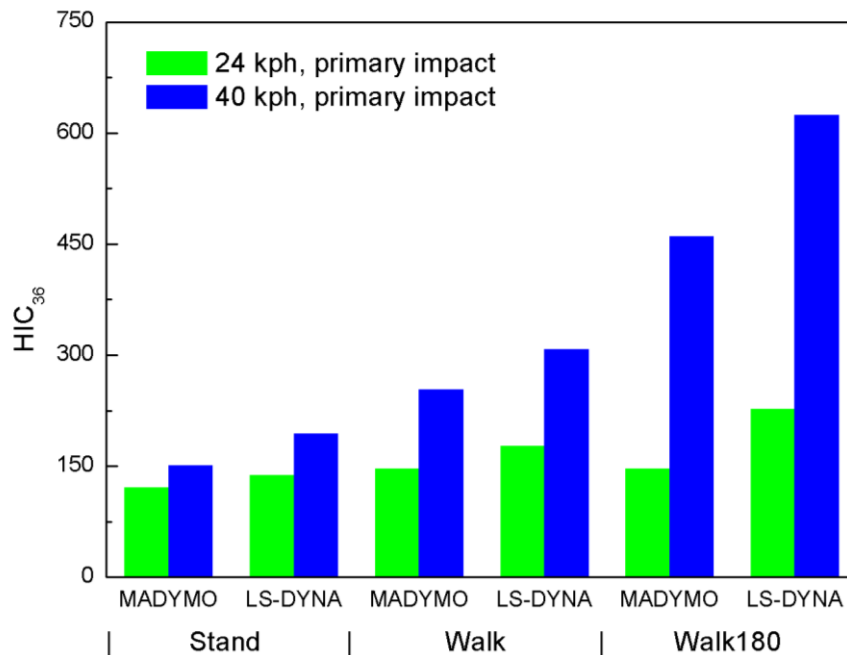
Both the difference values are smaller than 5%, which here is considered as an acceptable difference. Therefore, the LS-DYNA modeled spring system model is similar to the MADYMO model, and can be used for further study.

4.2 Comparison of results of MADYMO human model and LS-DYNA dummy model

Comparison between MADYMO and LS-DYNA is made through the following data: HIC₃₆, upper and lower torso 3ms clip acceleration, upper and lower neck resultant force and moment. Statistical analysis is carried out to figure out the similarity and difference between different pedestrian postures and also between LS-DYNA and MADYMO simulations.

In the following diagrams, ‘Primary impact’ and ‘Secondary impact’ implies the diagram only gather data from primary impact or secondary impact respectively. ‘General’ diagrams collect data from the entire collision, including primary and secondary impact. The detailed injury normalized values are shown in Appendix E, Table 9.2 to Table 9.7.

4.2.1 HIC₃₆



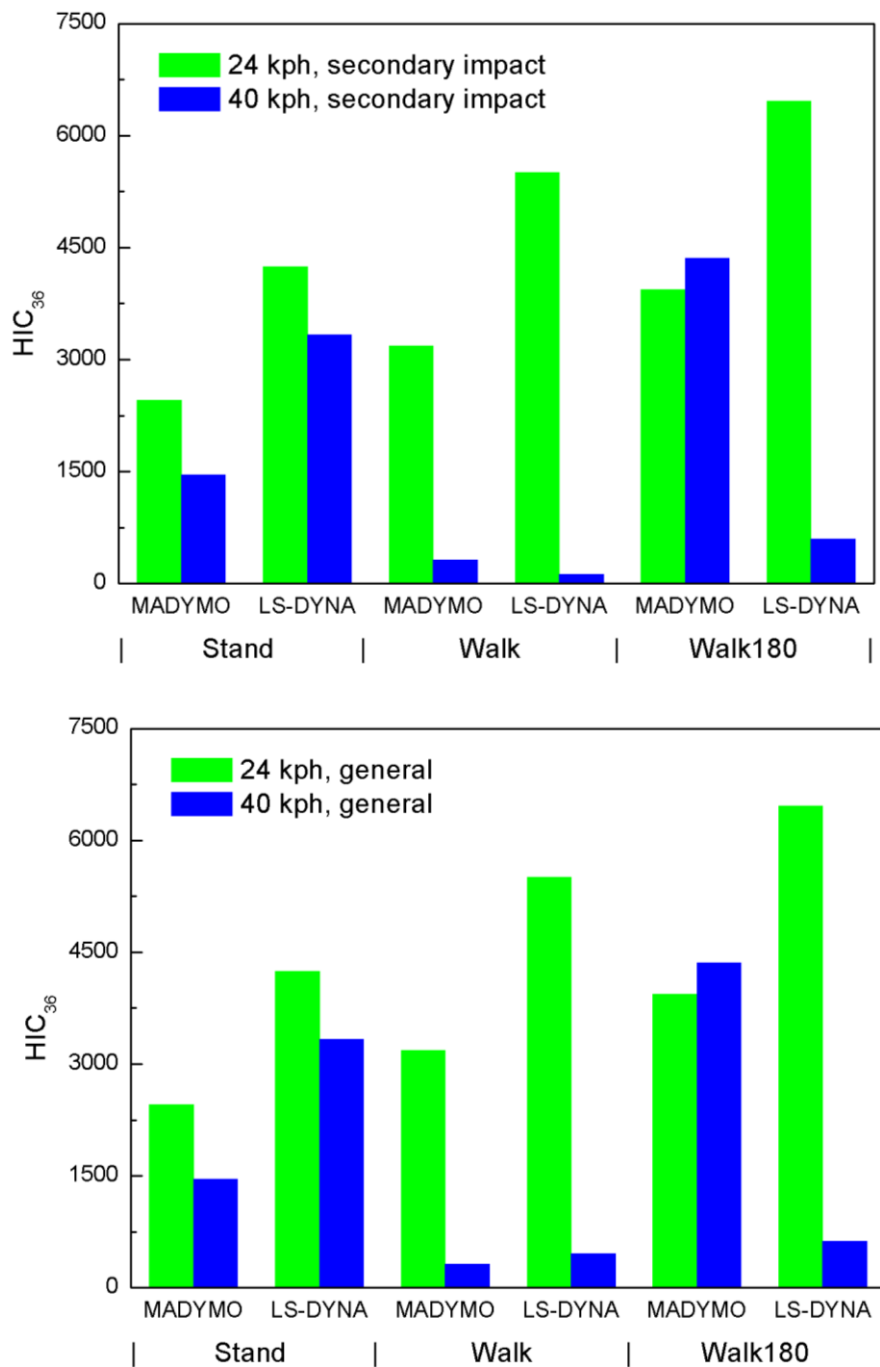
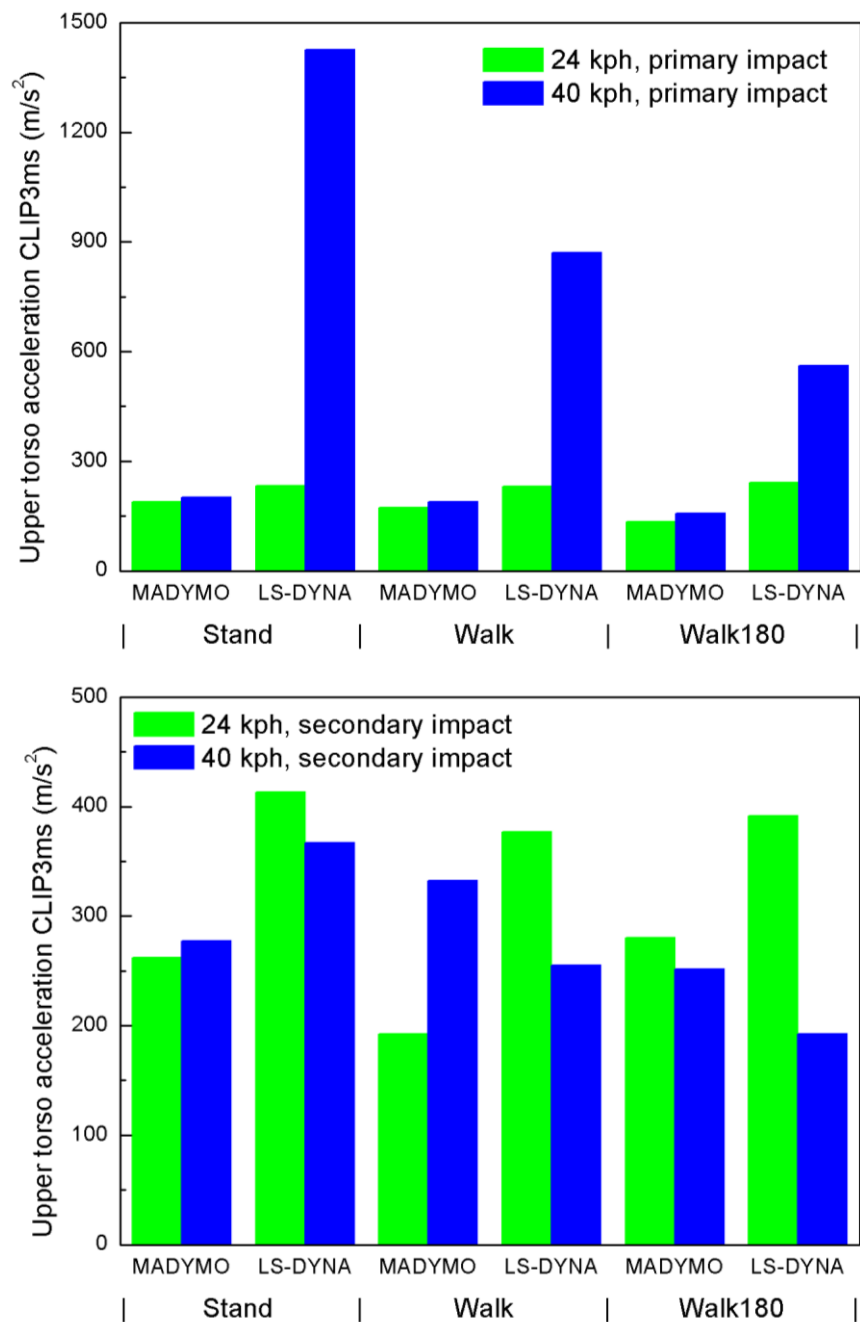


Figure 4.2 HIC_{36} comparison.

In primary impact, according to Figure 4.2, all models show that higher HIC_{36} value caused at higher impact speed. Besides, the stand posture results in the smallest HIC_{36} while “Walk 180” posture tends to lead to the most serious head injury levels.

Another phenomenon discovered during the primary impact is that FE dummy model’s HIC_{36} value is larger than MB model’s in all simulated scenarios. In addition, more severe head injury in all cases is estimated in secondary impact than in primary impact.

4.2.2 Torso acceleration



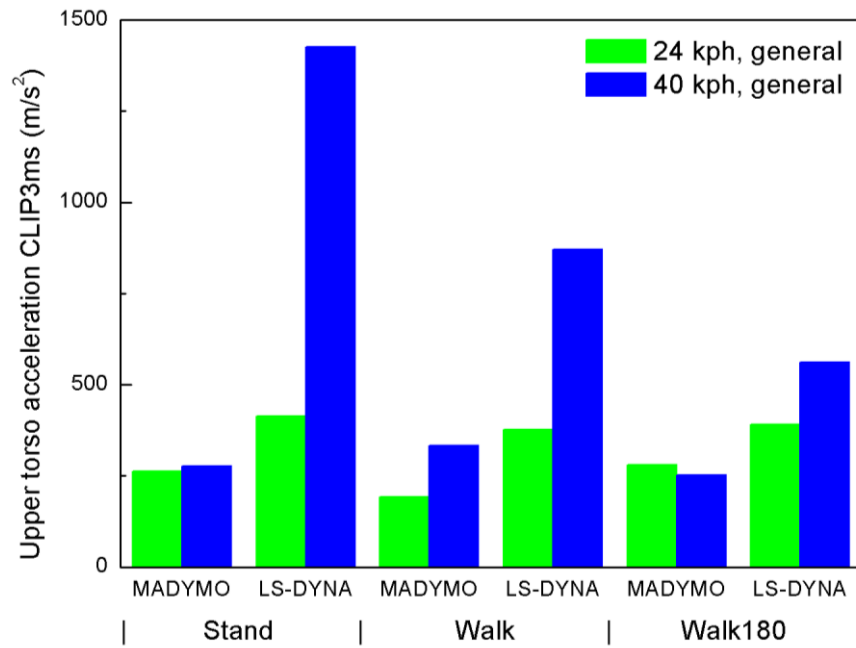
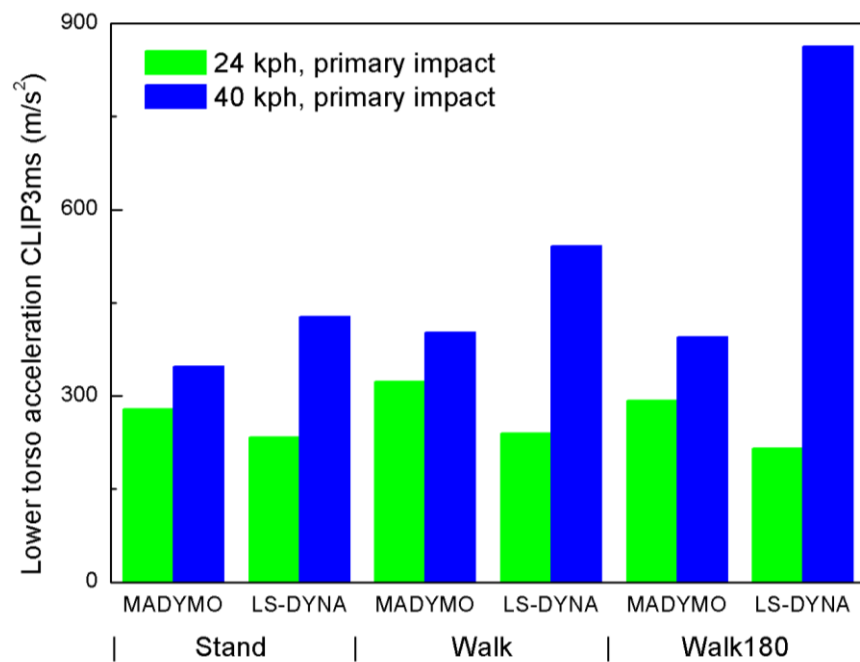


Figure 4.3 Upper torso 3ms clip acceleration comparison.



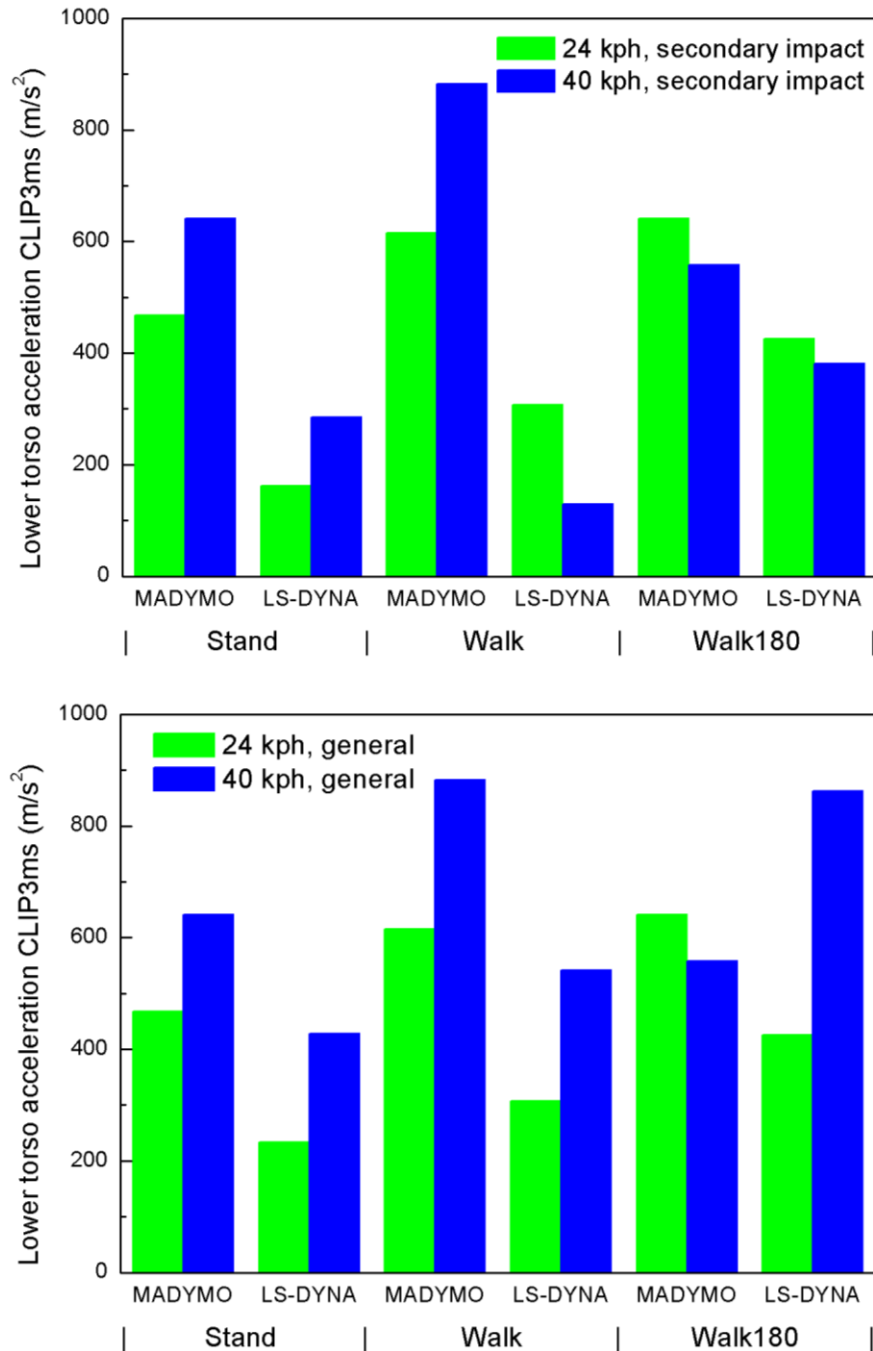
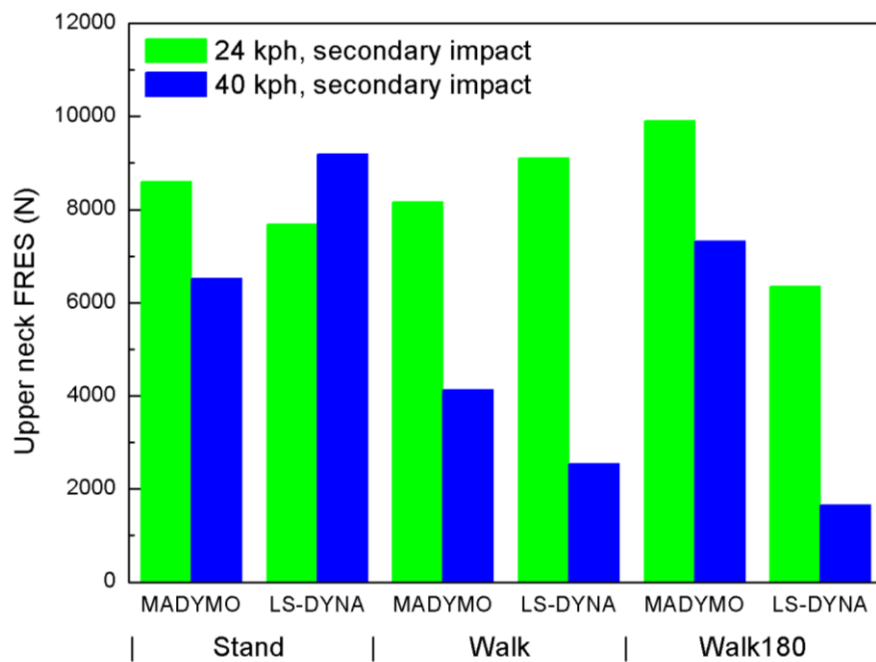
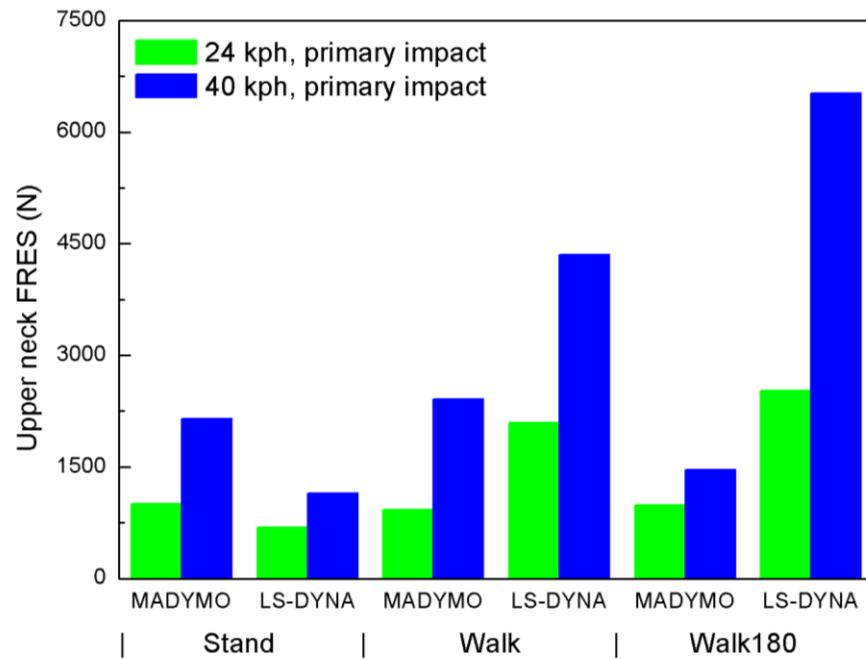


Figure 4.4 Lower torso 3ms clip acceleration comparison.

As seen in Figure 4.3 and 4.4, for primary impact, higher impact speed generally causes larger torso acceleration. These two figures also show that FE dummy model is more sensitive to impact speed. However, no clear discipline is found in secondary impact.

4.2.3 Neck resultant force



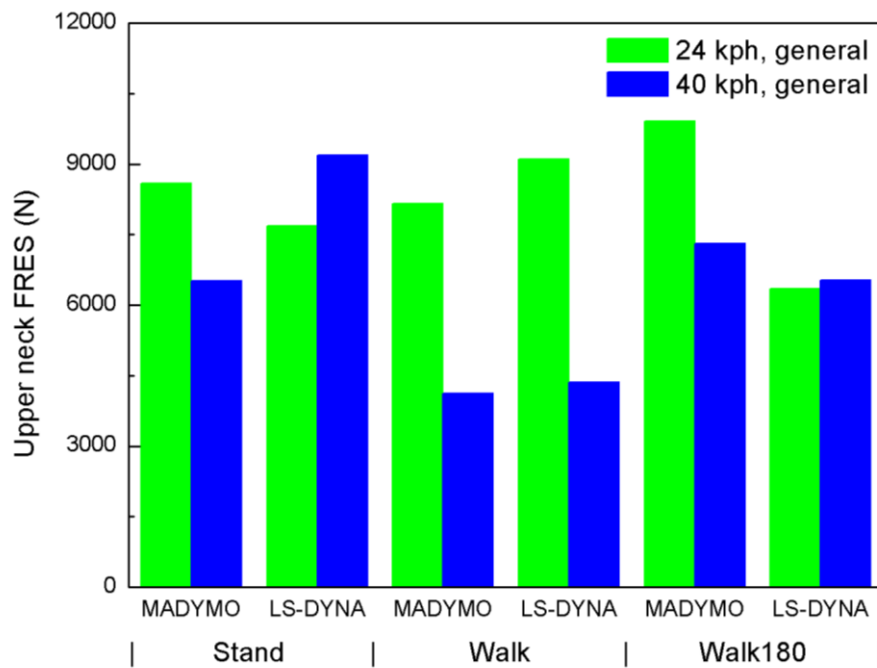
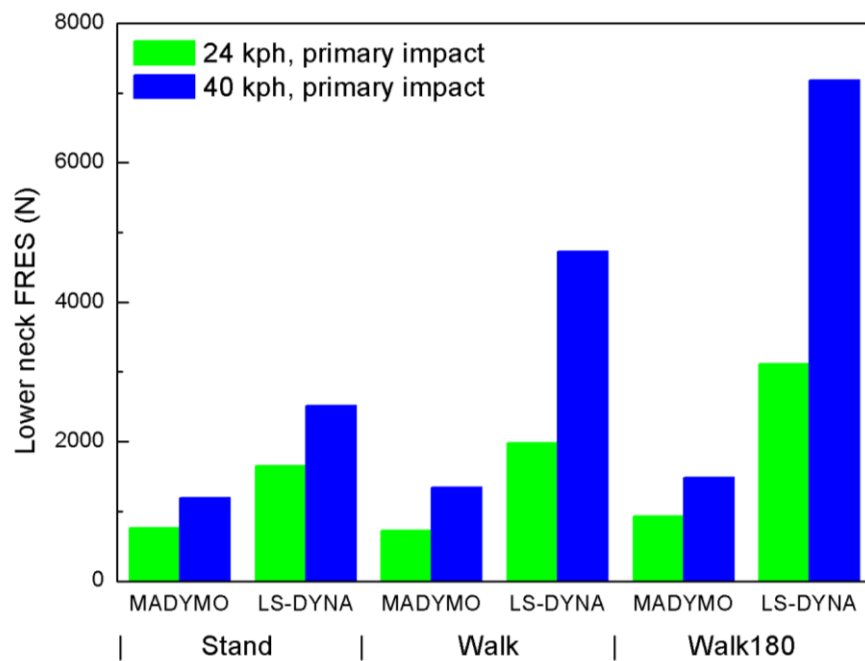


Figure 4.5 Upper neck maximum resultant force comparison.



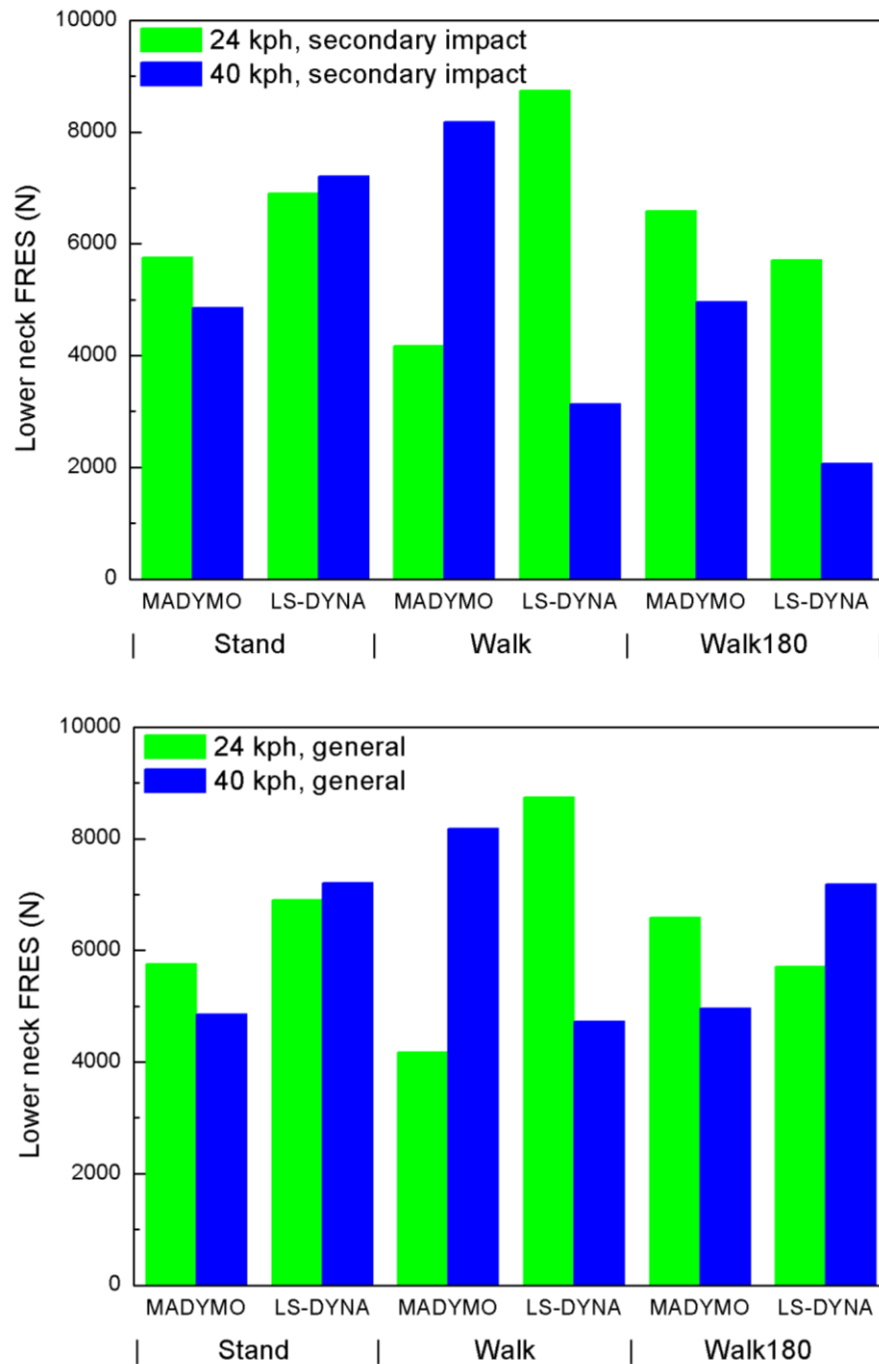
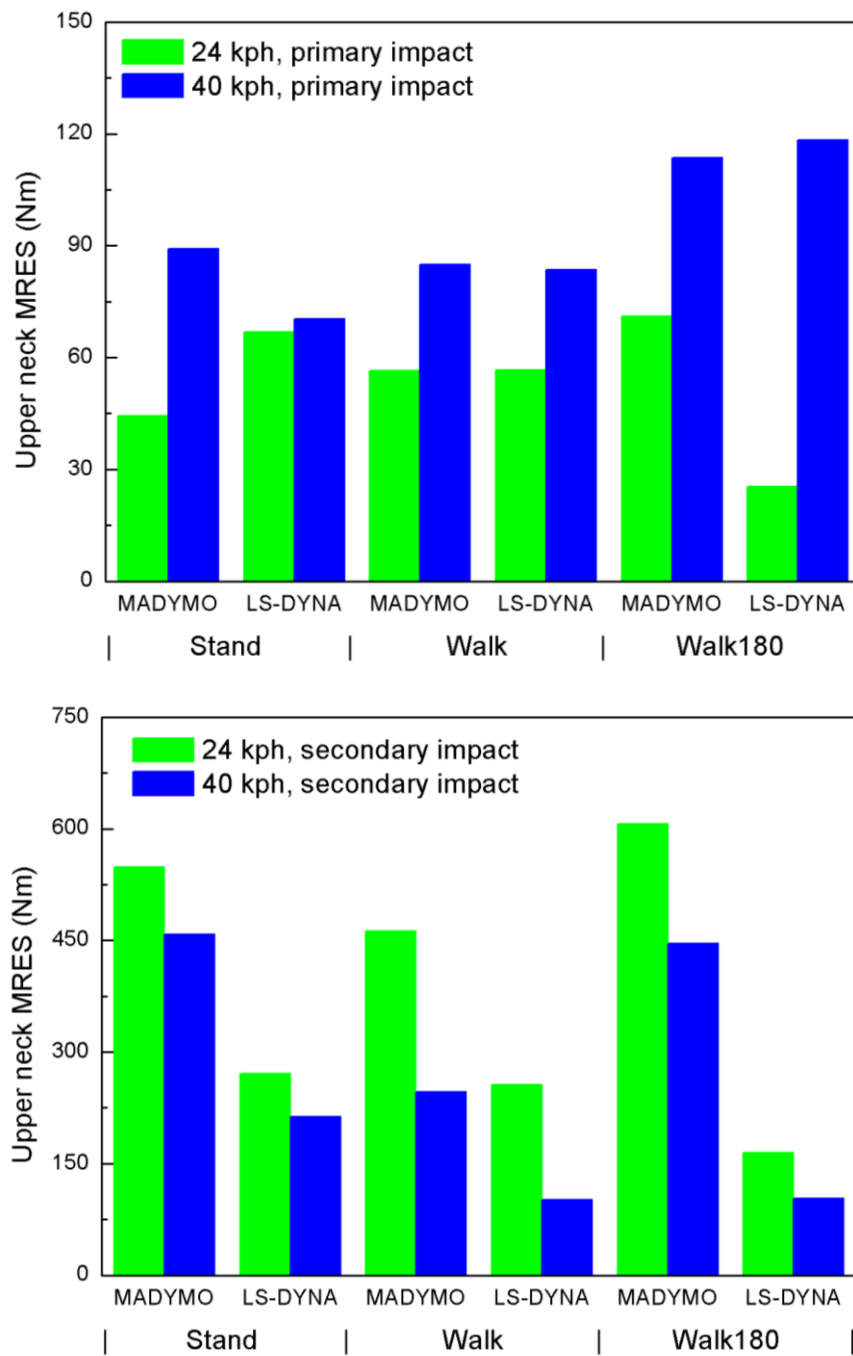


Figure 4.6 Lower neck maximum resultant force comparison.

Maximum upper and lower neck resultant forces are shown in Figure 4.5 and Figure 4.6. In primary impact, similar as head, FE model generally has higher “neck FRES” value. The secondary impact results are complex and disordered.

4.2.4 Neck resultant moment



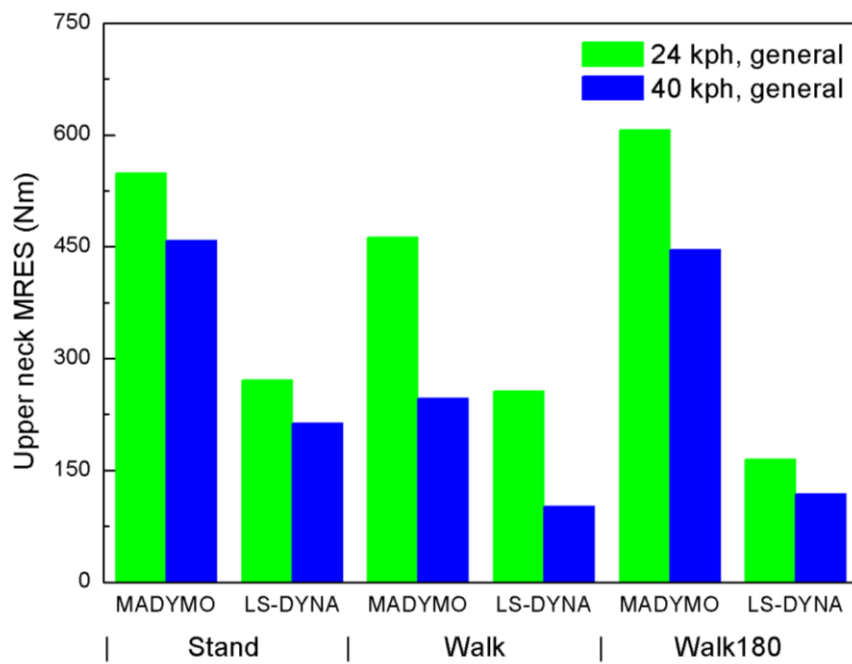
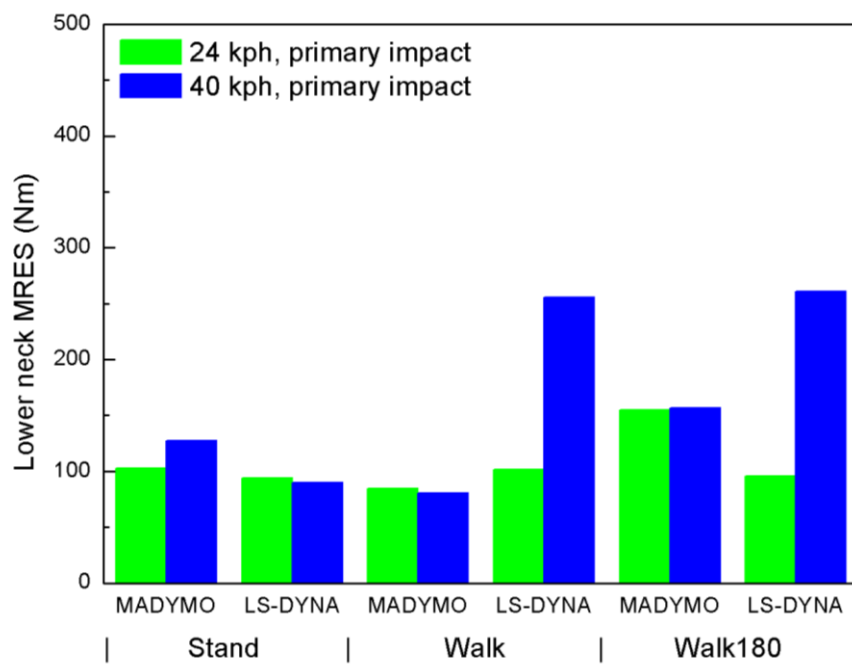


Figure 4.7 Upper neck maximum resultant moment comparison.



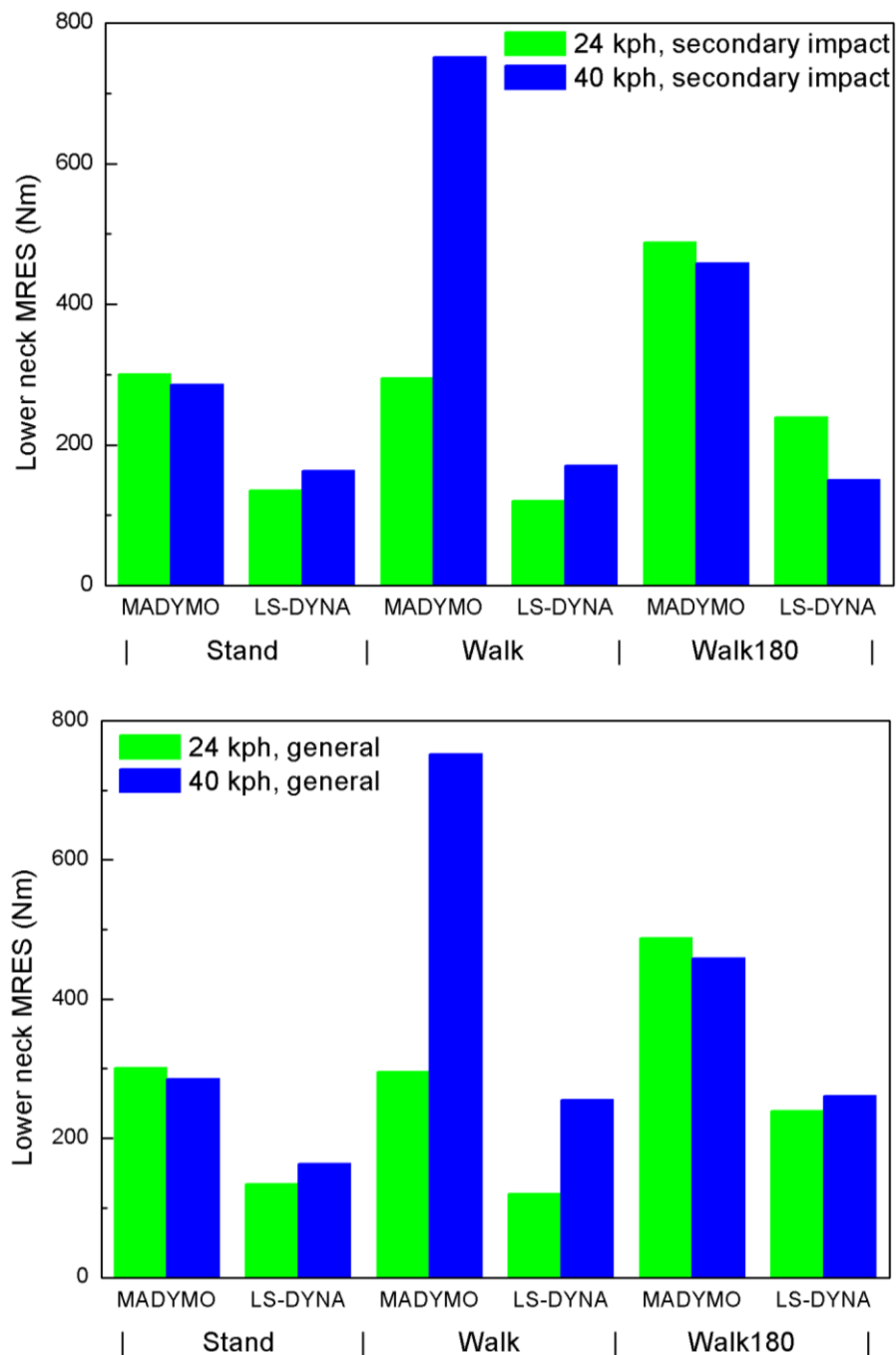


Figure 4.8 Lower neck maximum resultant moment comparison.

Figure 4.7 results show that higher impact speed results in more severe upper neck injury. Instead, lower neck resultant moment appears to be less relevant to impact speed.

As seen in Figure 4.7 and Figure 4.8, FE dummy model has smaller maximum moment in secondary impact compared to MB model. However, for the primary impact, the results vary from situation to situation.

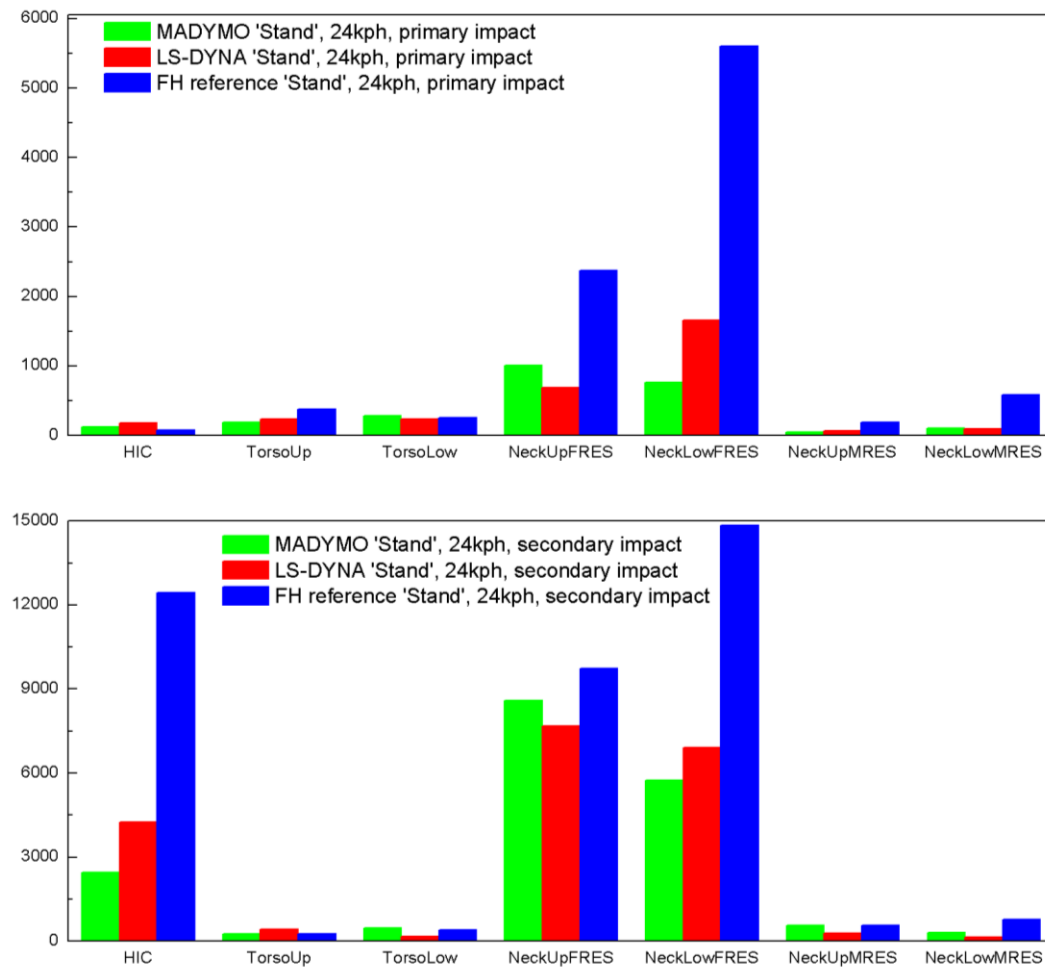
4.3 Comparison of results of reference FH truck and studied truck

The results of injury data from MADYMO and LS-DYNA simulations are compared between reference truck and the truck with spring system. The comparison is still made

through the following data: HIC_{36} , upper and lower torso acceleration, upper and lower neck resultant force, upper and lower neck resultant moment.

In the following diagrams, ‘Reference FH’ stands for the reference truck MADYMO modeled front described in Section 2.1.2. ‘TorsoUp/TorsoLow’ represents upper or lower torso 3ms clip acceleration. ‘NeckUpFRES/NeckLowFRES’ stands for upper or lower neck resultant force while ‘NeckUpMRES/NeckLowMRES’ for upper or lower neck resultant moment. The detailed statistics are shown in Appendix E, Table 9.2 to Table 9.7.

4.3.1 Stand posture with the impact speed of 24kph



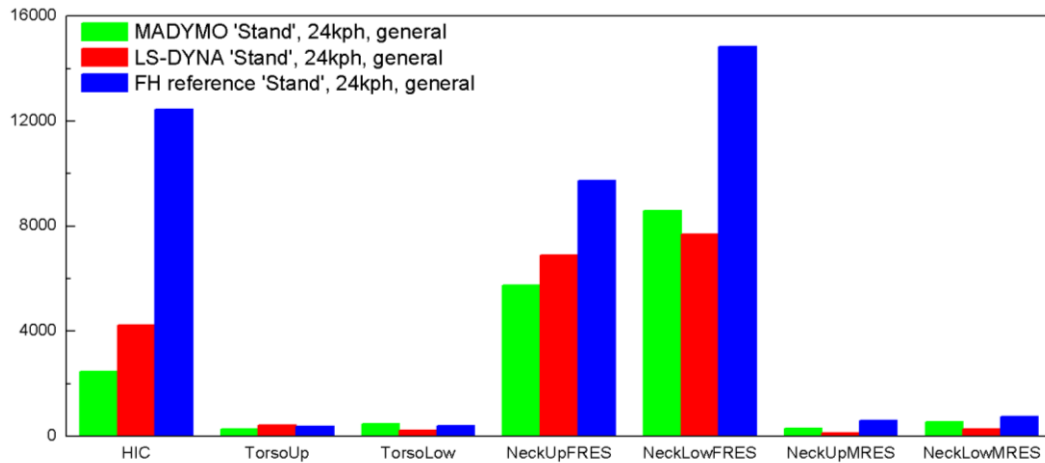


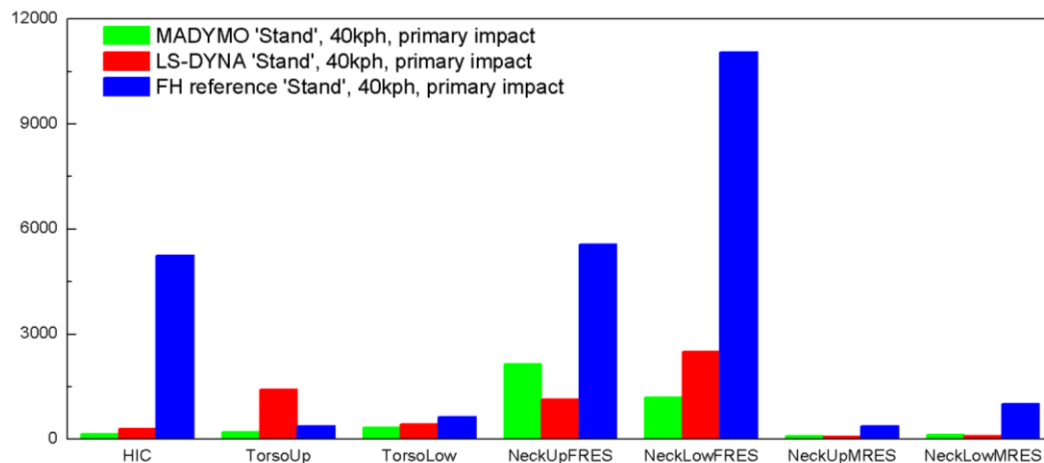
Figure 4.9 Comparison with reference in all aspects with the posture of 'Stand' at impact speed of 24kph.

In this scenario, FH reference model has highest value in most of the injury items except the following labels in Table 4.2.

Table 4.2 Exception items for 'Stand' at 24kph.

MADYMO value > FH reference value	"HIC" in primary impact, "TorsoLow" in primary impact, "TorsoLow" in secondary impact
LS-DYNA value > FH reference value	"HIC" in primary impact, "TorsoUp" in secondary impact

4.3.2 'Stand' posture with the impact speed of 40kph



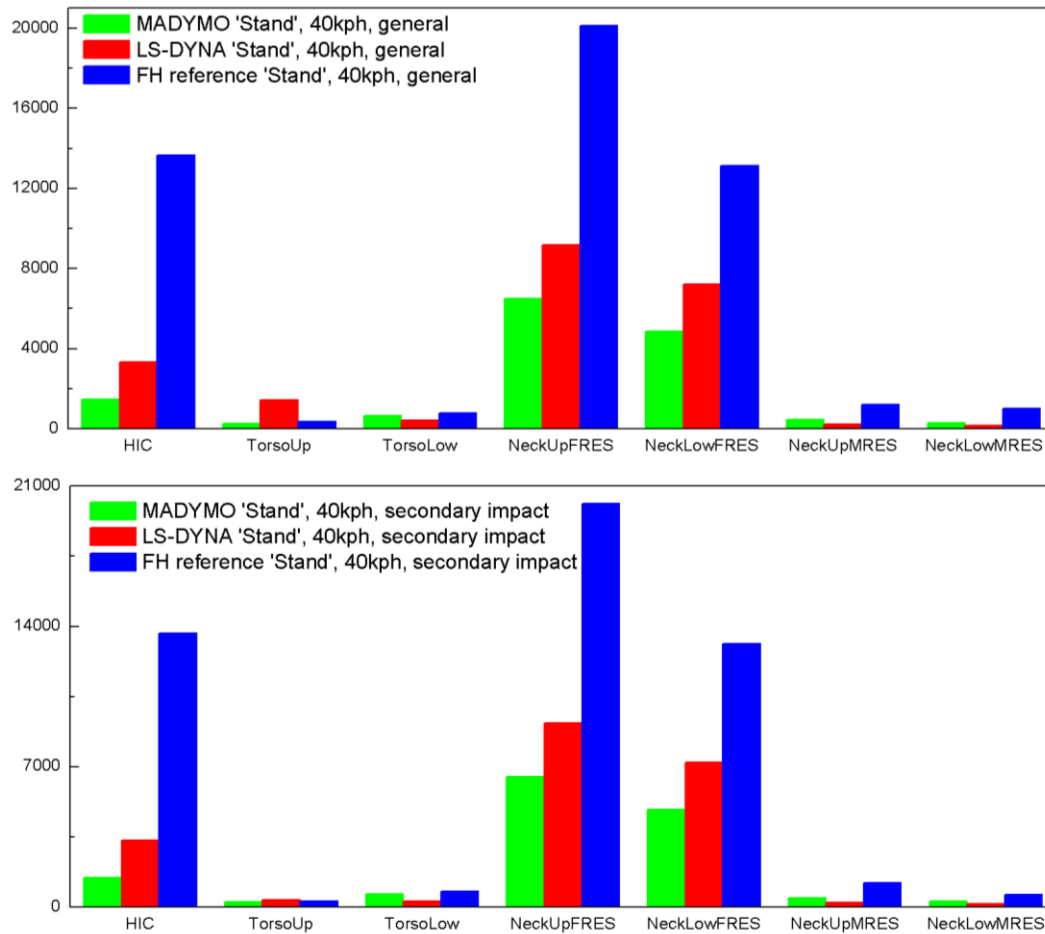


Figure 4.10 Comparison with reference in all aspects with the posture of 'Stand' at impact speed of 40kph.

In this scenario, the reference's results are mostly the largest in all items except the items listed in Table 4.3.

Table 4.3 Exception items for 'Stand' at 40kph.

MADYMO value > FH reference value	None
LS-DYNA value > FH reference value	"TorsoUp" in primary impact, "TorsoUp" in secondary impact

4.3.3 ‘Walk’ posture with the impact speed of 24kph

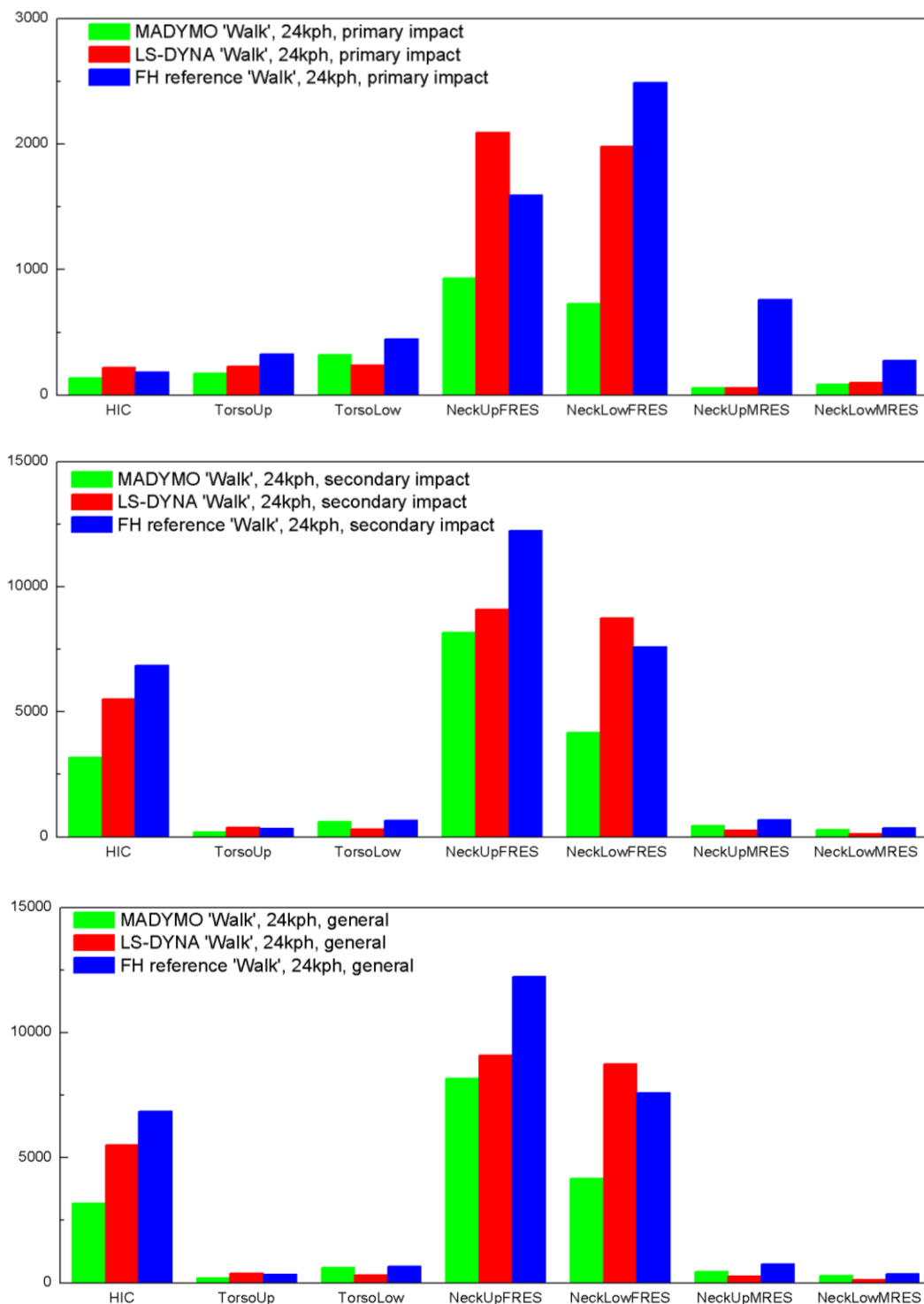


Figure 4.11 Comparison with reference in all aspects with the posture of ‘Walk’ at impact speed of 24kph.

The items that FH reference is not the highest are listed in Table 4.4.

Table 4.4 Exception items for ‘Walk’ at 24kph.

MADYMO value > FH reference value	None
-----------------------------------	------

LS-DYNA value > FH reference value	“HIC” in primary impact, “NeckUpFRES” in primary impact, “TorsoUp” in secondary impact, “NeckLowFRES” in secondary impact
------------------------------------	--

4.3.4 ‘Walk’ posture with the impact speed of 40kph

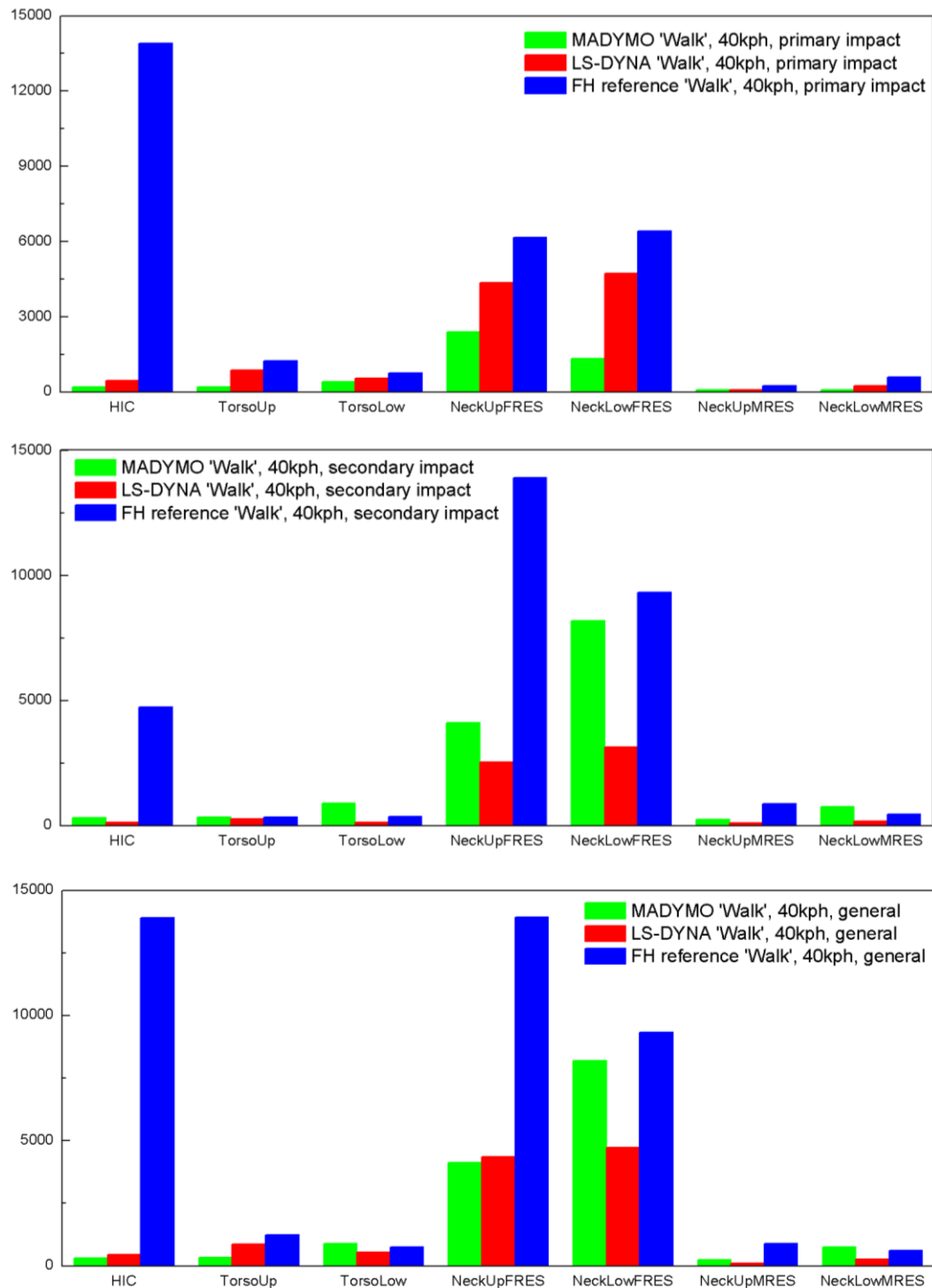


Figure 4.12 Comparison with reference in all aspects with the posture of ‘Walk’ at impact speed of 40kph

As seen in Figure 4.12, “MADYMO” or “LS-DYNA” leads in the comparison sometimes and as listed below.

Table 4.5 Exception items for ‘Walk’ at 40kph.

MADYMO value > FH reference value	“TorsoLow” in secondary impact,
LS-DYNA value > FH reference value	None

4.3.5 ‘Walk 180’ posture with the impact speed of 24kph

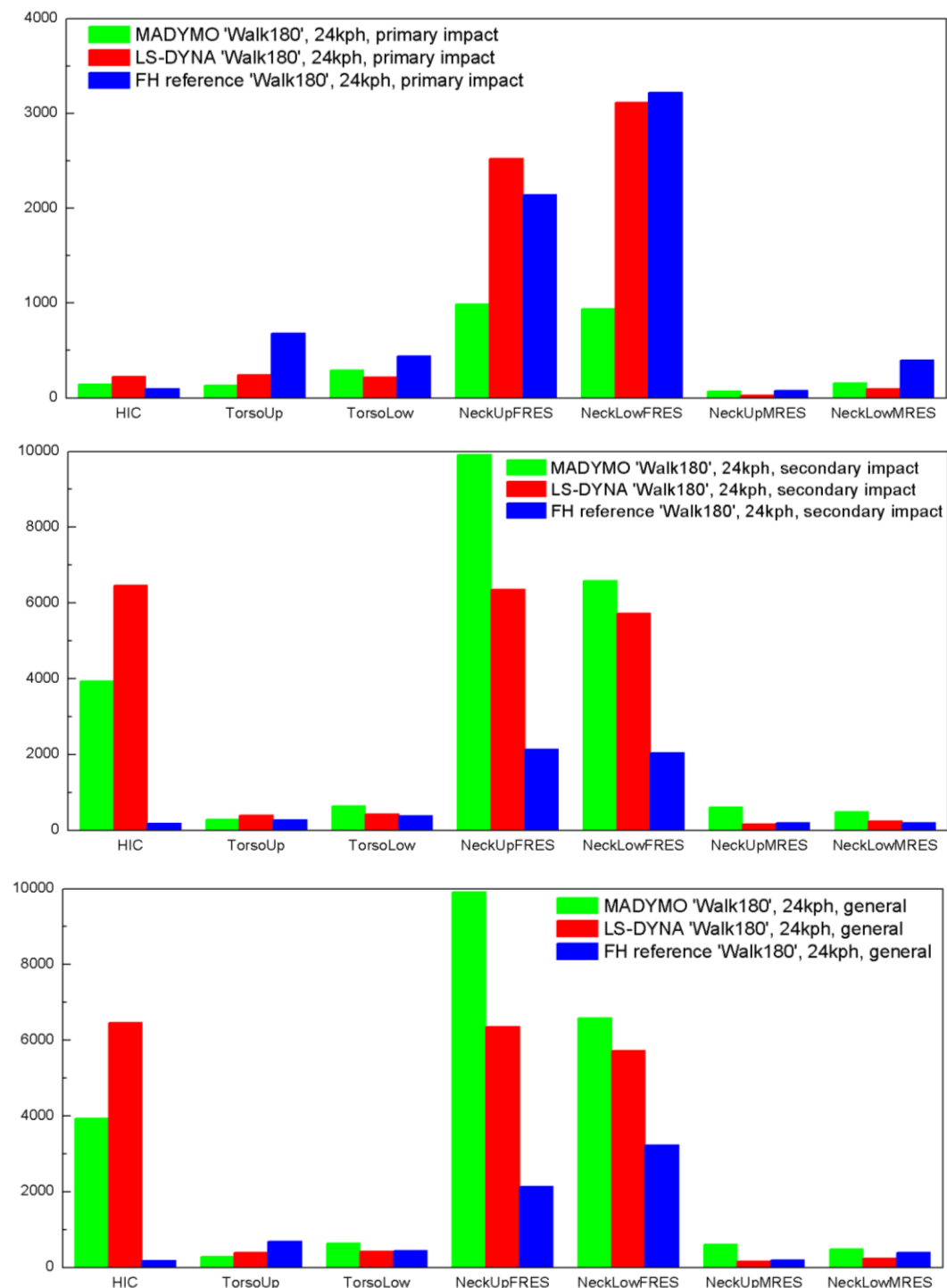


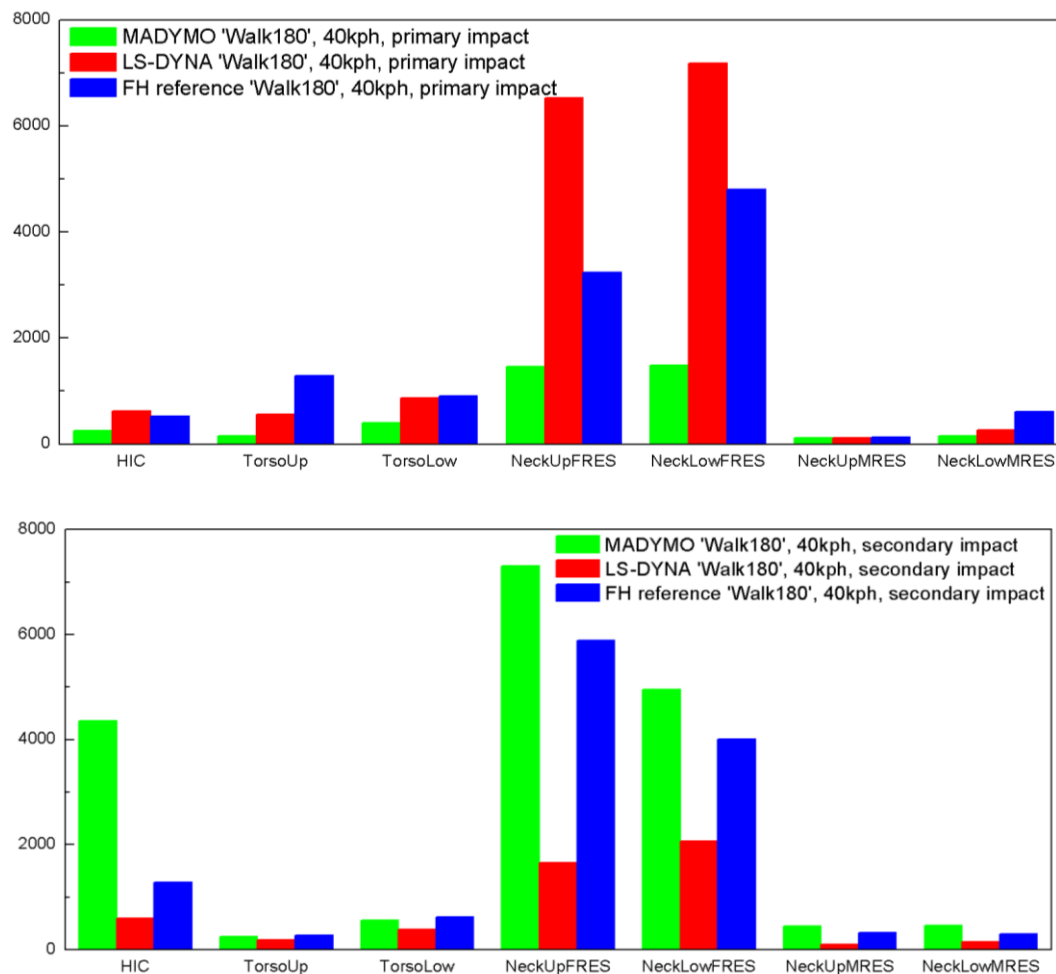
Figure 4.13 Comparison with reference in all aspects with the posture of ‘Walk180’ at impact speed of 24kph.

According to Figure 4.13, the labels where value is larger than corresponding FH reference values are shown in Table 4.6.

Table 4.6 Exception items for 'Walk180' at 24kph.

MADYMO value > FH reference value	"HIC ₃₆ " in primary impact, "HIC ₃₆ " in secondary impact, "TorsoLow" in secondary impact, "NeckUpFRES" in secondary impact, "NeckLowFRES" in secondary impact, "NeckUpMRES" in secondary impact, "NeckLoMFRES" in secondary impact
LS-DYNA value > FH reference value	"HIC ₃₆ " in primary impact, "NeckUpFRES" in primary impact, "HIC ₃₆ " in secondary impact, "TorsoUp" in secondary impact, "TorsoLow" in secondary impact, "NeckUpFRES" in secondary impact, "NeckLowFRES" in secondary impact, "NeckLowMRES" in secondary impact

4.3.6 'Walk 180' posture with the impact speed of 40kph



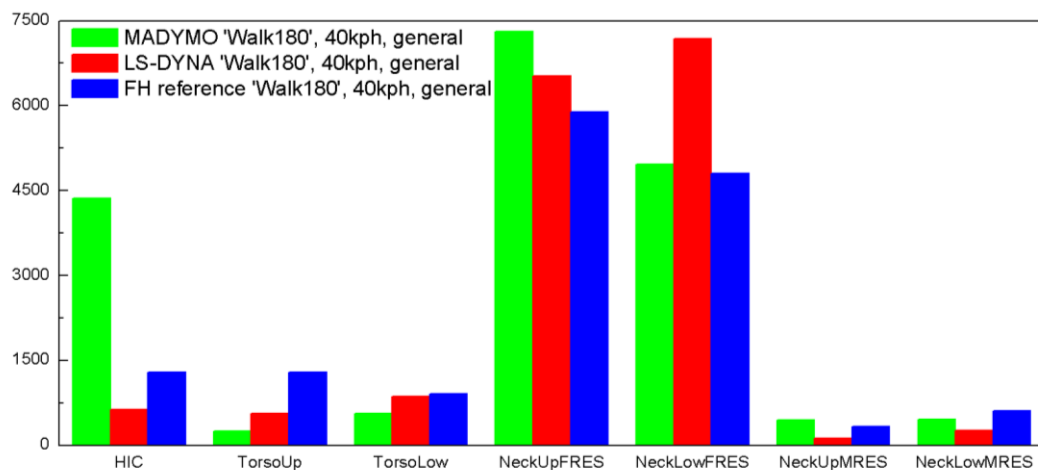


Figure 4.14 Comparison with reference in all aspects with the posture of 'Walk180' and impact speed of 40kph.

There are some aspects that FH reference model does not behave the worst. They are shown in Table 4.7

Table 4.7 Exception items for 'Walk180' at 40kph.

MADYMO value > FH reference value	"HIC" in secondary impact, "NeckUpFRES" in secondary impact, "NeckUpMRES" in secondary impact
LS-DYNA value > FH reference value	"HIC" in primary impact, "NeckUpFRES" in primary impact, "NeckLowFRES" in primary impact,

4.4 Comparison of results of Truck A and trucks with honeycomb.

The value of injury parameters for head, neck and torso injuries are shown in tables below. For all tables in this section, the green background color means the difference of injury value in truck with honeycomb compared to reference injury value in Truck B is in the range of $\pm 20\%$. Similarly, the yellow background represents the range of $\pm 30\%$. The blue background means the value is smaller than the reference value over 30% while the red background means the value is larger than the reference value over 30%.

4.4.1 Head injury

The HIC_{36} values in all simulations within Truck A and trucks with honeycomb are shown in Table 4.2.

Table 4.2 HIC_{36} values of simulations of Truck A and trucks with honeycomb.

HIC ₃₆								
Impact	Primary impact				Secondary impact			
Truck speed	24km/h		40km/h		24km/h		40km/h	
Truck 1	215	4.4%	759	12.9%	213	-77.1%	931	84.0%

Truck 2	200	-2.9%	744	10.7%	822	-11.6%	568	12.3%
Truck 3	202	-1.9%	546	-18.8%	1214	30.5%	1786	253.0%
Truck 4	208	1.0%	728	8.3%	2243	141.2%	2223	339.3%
Truck 5	206	0.0%	728	8.3%	387	-58.4%	1786	253.0%
Truck B	207	0.5%	722	7.4%	460	-50.5%	167	-67.0%
Truck A	206		672		930		506	

In primary impact of both low and high speed scenarios, the HIC₃₆ values of trucks with honeycomb are all close to that of Truck A, within variation value lower than 20%. In secondary impact, the variation of all HIC₃₆ values is large, from -77% to 340%. Only Truck 2's HIC₃₆ values are in green range.

For Truck B, the HIC₃₆ values in primary impact are in green range. However the values in secondary impact are both in blue range, lower than reference value by over 50%.

4.4.2 Neck injury

The magnitude of upper and lower neck's force and moment values in all simulations within Truck A and trucks with honeycomb are shown in Table 4.3 to 4.6.

Table 4.3 Magnitude of neck upper force of simulations of Truck A and trucks with honeycomb.

Magnitude of neck upper force (N)								
Impact	Primary impact				Secondary impact			
Truck speed	24km/h		40km/h		24km/h		40km/h	
Truck 1	1333	5.0%	4452	-24.4%	2081	-65.6%	4654	-23.1%
Truck 2	1245	-2.0%	4888	-16.9%	3283	-45.8%	7892	30.4%
Truck 3	1307	2.9%	4178	-29.0%	5350	-11.7%	3043	-49.7%
Truck 4	1238	-2.5%	5377	-8.6%	3565	-41.1%	4105	-32.1%
Truck 5	1235	-2.8%	4893	-16.9%	2511	-58.5%	4762	-21.3%
Truck B	1396	9.9%	3933	-33.2%	4079	-32.7%	2255	-62.7%
Truck A	1270		5885		6057		6050	

Table 4.4 Magnitude of neck upper moment of simulations of Truck A and trucks with honeycomb.

Magnitude of neck upper moment (N·m)								
Impact	Primary impact				Secondary impact			
Truck speed	24km/h		40km/h		24km/h		40km/h	
Truck 1	60	22.4%	147	-1.3%	57	-36.7%	138	25.5%
Truck 2	33	-32.7%	119	-20.1%	67	-25.6%	107	-2.7%
Truck 3	59	20.4%	62	-58.4%	93	3.3%	54	-50.9%
Truck 4	44	-10.2%	138	-7.4%	67	-25.6%	140	27.3%
Truck 5	47	-4.1%	140	-6.0%	59	-34.4%	170	54.5%
Truck B	42	-14.3%	85	-43.0%	84	-6.7%	54	-50.9%
Truck A	49		149		90		110	

Table 4.5 Magnitude of neck lower force of simulations of Truck A and trucks with honeycomb.

Magnitude of neck lower force (N)								
Impact	Primary impact				Secondary impact			
Truck speed	24km/h		40km/h		24km/h		40km/h	
Truck 1	1631	15.1%	6411	2.2%	2195	-63.9%	4392	-31.5%
Truck 2	1700	20.0%	6608	5.3%	3590	-41.0%	7064	10.2%
Truck 3	1520	7.3%	5315	-15.3%	5451	-10.4%	3591	-44.0%
Truck 4	1503	6.1%	6084	-3.0%	4491	-26.2%	4205	-34.4%
Truck 5	1375	-3.0%	6499	3.6%	2291	-62.4%	4996	-22.0%
Truck B	1700	20.0%	5333	-15.0%	4080	-32.9%	2674	-58.3%
Truck A	1417		6275		6085		6409	

Table 4.6 Magnitude of neck lower moment of simulations of Truck A and trucks with honeycomb.

Magnitude of neck lower moment (N·m)								
Impact	Primary impact				Secondary impact			
Truck speed	24km/h		40km/h		24km/h		40km/h	
Truck 1	90	0.0%	419	19.0%	135	6.3%	160	-4.8%
Truck 2	77	-14.4%	471	33.8%	130	2.4%	183	8.9%
Truck 3	80	-11.1%	168	-52.3%	107	-15.7%	161	-4.2%
Truck 4	91	1.1%	342	-2.8%	135	6.3%	166	-1.2%
Truck 5	90	0.0%	372	5.7%	172	35.4%	207	23.2%
Truck B	66	-26.7%	381	8.2%	156	22.8%	122	-27.4%
Truck A	90		352		127		168	

For primary impact in simulations at 24km/h, most injury parameters' values of all simulations are in green area while two in yellow and one in blue area.

For primary impact in simulations at 11m/s, the variation of values is larger. Although most of the values are in green and yellow range, 4 trucks have one or more values in blue or red range. However, only the neck lower moment of 'Truck 2' is larger than their reference value by over 30%.

For secondary impact in all simulations, most of the values are not in green range, except neck lower moment.

For Truck B, at low speed scenario, the injury parameters' values at primary impact are in green area except the magnitude of neck lower moment in yellow range. When at high speed scenario, the upper neck force and moment's values are in blue range while the lower neck force and moment's values in green range. Over 90% of the injury parameters in secondary impact are not in green range.

4.4.3 Torso injury

The 3ms clip value of upper and lower torso in all simulations within Truck A and trucks with honeycomb are shown in Table 4.7 and 4.8.

Table 4.7 *Ac value of upper torso in simulations of Truck A and trucks with honeycomb.*

Upper torso 3ms clip acceleration, m/s ²								
Impact	Primary impact				Secondary impact			
Truck speed	24km/h		40km/h		24km/h		40km/h	
Truck 1	200	0.5%	1104	3.0%	628	206.3%	581	-21.9%
Truck 2	195	-2.0%	847	-21.0%	594	189.8%	659	-11.4%
Truck 3	187	-6.0%	1048	-2.2%	579	182.4%	188	-74.7%
Truck 4	198	-0.5%	1114	3.9%	928	352.7%	299	-59.8%
Truck 5	205	3.0%	1061	-1.0%	200	-2.4%	453	-39.1%
Truck B	195	-2.0%	897	-16.3%	425	107.3%	219	-70.6%
Truck A	199		1072		205		744	

Table 4.8 *Clip3ms value of torso lower acceleration in simulations of Truck A and trucks with honeycomb.*

Lower torso 3ms clip acceleration, m/s ²								
Impact	Primary impact				Secondary impact			
Truck speed	24km/h		40km/h		24km/h		40km/h	
Truck 1	158	8.2%	932	4.0%	293	4.6%	429	30.0%
Truck 2	175	19.9%	760	-15.2%	297	6.1%	327	-0.9%
Truck 3	163	11.6%	848	-5.4%	313	11.8%	214	-35.2%
Truck 4	146	0.0%	1060	18.3%	328	17.1%	299	-9.4%
Truck 5	160	9.6%	860	-4.0%	149	-46.8%	358	8.5%
Truck B	194	32.9%	789	-11.9%	385	37.5%	199	-39.7%
Truck A	146		896		280		330	

In primary impact of both low and high speed scenarios, most of both torso upper and lower acceleration 3ms clip values are all in green range. However, for secondary impact, over 60% of the simulations with honeycomb's values are not in green range.

For Truck B in primary impact, most of the acceleration values are in green range except the lower torso 3ms clip acceleration value in 24km/h collision 32.9% larger than reference value.

4.4.4 Motion of pedestrian and impact condition for Truck B.

In scenarios at 24km/h, the figures of pedestrian motions and postures at 100ms, 200ms, 500ms, 600ms and 650ms, from primary impact to secondary impact, are shown in Appendix F. Generally, the motions of pedestrian in different scenarios are similar.

In scenarios at 40km/h, the figures of pedestrian motions and postures at 50ms, 100ms, 200ms, 400ms, 500ms and 600ms, from primary impact to secondary impact, are shown in Appendix F. Generally, the motions of pedestrian in different scenarios are different.

5 Discussion

5.1 MADYMO and LS-DYNA pedestrian model injury results

The discussion mainly focuses on the predicted injury in primary impact since the results from primary impact are more comparable. The results from secondary impact are more disordered. This is because compared to primary impact, more factors can influence the secondary impact in this case.

5.1.1 Secondary impact

Secondary impact is related to primary impact. The different kinetic energy and postures of the pedestrian after primary impact can lead to various kinematic behaviors of pedestrians when falling on the ground. These factors make the injury data lack of principal and difficult to predict or explain the phenomenon of secondary impact. Consequently, the comparison of secondary impact between LS-DYNA model and MADYMO model is not discussed in detail in this study.

5.1.2 Primary impact

Generally, the injuries predicted in primary impact of 24kph scenarios are smaller than that in corresponding 40kph scenarios except for the lower neck moment. This is because in 40kph scenarios, the collision causes larger kinetic energy and larger impact force to pedestrian compared to 24kph. Neck lower moment is connected to head and torso, where the influence factors are more complicated.

5.1.2.1 HIC₃₆

Figure 4.2 shows that the head injury of ‘Walk 180’ is largest while ‘Stand’ is lowest in both 24kph and 40kph collisions. The main reason is the deformation of arm caused by different postures.

For example, in 24kph collisions as seen in Figure 5.1, the ‘Stand’ pedestrian has the largest arm deformation while the arm deformation of ‘Walk 180’ posture is the smallest. During the deformation of arm, the kinetic energy of pedestrian’s head increases, resulting in increased velocity of head along truck motion direction. This can reduce the impact speed between truck and head, thus reducing the predicted head injury. Therefore, larger arm deformation leads to lower head injury. As a result, since the arm deformation of ‘Walk 180’ is smallest, the head injury is highest in primary impact. Similarly, the head injury of ‘stand’ pedestrian is lowest. The situation in 40kph collisions is similar.

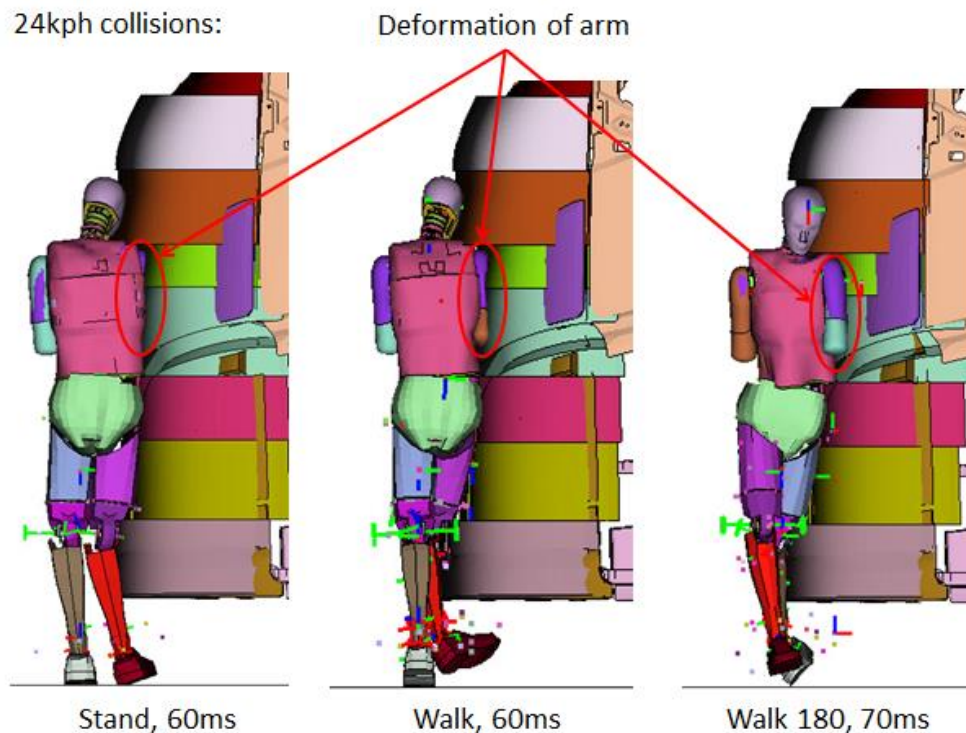


Figure 5.1 Impact behavior comparison of 3 postures at the moment when head acceleration reaches the peak.

In MADYMO simulations, the deformation of arm in FE model is replaced by penetration between arm and truck front plates. Larger penetration of can also cause higher velocity of head along truck motion direction, which reduces the impact speed, result in lower head acceleration. Therefore, the MB ‘Stand’ model has lowest HIC_{36} value while ‘Walk 180’ has highest one.

Figure 4.2 also shows that FE dummy model’s HIC_{36} value is larger than that of corresponding MB model. Different stiffness of neck structure is a potential reason. The different neck structures of FE dummy model and multi-body dummy model are shown as Figure 5.2 and Figure 5.3. The neck structure of MB model is a rigid ellipsoid while that of FE model consists of rubber material. As a result, FE dummy’s neck is able to bend but MB dummy’s neck can only rotate along joints between upper neck and head, lower neck and upper torso.

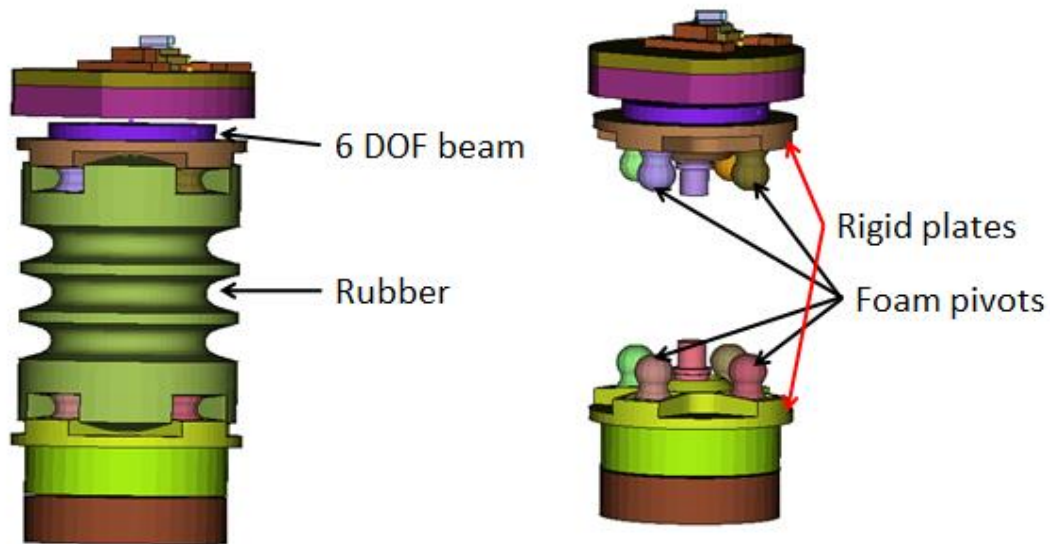


Figure 5.2 Neck structure of FE dummy model

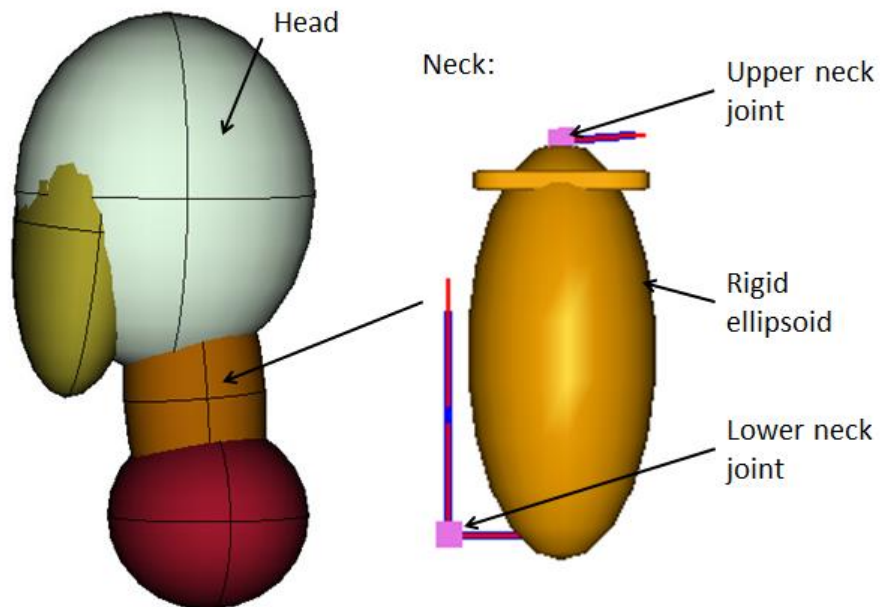


Figure 5.3 Neck structure of multi-body dummy model

For example, in 24kph collisions of ‘Stand’ pedestrian, although two dummy models’ postures are similar as shown in Figure 5.4, the neck of MB model with higher stiffness can provide larger resistance force to head during impact. Since the impact forces between head and truck front (yield stage of load curve) are same in two simulations, the head acceleration of FE model is larger than that of MB model. Other collision scenarios are similar to this case.

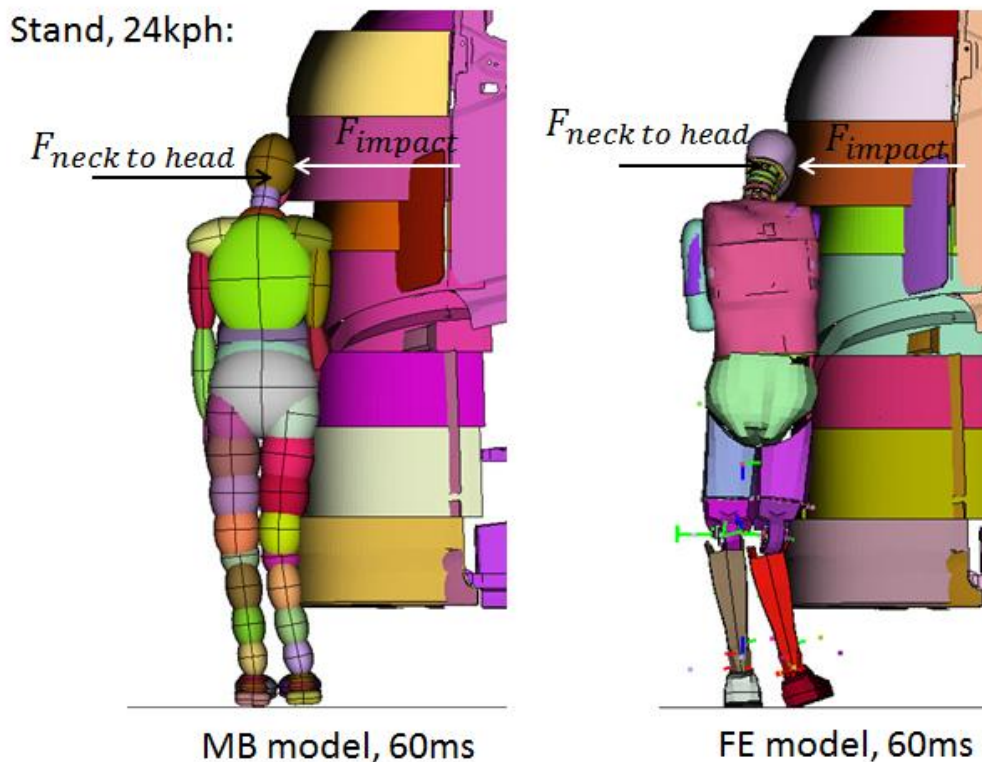


Figure 5.4 Impact behavior comparison of MADYMO and LS-DYNA model at the moment when head acceleration reaches the peak

5.1.2.2 Neck injury

Figure 4.6 shows that the lower neck forces of the FE model are all larger than that of the MB model in same collision scenarios. The main reason is that the FE neck is able to deform while MB neck is rigid as discussed in Section 5.1.1.1.

For example, in ‘Stand’ at 24kph collision scenario, the MB neck is not directly contacted by the truck front plate during the collision because of its rigid property while the FE lower neck is impacted, see Figure 5.5. As a result, the total force on the FE lower neck becomes higher. In other scenarios, the neck impact situations are similar.



Figure 5.5 Neck motion comparison at the moment of peak neck FRES

5.1.2.3 Torso injury

Both upper and lower torso results show that FE models have higher upper and lower torso acceleration than MB models in same scenarios when impact speed is 40kph. However, for the impact speed of 24kph, the data do not show the same tendency.

The potential reason, as seen the example of ‘Stand’ at 40kph impact pattern in Figure 5.6, is the deformable torso having larger deformation in the parts above and under abdomen part, where the acceleration data are collected. This is caused by larger deformation of spring between abdomen and pelvis. The inertia of these two parts is smaller, resulting in higher acceleration of upper and lower torso.

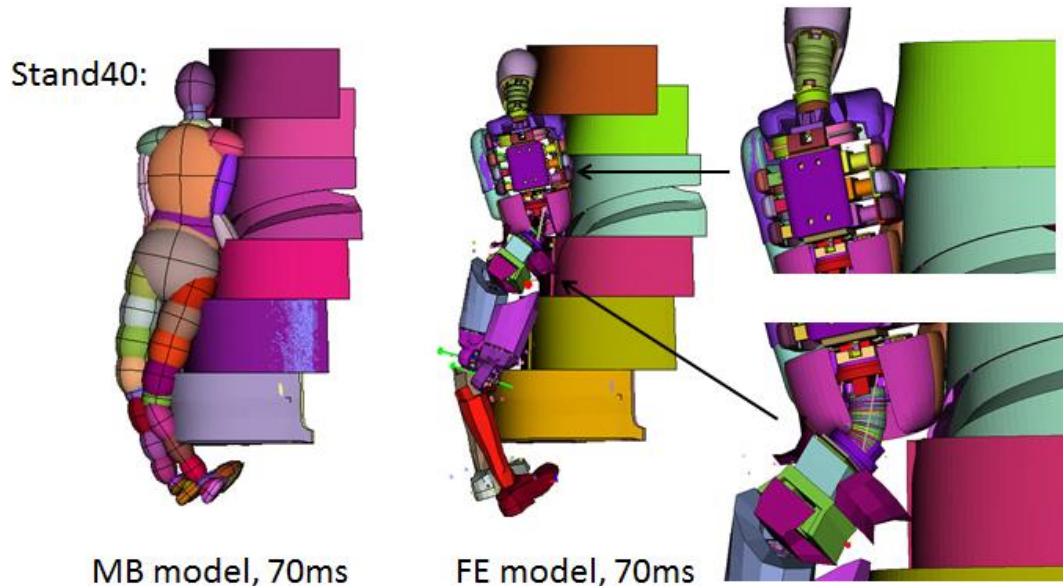


Figure 5.6 Pedestrian model behavior comparison at 70ms

5.2 The performance of mass-spring system

To indicate how effective the mass-spring system is, the ‘improved items’ have to be counted. ‘MADYMO improved items’ and ‘LS-DYNA improved items’ refer to the items in which the FH reference model has the higher value than MADYMO model or LS-DYNA model respectively from Figure 4.8 to Figure 4.14. In additional, only primary and secondary impact are included. Total item number counts the listed items of the primary and secondary impact. ‘MADYMO improved percentage’ and ‘LS-DYNA improved percentage’ is the calculation that corresponding ‘improved item number’ divided by ‘Total item number’. The data are listed in Table 5.1.

Table 5.1 Improved item statistics

Model	MADYMO improved item number	LS-DYNA improved item number	Total item number	MADYMO improved percentage	LS-DYNA improved percentage
Stand at 24kph	11	12	14	78.6%	85.7%
Stand at 40kph	14	12	14	100%	85.7%
Walk at 24kph	14	10	14	100%	71.4%
Walk at 40kph	13	14	14	92.9%	100%
Walk180 at 24kph	7	6	14	50.0%	42.9%
Walk180 at 40kph	11	11	14	78.6%	78.6%
In total	70	65	84	83.3%	77.4%

As shown in Table 5.1, generally 83.3% of MADYMO model's injury data and 77.4% of LS-DYNA model's injury data have been improved by installing the mass-spring system. This is because that compared to reference truck, the mass-spring system absorbs more kinetic energy of human body, reducing the human body acceleration during and after primary impact. Consequently, less impact force can be achieved.

Table 5.1 also shows that the 'improved item number' of each posture in MADYMO and LS-DYNA are close, which proves the similar performance of mass-spring system in both MB and FE simulations.

5.3 The performance of honeycomb structure

5.3.1 Primary impact

As seen in Figure 5.7, in 24km/h collisions, over 95% of upper body injury parameters for trucks with honeycombs are in green and yellow level, except the neck upper force value in Truck 2 case and torso lower acceleration Clip3ms value in Truck B case. In addition, 38(90%) of the total 42 values are in green range. Therefore, the honeycomb performs well in low speed collisions.

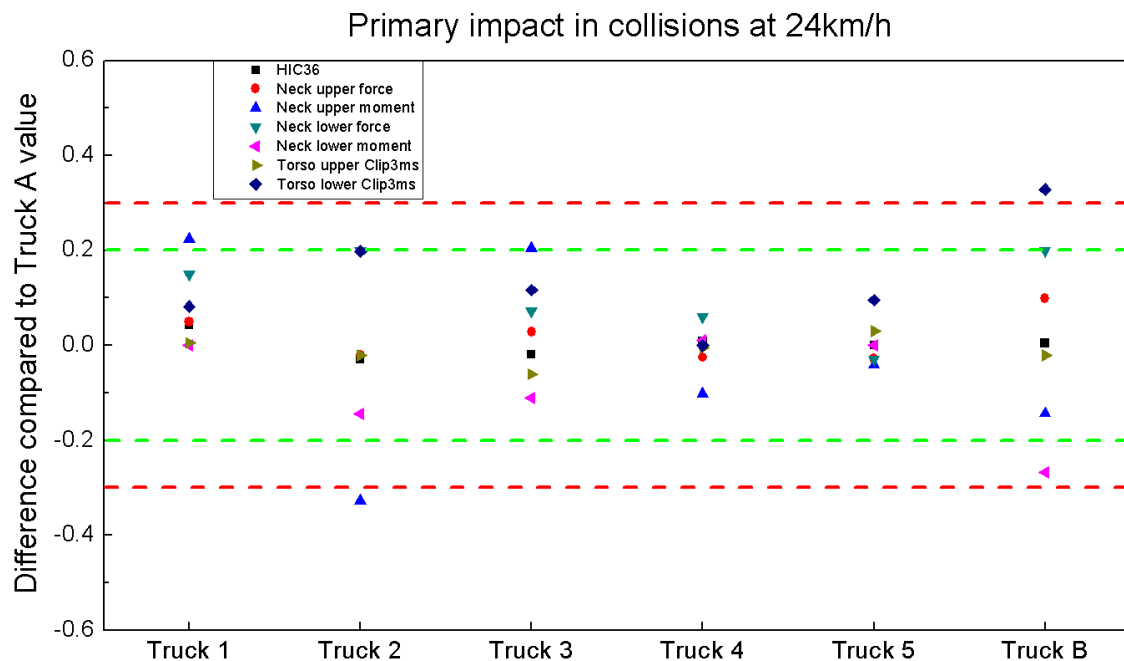


Figure 5.7 The injury result of primary impact in 24kph collisions.

As seen in Figure 5.8, when at high speed collision, 88% of 42 injury values are in green or yellow range and 81% of them are in green range. Specifically, for Truck 4 and Truck 5, all values are in green range. The big difference happens in terms of neck injury parameters.

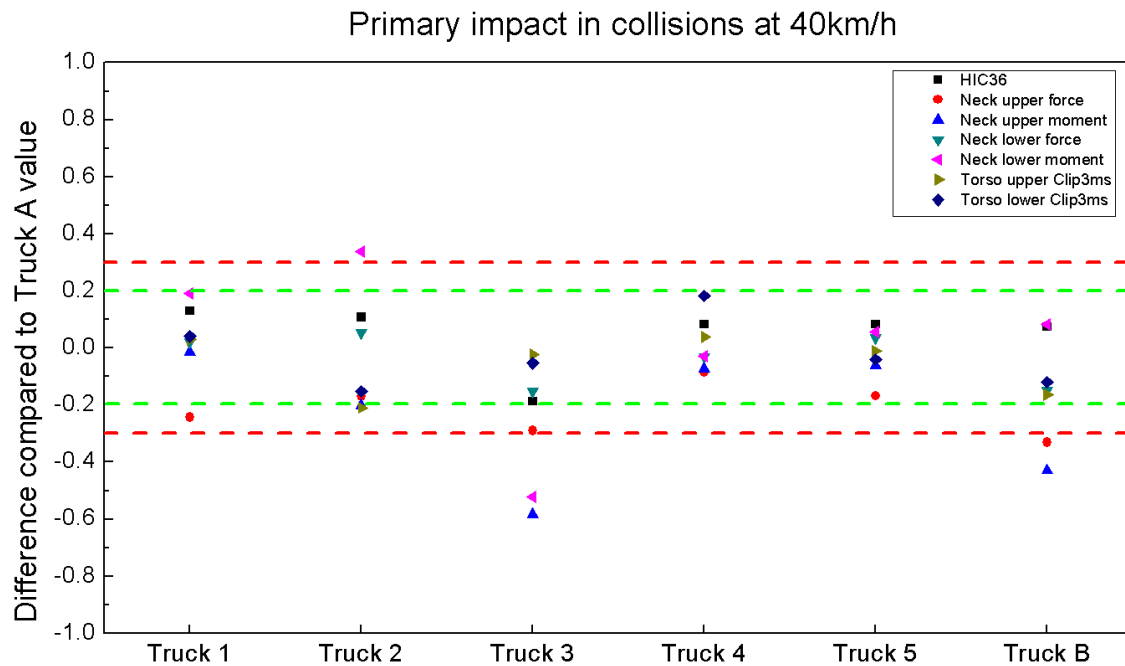


Figure 5.8 The injury result of primary impact in 40kph collisions.

One of the main reasons of this result is the influence of strain rate of honeycomb on resistance force. The selected thickness is based on the bench test at 0.35m/s. However, if the impact speed of bench test mentioned in Section 3.5.2 is changed from 0.35m/s to 11m/s, the resistance force of honeycomb become larger. For example, the result of 'Lid lower 1' honeycomb shown in Figure 5.9 shows that the resistance force at 11m/s condition becomes 250% higher than original force level.

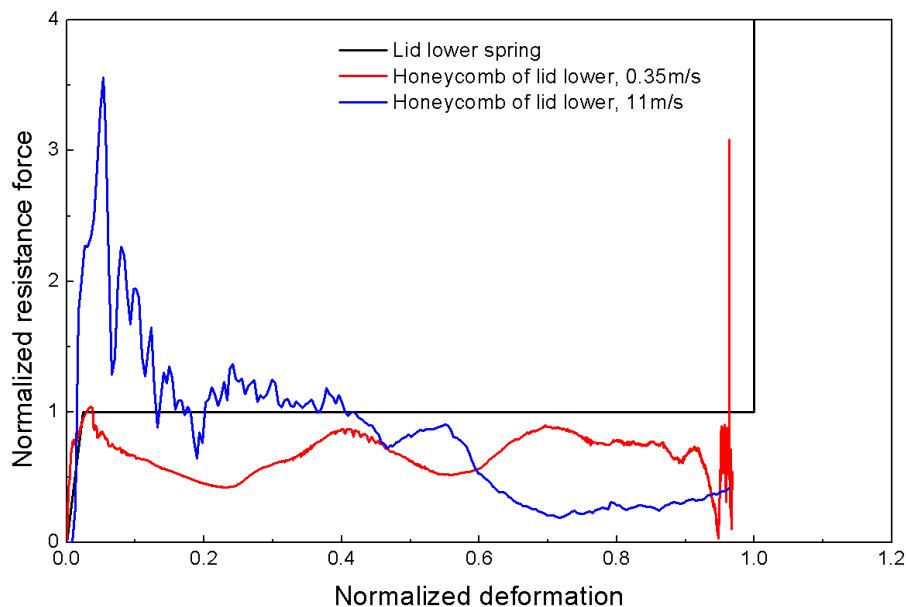


Figure 5.9 Dynamic effect on Lid lower 1 honeycomb's normalized resistance force versus normalized deformation.

Another import factor is that the honeycomb's bottom out length is smaller than its total length. For instance, as seen in Figure 5.9, the real bottom out length in bench test is around 96% of the spring's bottom out length. This may cause easier to reach large bottom out force.

At low speed condition, these two factors' influence is not large, thus the primary impact is still close. However, in high speed collisions, the larger force may cause more severe pedestrian's injury.

5.3.1.1 Primary impact of Truck 1

At 11m/s, specifically for Truck 1, the contact force between head and 'Lid mid 1' becomes larger, resulting in around 13% higher HIC_{36} value. This force also enlarges the moment of pedestrian body, thus increasing the torso upper and lower acceleration, which causing higher torso upper and lower injury, as seen in Figure 5.10.

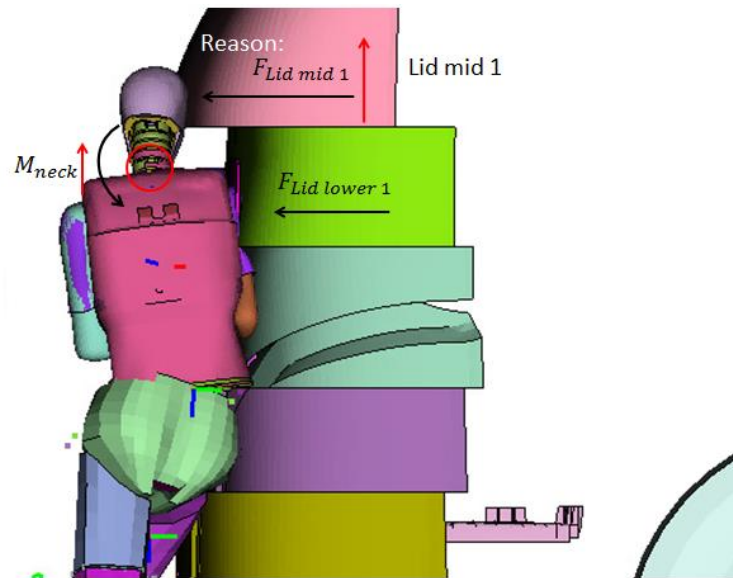


Figure 5.10 Truck 1 collision in 11m/s collision.

5.3.1.2 Primary impact of Truck 2

For Truck 2 collision at 11m/s, the neck lower moment is 33.8% higher than the reference value and both Truck 2 and Truck A get largest neck lower moment at around 60ms. This because that the contact force between shoulder and 'Lid lower 1' becomes larger and this causes larger bending moment for neck lower part as seen in Figure 5.11. This also causes larger head impact force which is supported by HIC_{36} increases by 10.7%.

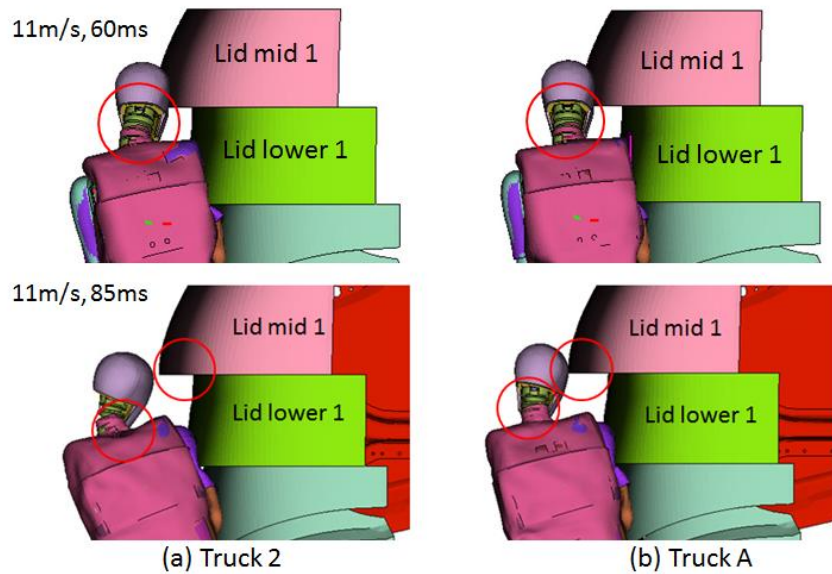


Figure 5.11 Truck 2 and Truck A collisions at 60ms and 85ms in 11m/s collision.

5.3.1.3 Primary impact of Truck 3

For Truck 3 collision at 11m/s, the data show that the all injury parameters of head and neck injury decrease by over 15%. The reason is that the 'Grille upper 1' impact force on torso part becomes larger but for the whole body, the bending moment becomes smaller as seen in Figure 5.12. Therefore, the impact force of 'Lid mid 1' and 'Lid lower 1' become smaller, resulting in lower head and neck injury.

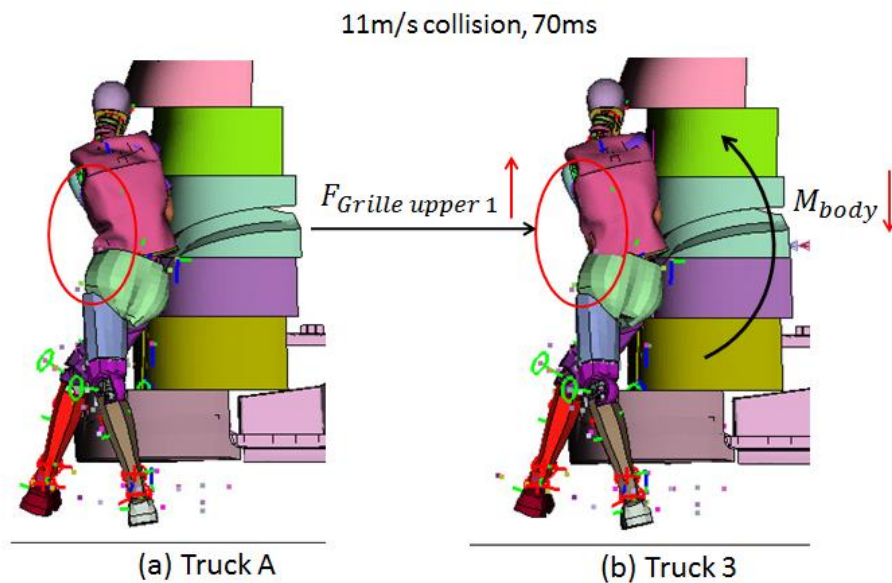


Figure 5.12 Truck 3 and Truck A collisions at 70ms in 11m/s collision.

5.3.1.4 Primary impact of Truck 4

For Truck 4, since 'Grille lower 1' impacts on pelvis part, which causes larger torso lower acceleration.

5.3.1.5 Primary impact of Truck 5

For Truck 5, since 'Bumper upper 1' impacts on right leg, the difference mainly happens in lower body, which causes relatively small difference to upper body

5.3.1.6 Primary impact of Truck B

For Truck B, since 5 springs are all replaced by honeycombs, the united influence can be complicated. Generally, all contact parts' stiffness becomes larger and this may balance the difference. This is supported by the injury result, most in green and yellow range and only two neck upper values in blue range. The reason is that the 'Grille upper 1' parts have the major influence on Truck B's performance. Similar to Truck 3 collision, the increased impact force of 'Grille upper 1' reduces the moment of pedestrian body, thus reducing the neck injury. As for head injury, since it is mainly related to 'Lid mid 1' part, the head injury still increases by 7.4%, which is acceptable.

5.3.2 Secondary impact

For secondary impact, in both low and high speed collisions, few injury parameters are in green or yellow level, as seen in Figure 5.13 and 5.14.

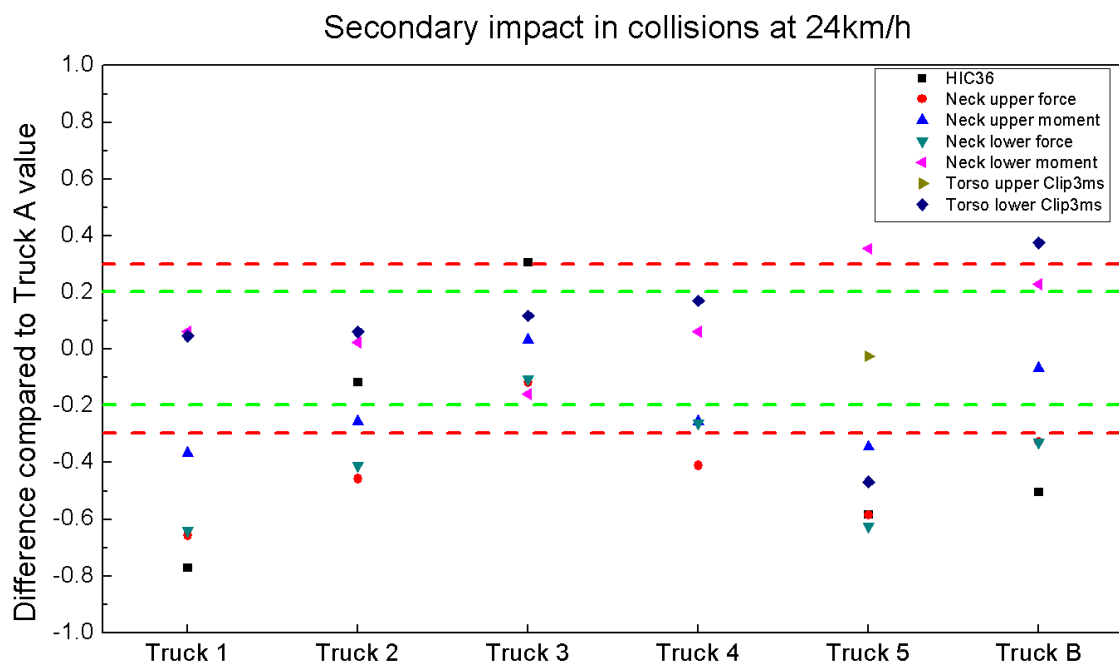


Figure 5.13 The injury result of secondary impact in 24kph collisions.

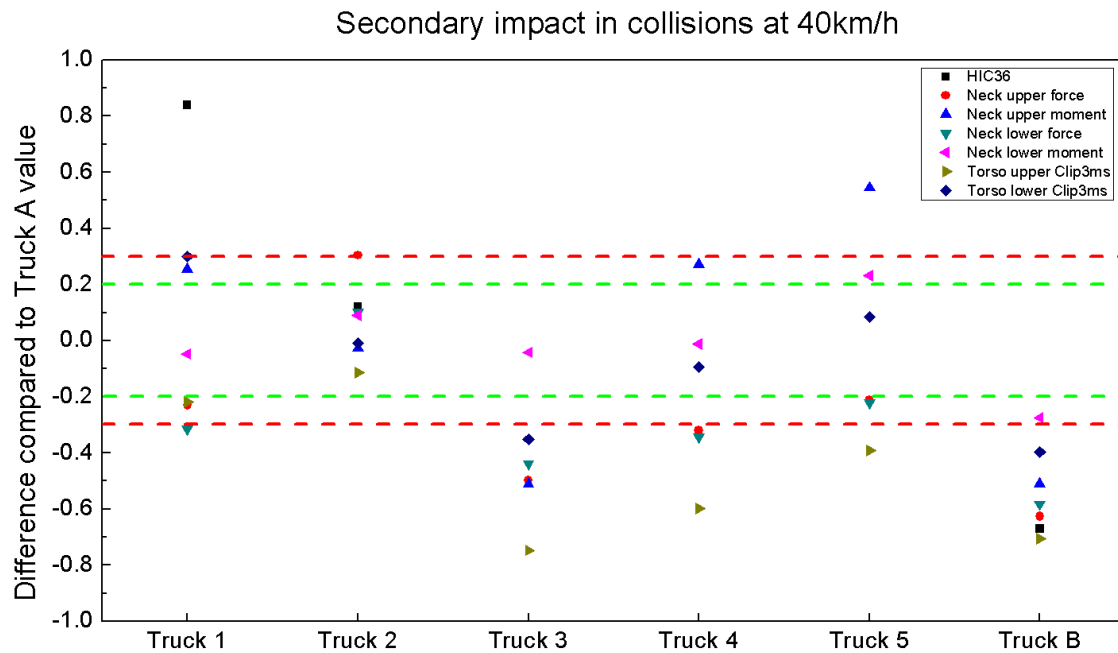


Figure 5.14 The injury result of secondary impact in 40kph collisions.

The secondary injury is mainly related to the motion of pedestrian. Small change can result in big difference of pedestrian motion although the motion in primary impact is similar.

5.3.2.1 Secondary impact in 24kph scenario

Generally, the motion of pedestrian in 7 scenarios are similar, all facing to ground as seen in Appendix F. However, the contact parts, the kinetic energy of pedestrian et al. can influence the injury to a large extent.

For example, for Truck B, the primary impact is similar in terms of injury level and motion of pedestrian compared to Truck A collision. However, in secondary impact, for truck A, the first contact part of upper body is head at 620ms, while in Truck B collision left arm at 595ms followed by the head impacting to ground at 605ms, see Figure 5.15 to 5.17. The left arm's deformation can absorb energy, which reduces the injury of head and upper neck. The impact force from left arm could transfer to torso part, resulting in higher upper and lower torso compared to Truck A collision.

The pedestrian posture and motion in secondary impact in all collisions are different. Hence, the difference between most of the secondary impact injury parameters and corresponding reference values are out of acceptable range.

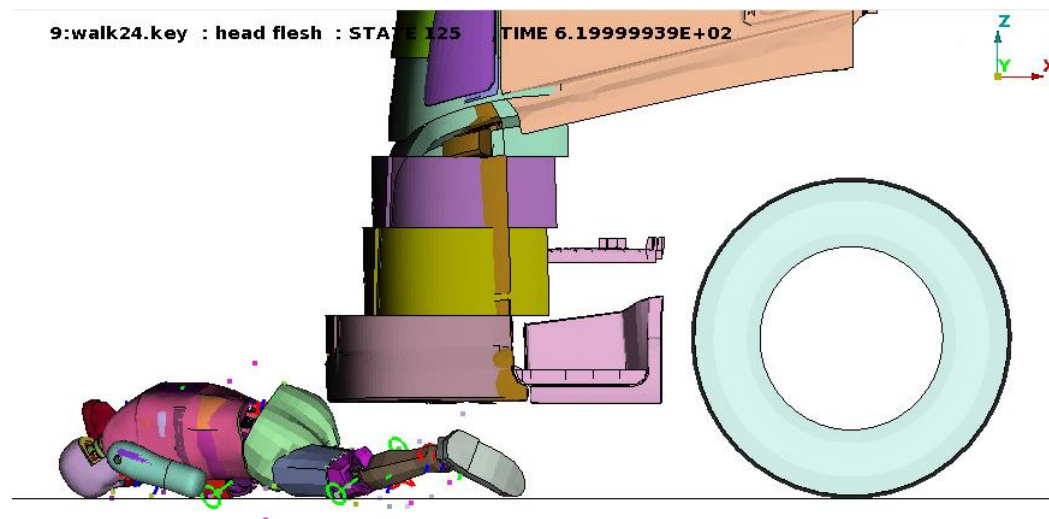


Figure 5.15 The collision scenario at 620ms in Truck A, 24kph collision.

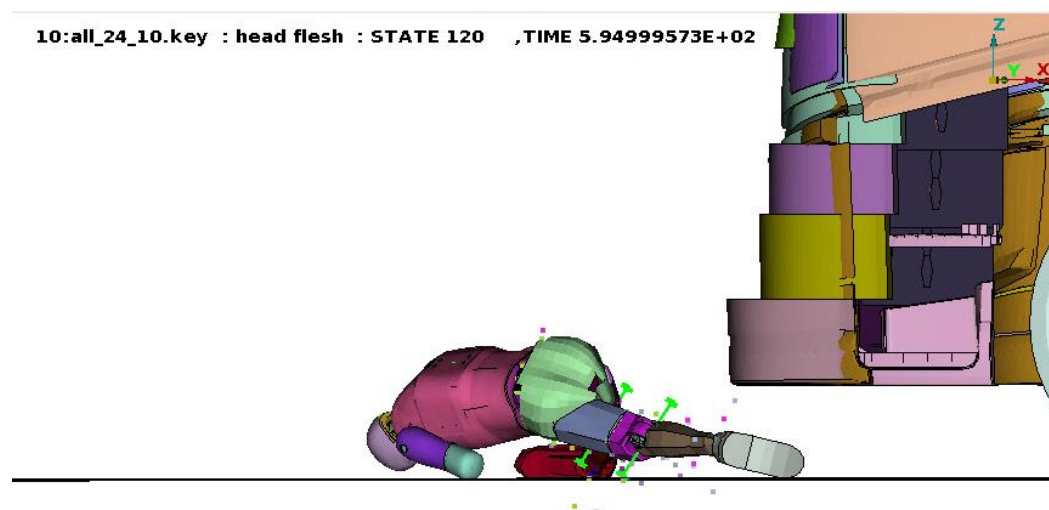


Figure 5.16 The collision scenario at 595ms of Truck B, 24kph collision.

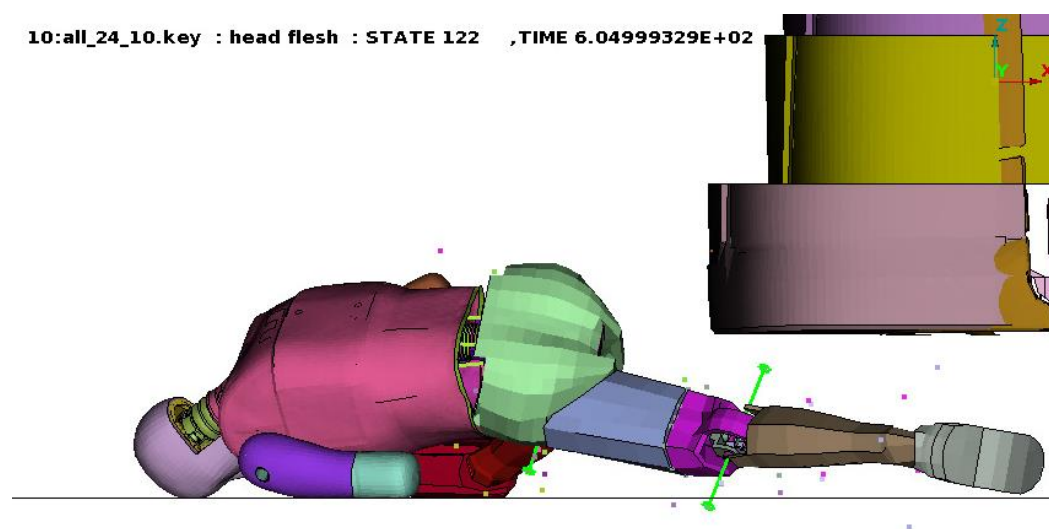


Figure 5.17 The collision scenario at 605ms of Truck B, 24kph collision.

5.3.2.2 Secondary impact in 40kph scenario

Compare to 24kph collisions, the 40kph collisions are less similar to reference collision. This is mainly because the similarity of primary impact is worse than in that of 24kph collisions as discussed in Section 5.3.1. The secondary impact condition, including contact parts, impact speed, etc. could explain the difference of some injury parameters.

For example, the upper body injury level in Truck B is much lower than that in reference Truck A collision. The reason is similar, in Truck B collision, the right arm and pelvis first impact on the ground at 505ms and after 55ms, the head impacts on the ground as seen in Figure 5.18 and 5.19. The deformation of arm, torso and pelvis in this 55ms duration can absorb large amount of kinetic energy, result in lower injury level of head and neck. The situation in Truck A collision is different as seen in Figure 5.20 and 5.21, although some energy is absorbed by pelvis, the back impacts on ground, causing high upper torso injury and neck lower bending moment, which increases head and neck injury.

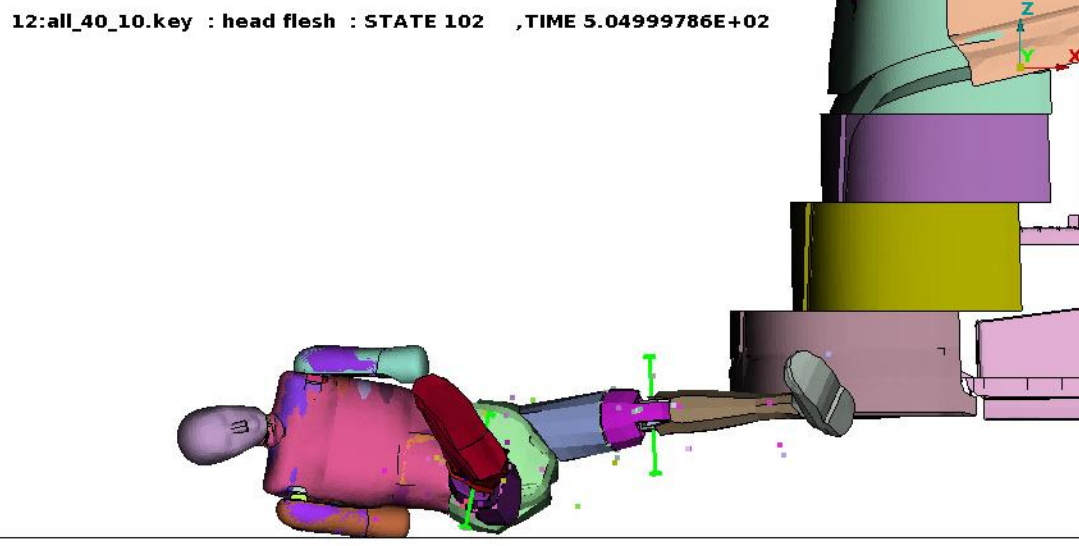


Figure 5.18 The collision scenario at 505ms of Truck B, 40kph collision.

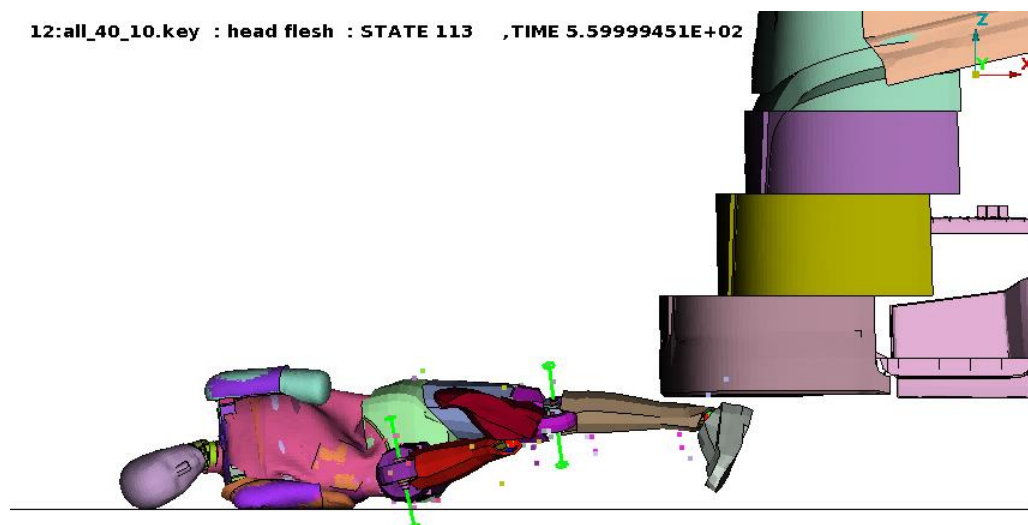


Figure 5.19 The collision scenario at 560ms of Truck B, 40kph collision.

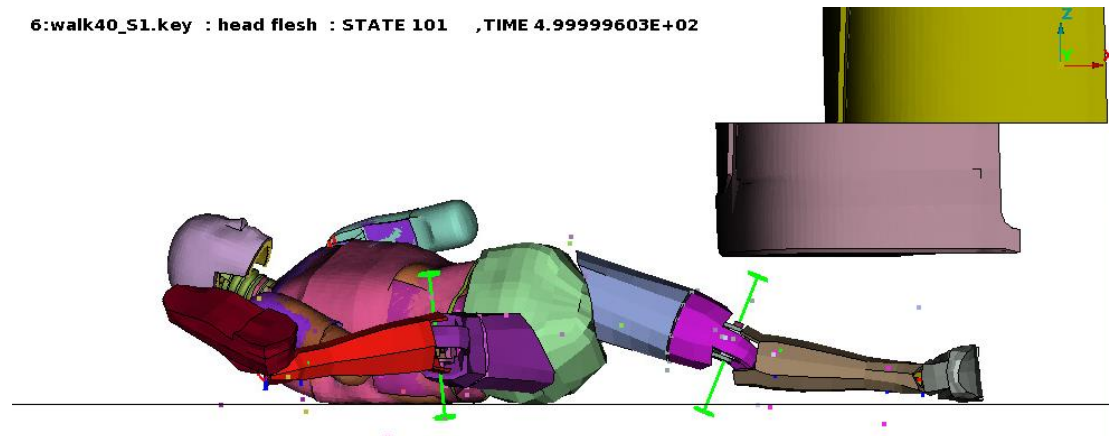


Figure 5.20 The collision scenario at 500ms of Truck A, 40kph collision.

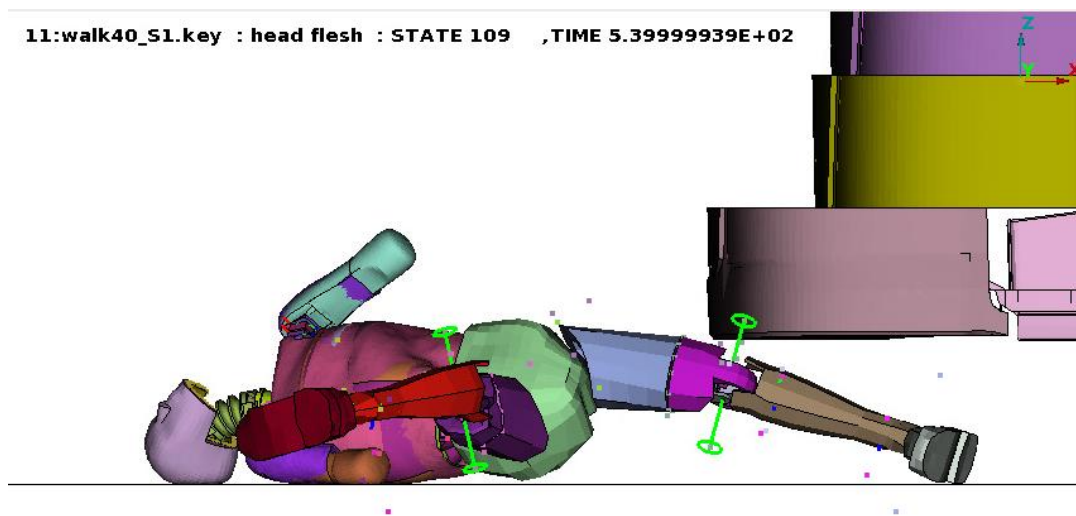


Figure 5.21 The collision scenario at 540ms of Truck A, 40kph collision.

5.4 Limitation of the work

5.4.1 Lack of pedestrian models in different sizes

In this study, only 50th percentile male pedestrian model was studied. Different situation or result may occur in collisions between this truck front and other pedestrians of different sizes, such as 6-year child, 5th percentile female model, etc.

5.4.2 Lack of collision scenarios

In this study, only 3 side impact postures were studied. More postures including front impact postures may need to be further studied.

In addition, the moving speed of truck used in this study is 24km/h and 40km/h and more speed may need to be studied in the future. Lack of lower body injury

In this study, only upper body injury, including head, neck and torso injury have been studied. The lack of lower body injury may limit the accuracy of human body injury analysis.

5.4.3 Lack of secondary impact analysis

Among the injury results, secondary impact data are disordered to be analyzed. To deal with this problem, new feasible method needs to be developed and more statistics should be collected.

5.4.4 Difficulty to create the same impact scenarios

To compare with and verify the MADYMO results, the same impact scenarios have to be reproduced in LS-DYNA simulations. However, due to different dummy models, it is impossible to recreate exactly the same positions or postures. In this study, the scenarios are fairly similar but still, differences exist. The distinctiveness of LS-DYNA model itself may also lead to different results.

6 Conclusion

6.1 The similarities and difference between MADYMO and LSDYNA pedestrian model

The deformable neck of FE 50th percentile male pedestrian may cause larger head and neck injury. The deformable arm is able to absorb energy and potential to reduce the head injury during side impact conditions. The spring between abdomen and pelvis may cause large deformation or movement of abdomen and pelvis, thus increasing upper and lower torso injury.

6.2 The performance of mass-spring system

Generally, the mass-spring system is verified to have significant effect on reducing upper body injury. Over 75% of the injury items are improved after installing this mass-spring system in FE study. Therefore, it is worth to implement it in future truck front concept design.

Although the ideal mass-spring system is not the realistic product solution, the study of it could help understand the target values on stiffness, shape, etc. on the future physical deformable structure.

6.3 The performance of honeycomb B

The designed 5 honeycombs perform well in primary impact of both low and high impact speed collisions. 90% of values in low speed collision and 81% in high speed collision have absolute difference value smaller than 20% compared to reference value. The main reason why it performs worse in high speed collision is the effect of strain rates (impact speed). With larger impact speed, the resistance force of honeycomb becomes larger than demanded yield force.

Most of the injury predicted in secondary impact is out of acceptable range (the difference is larger than 30%). This is because the secondary impact is related to primary impact in large content. The small difference in primary injury can result in different pedestrian motion speed and direction, resulting in different injury.

7 Future work

7.1 Validation of spring system

More postures including front impact postures may need to be further studied since only 3 side impact postures were studied in this study. More moving speed of truck may also need to be studied in the future.

In addition, other pedestrian models of difference sizes, such as 6-year child, 5th percentile female model, etc. needs to be further studied to validate this spring system's performance.

The concern of lower body injury and the condition of run-over, as well as more scientific injury criteria also need to be considered in the future work to make a more scientific injury comparison.

7.2 Honeycomb and truck front surface development

More material and structure of honeycomb can be studied to make a better design of honeycomb, including reducing the sensitivity to impact speed.

In the reality, the truck front is deformable. Therefore, different impact position of truck front will cause different injury result. To solve this, more honeycombs or other energy absorption structure needs to be developed and located behind the deformable front surface to make the force distribution evenly. In this way, the influence of impact position can be reduced so that the structure is able to fit more impact scenarios. Some structure such as cladding sheet can be used to distribute impact force.

Also, the consideration of air flow for air drag or cooling demand can be achieved by change the front surface structure since the honeycomb structure is able to induct the air flow. The position of honeycomb can be modified to create better air flow. A balance between safety performance and other demand can be achieved.

In this way, a feasible concept truck front design based on honeycombs can be developed.

References

- European Commission (2016). Traffic Safety Basic Facts 2016 Report – Pedestrians. Available at: https://ec.europa.eu/transport/road_safety/sites/roadsafety/files/pdf/statistics/dacota/bfs2016_pedestrians.pdf. Accessed: 2017-05-01
- European Commission (2016). Traffic Safety Basic Facts 2016 Report - Heavy Goods Vehicles and Buses. Available at: http://ec.europa.eu/transport/road_safety/sites/roadsafety/files/pdf/statistics/dacota/bfs2016_hgvs.pdf. Accessed: 2017-05-01
- Almqvist, C. J., & Heinig, K. (2013). European Accident Research and Safety Report 2013. *Volvo Trucks*.
- Mesina, C. T., & Margaritis, D. (2005). Characteristics of Heavy Trucks versus Pedestrians and/or Cyclists. Deliverable D8.3.5 from *APROSYS SP 8.3 (AP-SP83-D835)*.
- Puthan, P., Fredriksson, R., Thorn, S., & Törnvall, F. (2016). Real World Accident Analysis of Truck Front Impact to Pedestrians. In *IRCOBI Conference Proceedings*.
- Gandhi, T., & Trivedi, M. M. (2007). Pedestrian protection systems: Issues, survey, and challenges. *IEEE Transactions on Intelligent Transportation Systems*, 8(3), 413-430.
- Chawla, A., Mohan, D., Sharma, V., & Kajzer, J. (2000). Safer truck front design for pedestrian impacts. *Journal of Crush Prevention and Injury Control*, 2(1), 33-43.
- Feist, F., Gugler, J., Arregui-Dalmases, C., Del Pozo de Dios, E., Lopez-Valdes, F., Deck, D., & Willinger, R. (2009). Pedestrian collisions with flat-fronted vehicles: injury patterns and importance of rotational accelerations as a predictor for traumatic brain injury (TBI). In *21st International Conference on the Enhanced Safety of Vehicles (ESV)*, National Highway Traffic Safety Administration. Stuttgart: Germany. pps (pp. 1-19).
- Akiyama, A., Okamoto, M., & Rangarajan, N. (2001, June). Development and application of the new pedestrian dummy. In *17th ESV Conference, Paper* (No. 463).
- Crash test dummy (2016, December 14th). *Wikipedia*. Available at: https://en.wikipedia.org/wiki/Crash_test_dummy. Accessed: 2017-01-06.
- Backaitis, S. H., & Mertz, H. J. (1993). Hybrid III: The first human-like crash test dummy. Warrendale, PA: *Society of Automotive Engineers*, 1993. 830.
- Moss, S., Wang, Z., Salloum, M., Reed, M. P., Van Ratingen, M., Cesari, D., ... & Beusenberg, M. (2000). *Anthropometry for WorldSID a world-harmonized midsize male side impact crash dummy* (No. 2000-01-2202). SAE Technical Paper.
- Neilson, L., Lowne, R., Tarriere, C., Bendjellal, F., Gillet, D., Maltha, J., ... & Bouquet, R. (1985). *The EUROSID side impact dummy* (No. 856029). SAE Technical Paper.
- Elmasoudi, S. (2015). Finite element modelling of a pedestrian impact dummy (Unpublished master's thesis). KTH ROYAL INSTITUTE OF TECHNOLOGY. Available at: <https://kth.diva-portal.org/smash/get/diva2:912550/FULLTEXT01.pdf>. Accessed: 2016-09-15.
- L. S. T. C. (2014). LS-DYNA Keyword User's Manual Version R7.1, Volume I. California, The United States of America.

- Automotive, T. N. O. (2015). MADYMO Theory Manual Version 7.6. *TNO Automotive. Delft, The Netherlands*.
- Automotive, T. N. O. (2015). Manual: MADYMO Human Body Models Version 7.6. *TNO Automotive. Delft, The Netherlands*.
- Kirkpatrick, S. W., Holmes, B. S., Hollowell, W. T., Gabler, H. C., & Trella, T. J. (1993). *Finite element modeling of the side impact dummy (SID)* (No. 930104). SAE Technical Paper.
- Himmetoglu, S., Acar, M., Taylor, A. J., & Bouazza-Marouf, K. (2007). A multi-body head-and-neck model for simulation of rear impact in cars. *Proceedings of the Institution of Mechanical Engineers, Part D: Journal of Automobile Engineering*, 221(5), 527-541.
- Verhoeve, R., Kant, R., & Margerie, L. (2001, January). Advances in numerical modelling of crash dummies. In *ESV Conference 2001, Paper Number* (Vol. 152).
- Wismans, J., Bermond, F., Gertosio, G., Kreuzinger, T., Roberts, A., Ratingen, M., ... & Leyer, H. (2001). *Development and Evaluation of the ES-2 Dummy*. EEVC (European Enhanced Vehicle-safety Committee).
- Mohan, P., Park, C. K., Marzougui, D., Kan, C. D., Guha, S., Maurath, C., & Bhalsod, D. (2010, June). LSTC/NCAC dummy model development. In *11th International LS-Dyna Users Conference*.
- Beillas, P., Mero, M., Belon, S., Maupas, A., Desfontaines, H., Deloffre, P., ... & Charnaux, S. (2011). Accidents between pedestrians and industrial vehicles: from injury patterns to dummy and truck prototypes. In *International Technical Conference on Enhanced Safety of Vehicles (ESV), June, Washington, DC* (pp. 13-16).
- Fernando C, Jardinier W. (Master thesis 2002) Development and evaluation of a pedestrian anthropomorphic test device phase II. Chalmers University of technology, Göteborg Sweden
- RAMSIS (1997). RAMSIS Manual version 3.1. *Tecmath GmbH, Kaiserlautern, Germany*.
- Versace, J. (1971). *A review of the severity index* (No. 710881). SAE Technical Paper.
- Eppinger, R., Sun, E., Bandak, F., Haffner, M., Khaewpong, N., Maltese, M., ... & Zhang, A. (1999). Development of improved injury criteria for the assessment of advanced automotive restraint systems—II. *National Highway Traffic Safety Administration*, 1-70.
- Klinich, K. D., Saul, R. A., Auguste, G., Backaitis, S., & Kleinberger, M. (1996). Techniques for developing child dummy protection reference values.
- Eppinger, R. H., Marcus, J. H., & Morgan, R. M. (1984). *Development of dummy and injury index for NHTSA's thoracic side impact protection research program* (No. 840885). SAE Technical Paper.
- Morgan, R. M., Marcus, J. H., & Eppinger, R. H. (1986). *Side impact-the biofidelity of NHTSA's proposed ATD and efficacy of TTI* (No. 861877). SAE Technical Paper.
- Forbes, P. A., Cronin, D. S., Deng, Y. C., & Boismenu, M. (2005). Numerical human model to predict side impact thoracic trauma. In *IUTAM symposium on impact biomechanics: from fundamental insights to applications* (pp. 441-450). Springer Netherlands.

Lau, I. V., & Viano, D. C. (1986). *The viscous criterion-bases and applications of an injury severity index for soft tissues* (No. 861882). SAE Technical Paper.

Viano, D. C., Lau, I. V., Asbury, C., King, A. I., & Begeman, P. (1989). Biomechanics of the human chest, abdomen, and pelvis in lateral impact. *Accident Analysis & Prevention*, 21(6), 553-574.

Kuppa, S. (2004). Injury criteria for side impact dummies. *Washington, DC: National Transportation Biomechanics Research Center, National Highway Safety Administration, US DOT*, 67.

Appendix

Appendix A Contact between pedestrian and truck

Table 9.1 The contact between body part and corresponding truck front contact part in MADYMO study.

Dummy contact parts	Head	Arms and chest	Pelvis	Upper legs	Lower legs
Corresponding truck front contact parts	lid mid 2	lid mid 1	grille upper 1	grille lower 1	grille lower 1
	lid lower 2	lid lower 1	grille lower 2	bumper upper 1	bumper upper 1
		grille upper 1	bumper upper 1	bumper lower 1	bumper lower 1
			bumper lower 2		

Appendix B Material card in FE model

MAT205 MAT_SPRING_GENERAL_NONLINEAR [MAT205 MAT_SPRING_GENERAL_NONLINEAR]

Name: Lid mid spring

FROZEN_ID: NO FROZEN_DELETE: NO DEFINED: YES

MID	LCDL	LCDU	BETA	TYI	CYI
47	8	10		2.	-2.

*MAT_ADD_EROSION: NO

Lid mid spring

OK ColorEdit Cancel

Figure 9.1 The material card of the springs of 'Lid Mid 1' and 'Lid Mid 2'.

MAT204 MAT_DAMPER_NONLINEAR_VISCOUS [MAT204 MAT_DAMPER_NONLINEAR_VISCOUS]

Name: **DAMPER**

FROZEN_ID: **NO** FROZEN_DELETE: **NO** DEFINED: **YES**

MID: **49** LCDR: **11**

*MAT_ADD_EROSION: **NO**

DAMPER

OK ColorEdit Cancel

Figure 9.2 The material card of all dampers.

MAT24 MAT_PIECEWISE_LINEAR_PLASTICITY [MAT24 MAT_PIECEWISE_LINEAR_PLASTICITY]

Name: **Zytel® ST811HS NC010, PA6-I**

FROZEN_ID: **NO** FROZEN_DELETE: **NO** DEFINED: **YES**

MID	RO	E	PR	SIGY	ETAN	FAIL	TDEL
100671	1.04E-6	0.4	0.35		0	1.E20	0

C	P	LCSS	LCSR	VP
0	0	3457		0

EPS1	EPS2	EPS3	EPS4	EPS5	EPS6	EPS7	EPS8
0	0	0	0	0	0	0	0

Figure 9.3 Material card for Zytel® ST811HS NC010.

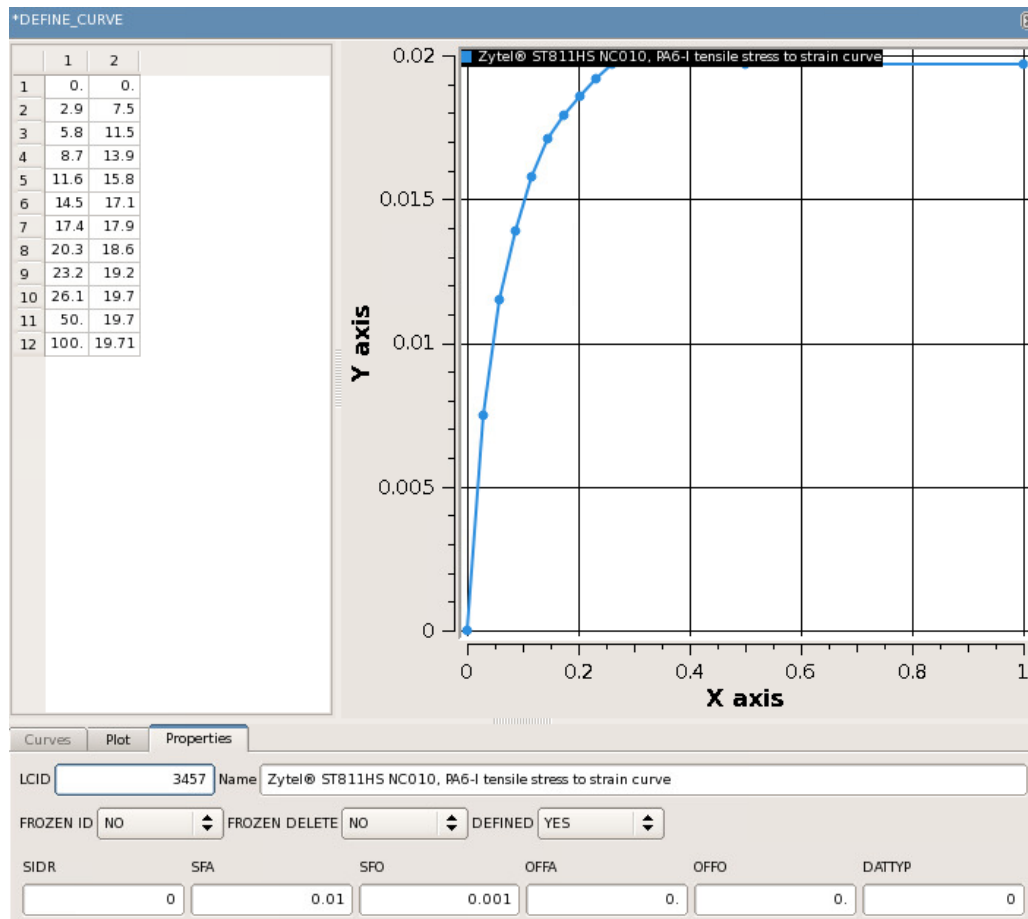


Figure 9.4 Tensile stress to strain curve of Zytel® ST811HS NC010 used in material card.

Appendix C Modification of IA pedestrian dummy model

Head flesh material substitution

The original head flesh is a rigid body which is attached to skull by 'CONSTRAINED_RIGID_BODIES'. After the substitution, this constrain should be deleted to avoid potential errors. Besides, the 'N' option (Number of constants to solve for) in this material card needs to be set to 3 manually.

Head accelerometer

Original head accelerometers are fixed on 'UPPER NECK MOUNTING PLATE' which is moving separately with the skull. As a result, accelerometers are actually not measuring head's acceleration. One way to solve this problem is to bind 'UPPER NECK MOUNTING PLATE' and skull by 'CONSTRAINED_RIGID_BODIES'.

Dummy self-contact

Simulations occasionally end up with that the lower parts of knee detach from the clevis. The reason is that dummy self-contact does not include knee axis and knee clevis, which causing no limitation for the knee foam material movement. Therefore, these parts should be included in dummy self-contact in case of unexpected knee motion.

Robustness

During the simulations, some dummy body parts exploded frequently, resulting in ‘Negative volume’ error in LS-DYNA. The problematic parts are: knees, arms, ribs and pelvis. The “ELFORM” of these parts are originally set to ‘1’ (Constant stress solid element). To solve this, one of the efficient way is to change the “ELFORM” value to ‘2’ (Fully integrated S/R solid). However, this change may reduce the calculation accuracy to some extent but acceptable as well as making the simulation more time consuming.

Appendix D Contact card in FE model

Example: Pelvis and bumper lower 2

The screenshot shows the LS-DYNA CONTACT card input form. The title bar is '*CONTACT [CONTACT]'. The Name field is 'Pelvis to bumper lower2'. Below the Name field are three dropdown menus: FROZEN_ID (NO), FROZEN_DELETE (NO), and AUXILIARY (NO). The main form is divided into several sections. The first section contains ID (28) and TYPE (AUTOMATIC_SURFACE_TO_SURFACE). The second section contains SSID (100120), MSID (19), SSTYPE (2: Part set), MSTYP (3: Part id), SBOXID, MBOXID, SPR (0), and MPR (0). The third section contains FRIC (NO), FS (0.3), FD, DC, VC, VDC, PENCHK (0), BT, and DT. The fourth section contains SF5, SFM, SST, MST, SFST, SFMT, FSF, and VSF. The fifth section is titled 'OPTIONAL CARDS A,B,C,D,E' and contains a dropdown menu set to 'A & B & C & D & E'. Below this are various parameters: SOFT (2), SOFSC (0.1), LCIDAB, MAXPAR (1.025), SBOPT (3), DEPTH/LCID (DEPTH), DEPTH (5), BSORT/LCID (BSORT), BSORT (200), FRCFRQ (0), PENMAX, THKOPT, SHLTHK, SNLOG, ISYM, I2D3D, SLDTHK, SLDSTF, IGAP, IGNORE, DPFAC, DTSTIF, FLANGL, CID_RCF, Q2TRI, DTPCHK, SFNBR, TIEDID, SHLEDG, SHAREC, CARM8, IPBACK, and _MPP.

Figure 9.5 Contact card of contact between Pelvis and bumper lower 2.

*CONTACT [CONTACT]

Name: **Pedestrian body part to road**

FROZEN_ID: **NO** FROZEN_DELETE: **NO** AUXILIARY: **NO**

ID: **2** TYPE: **AUTOMATIC_SURFACE_TO_SURFACE**

SSID: **63** MSID: **100130** SSTYP: **3: Part id** MSTYP: **2: Part set** SBOXID: **0** MBXID: **0** SPR: **0** MPR: **0**

FRIC: **NO** FS: **0.5** FD: **0** DC: **0** VC: **0** VDC: **0** PENCHK: **0** BT: **0** DT: **0**

SFS: **0** SFM: **0** SST: **0** MST: **0** SFST: **0** SFMT: **0** FSF: **0** VSF: **0**

OPTIONAL CARDS A,B,C,D,E

A & B & C & D & E

SOFT: **2** SOFSL: **0.1** LCIDAB: **0** MAXPAR: **1.025** SBOPT: **3** DEPTH/LCID: **DEPTH** DEPTH: **5** BSORT/LCID: **BSORT** BSORT: **0** FRCFRQ: **0**

PENMAX: **0** THKOPT: **0** SHLTHK: **0** SNLOG: **0** ISYM: **0** I2D3D: **0** SLDTHK: **0** SLDSTF: **0**

IGAP: **1** IGNORE: **0** DPRFAC: **0** DTSTIF: **0** FLANGL: **0** CID_RCF: **0**

Q2TRI: **0** DTPCHK: **0** SFNBR: **0** TIEDID: **0** SHLEDG: **0**

SHAREC: **0** CARM8: **0** IPBACK: **0**

_MPP: **0**

Figure 9.6 Contact card of contact between pedestrian body parts and road.

*CONTACT [CONTACT]

Name: **Shoes to road**

FROZEN_ID: **NO** FROZEN_DELETE: **NO** AUXILIARY: **NO**

ID: **1** TYPE: **AUTOMATIC_SURFACE_TO_SURFACE**

SSID: **63** MSID: **100131** SSTYP: **3: Part id** MSTYP: **2: Part set** SBOXID: **0** MBXID: **0** SPR: **0** MPR: **0**

FRIC: **NO** FS: **0.58** FD: **0** DC: **0** VC: **0** VDC: **0** PENCHK: **0** BT: **0** DT: **0**

SFS: **0** SFM: **0** SST: **0** MST: **0** SFST: **0** SFMT: **0** FSF: **0** VSF: **0**

OPTIONAL CARDS A,B,C,D,E

A & B & C & D & E

SOFT: **2** SOFSL: **0.1** LCIDAB: **0** MAXPAR: **1.025** SBOPT: **3** DEPTH/LCID: **DEPTH** DEPTH: **5** BSORT/LCID: **BSORT** BSORT: **0** FRCFRQ: **0**

PENMAX: **0** THKOPT: **0** SHLTHK: **0** SNLOG: **0** ISYM: **0** I2D3D: **0** SLDTHK: **0** SLDSTF: **0**

IGAP: **1** IGNORE: **0** DPRFAC: **0** DTSTIF: **0** FLANGL: **0** CID_RCF: **0**

Q2TRI: **0** DTPCHK: **0** SFNBR: **0** TIEDID: **0** SHLEDG: **0**

SHAREC: **0** CARM8: **0** IPBACK: **0**

_MPP: **0**

Figure 9.7 Contact card of contact between IA pedestrian model's shoes and road.

*CONTACT [CONTACT]

Name: Pedestrian to front surface

FROZEN_ID: NO FROZEN_DELETE: NO AUXILIARY: NO

ID: 40 TYPE: AUTOMATIC_SURFACE_TO_SURFACE

SSID: 100148 MSID: 100150 SSTYPE: 2: Part set MSTYP: 2: Part set SBOXID: MBQID: SPR: 0 MPR: 0

FRIC: NO FS: 0.3 FD: DC: VC: VDC: PENCHK: 0 BT: DT:

SFS: SFM: SST: MST: SFST: SFMT: FSF: VSF:

OPTIONAL CARDS A,B,C,D,E

A & B & C & D & E

SOFT: 2 SOFSCL: 0.1 LCIDAB: MAXPAR: 1.025 SBOPT: 2 DEPTH/LCID: DEPTH: 5 BSORT/LCID: BSORT: 0 FRCFRQ: 0

PENMAX: THKOPT: SHLTHK: SNLOG: ISYM: I2D3D: SLDTHK: SLDSTF:

IGAP: IGNORE: DPFAC: DTSTIF: FLANGL: CID_RCF:

Q2TRI: DTPCHK: SFNBR: TIEDID: SHLEDG:

SHAREC: CPARAM: IPBACK:

_MPP:

Figure 9.8 Contact card of contact between IA pedestrian model's whole body and truck front surface.

*CONTACT [CONTACT]

Name: honeycomb single surface

FROZEN_ID: NO FROZEN_DELETE: NO AUXILIARY: NO

ID: 53 TYPE: AUTOMATIC_SINGLE_SURFACE

SSID: 100183 SSTYPE: 2: Part set SBOXID: SPR: 0

FRIC: NO FS: 0.2 FD: 0.2 DC: VC: VDC: 40. PENCHK: 0 BT: DT:

SFS: SFM: SST: MST: SFST: SFMT: FSF: VSF:

Figure 9.9 Automatic_Single_Surface contact card of honeycomb and two rigid plates.

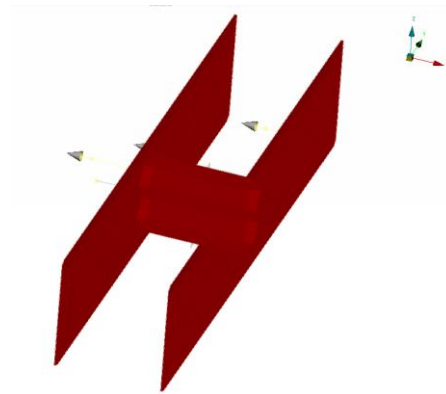


Figure 9.10 Automatic_Single_Surface contact of honeycomb and two rigid plates.

*CONTACT [CONTACT]

Name: honeycomb to rigid plate 1

FROZEN_ID: NO FROZEN_DELETE: NO AUXILIARY: NO

ID	TYPE	SSID	MSID	SSTYP	MSTYP	MBQID	SPR	MPR
51	TIED_NODES_TO_SURFACE_OFFSET	100182	3834	4: Node set	3: Part id		0	0
		FS	FD	DC	VC	VDC	PENCHK	BT
		0.3					0	
		SFS	SFM	SST	MST	SFST	SFMT	FSF
								VSF

Figure 9.11 Tied_Nodes_to_Surface_Offset contact card of contact between honeycomb and rigid plate 1.

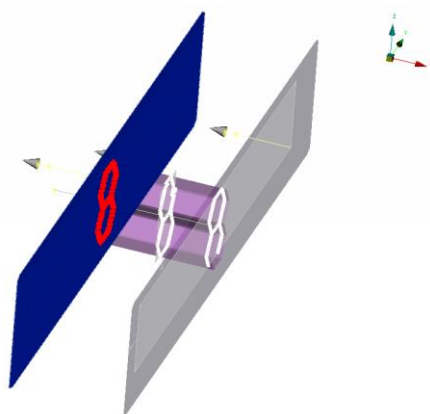


Figure 9.12 Tied_Nodes_to_Surface_Offset contact between honeycomb and rigid plate 1.

*CONTACT [CONTACT]

Name: honeycomb to rigid plate 2

FROZEN_ID: NO FROZEN_DELETE: NO AUXILIARY: NO

ID: 24 TYPE: TIED_NODES_TO_SURFACE_OFFSET

SSID: 100149 MSID: 3788 SSTYPE: 4: Node set MSTYP: 3: Part id MBOXID: SPR: 0 MPR: 0

FS: 0.3 FD: DC: VC: VDC: PENCHK: 0 BT: DT:

SFS: SFM: SST: MST: SFST: SFMT: FSF: VSF:

Figure 9.13 Tied_Nodes_to_Surface_Offset contact card of contact between honeycomb and rigid plate 2.

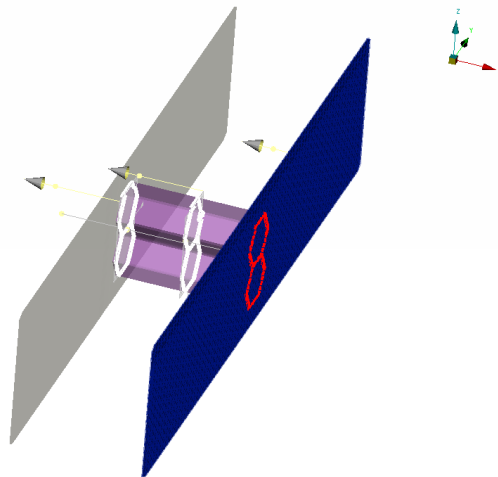


Figure 9.14 Tied_Nodes_to_Surface_Offset contact between honeycomb and rigid plate 2.

Appendix E Injury data

Table 9.2 'Stand' 24kph normalized results

Primary impact			
	MADYMO	LS-DYNA	FH reference
HIC	1.54	2.25	1
TorsoUp (m/s ²)	0.11	0.10	1
TorsoLow (m/s ²)	0.23	0.90	1
NeckUpFRES (N)	0.42	0.29	1
NeckLowFRES (N)	0.14	0.30	1
NeckUpMRES (Nm)	0.24	0.36	1
NeckLowMRES (Nm)	0.18	0.16	1
Secondary impact			
HIC	0.20	0.34	1
TorsoUp (m/s ²)	0.62	3.69	1
TorsoLow (m/s ²)	1.15	0.30	1

NeckUpFRES (N)	0.88	0.79	1
NeckLowFRES (N)	0.39	0.46	1
NeckUpMRES (Nm)	0.96	0.47	1
NeckLowMRES (Nm)	0.40	0.18	1
General			
HIC	0.20	0.34	1
TorsoUp (m/s ²)	0.16	0.94	1
TorsoLow (m/s ²)	1.15	0.31	1
NeckUpFRES (N)	0.88	0.79	1
NeckLowFRES (N)	0.39	0.46	1
NeckUpMRES (Nm)	0.94	0.46	1
NeckLowMRES (Nm)	0.40	0.18	1

Table 9.3 'Stand' 40kph normalized results

Primary impact			
	MADYMO	LS-DYNA	FH reference
HIC	0.03	0.06	1
TorsoUp (m/s ²)	0.10	0.35	1
TorsoLow (m/s ²)	0.16	1.13	1
NeckUpFRES (N)	0.38	0.21	1
NeckLowFRES (N)	0.11	0.23	1
NeckUpMRES (Nm)	0.24	0.19	1
NeckLowMRES (Nm)	0.13	0.09	1
Secondary impact			
HIC	0.11	0.24	1
TorsoUp (m/s ²)	0.70	2.89	1
TorsoLow (m/s ²)	1.49	0.65	1
NeckUpFRES (N)	0.32	0.46	1
NeckLowFRES (N)	0.37	0.55	1
NeckUpMRES (Nm)	0.38	0.18	1
NeckLowMRES (Nm)	0.45	0.26	1
General			
HIC	0.11	0.24	1
TorsoUp (m/s ²)	0.13	0.55	1
TorsoLow (m/s ²)	1.49	0.65	1
NeckUpFRES (N)	0.32	0.46	1
NeckLowFRES (N)	0.37	0.55	1
NeckUpMRES (Nm)	0.38	0.18	1
NeckLowMRES (Nm)	0.28	0.16	1

Table 9.4 'Walk' 24kph normalized results

Primary impact			
	MADYMO	LS-DYNA	FH reference
HIC	0.74	1.18	1

TorsoUp (m/s ²)	0.18	0.25	1
TorsoLow (m/s ²)	0.74	0.56	1
NeckUpFRES (N)	0.59	1.31	1
NeckLowFRES (N)	0.29	0.80	1
NeckUpMRES (Nm)	0.07	0.07	1
NeckLowMRES (Nm)	0.31	0.37	1
Secondary impact			
HIC	0.47	0.81	1
TorsoUp (m/s ²)	1.36	0.96	1
TorsoLow (m/s ²)	1.74	1.95	1
NeckUpFRES (N)	0.67	0.74	1
NeckLowFRES (N)	0.55	1.15	1
NeckUpMRES (Nm)	0.67	0.37	1
NeckLowMRES (Nm)	0.82	0.33	1
General			
HIC	0.47	0.81	1
TorsoUp (m/s ²)	0.97	0.69	1
TorsoLow (m/s ²)	1.74	1.66	1
NeckUpFRES (N)	0.67	0.74	1
NeckLowFRES (N)	0.55	1.15	1
NeckUpMRES (Nm)	0.61	0.34	1
NeckLowMRES (Nm)	0.82	0.33	1

Table 9.5 'Walk' 40kph normalized results

Primary impact			
	MADYMO	LS-DYNA	FH reference
HIC	0.01	0.03	1
TorsoUp (m/s ²)	0.13	0.53	1
TorsoLow (m/s ²)	0.62	1.36	1
NeckUpFRES (N)	0.39	0.71	1
NeckLowFRES (N)	0.21	0.74	1
NeckUpMRES (Nm)	0.35	0.35	1
NeckLowMRES (Nm)	0.13	0.42	1
Secondary impact			
HIC	0.07	0.03	1
TorsoUp (m/s ²)	5.04	0.38	1
TorsoLow (m/s ²)	1.58	3.00	1
NeckUpFRES (N)	0.30	0.18	1
NeckLowFRES (N)	0.88	0.34	1
NeckUpMRES (Nm)	0.28	0.12	1
NeckLowMRES (Nm)	1.63	0.37	1
General			
HIC	0.02	0.03	1
TorsoUp (m/s ²)	1.14	0.53	1

TorsoLow (m/s ²)	3.00	1.19	1
NeckUpFRES (N)	0.30	0.31	1
NeckLowFRES (N)	0.88	0.51	1
NeckUpMRES (Nm)	0.28	0.12	1
NeckLowMRES (Nm)	1.25	0.42	1

Table 9.6 'Walk180' 24kph normalized results

Primary impact			
	MADYMO	LS-DYNA	FH reference
HIC	1.57	2.44	1
TorsoUp (m/s ²)	1.65	0.45	1
TorsoLow (m/s ²)	1.04	0.70	1
NeckUpFRES (N)	0.87	1.18	1
NeckLowFRES (N)	1.06	0.97	1
NeckUpMRES (Nm)	1.14	0.32	1
NeckLowMRES (Nm)	1.03	0.24	1
Secondary impact			
HIC	21.76	35.70	1
TorsoUp (m/s ²)	0.50	1.02	1
TorsoLow (m/s ²)	0.87	0.15	1
NeckUpFRES (N)	2.42	2.97	1
NeckLowFRES (N)	1.87	2.80	1
NeckUpMRES (Nm)	2.02	0.85	1
NeckLowMRES (Nm)	1.40	1.22	1
General			
HIC	21.76	35.70	1
TorsoUp (m/s ²)	1.63	1.02	1
TorsoLow (m/s ²)	0.87	0.15	1
NeckUpFRES (N)	2.42	2.97	1
NeckLowFRES (N)	1.18	1.77	1
NeckUpMRES (Nm)	2.02	0.85	1
NeckLowMRES (Nm)	1.03	0.60	1

Table 9.7 'Walk180' 40kph normalized results

Primary impact			
	MADYMO	LS-DYNA	FH reference
HIC	0.48	1.19	1
TorsoUp (m/s ²)	0.44	1.00	1
TorsoLow (m/s ²)	0.48	1.31	1
NeckUpFRES (N)	0.45	2.02	1
NeckLowFRES (N)	0.31	1.50	1
NeckUpMRES (Nm)	0.90	0.93	1
NeckLowMRES (Nm)	0.26	0.43	1
Secondary impact			

HIC	3.38	0.46	1
TorsoUp (m/s ²)	0.33	0.33	1
TorsoLow (m/s ²)	0.75	0.23	1
NeckUpFRES (N)	1.24	0.28	1
NeckLowFRES (N)	1.24	0.52	1
NeckUpMRES (Nm)	1.36	0.32	1
NeckLowMRES (Nm)	1.54	0.51	1
General			
HIC	3.38	0.48	1
TorsoUp (m/s ²)	0.44	1.00	1
TorsoLow (m/s ²)	0.75	0.49	1
NeckUpFRES (N)	1.24	1.11	1
NeckLowFRES (N)	1.03	1.50	1
NeckUpMRES (Nm)	1.36	0.36	1
NeckLowMRES (Nm)	0.75	0.43	1

Appendix F Pedestrian motion in collisions of Truck A and trucks with honeycombs

24kph collisions

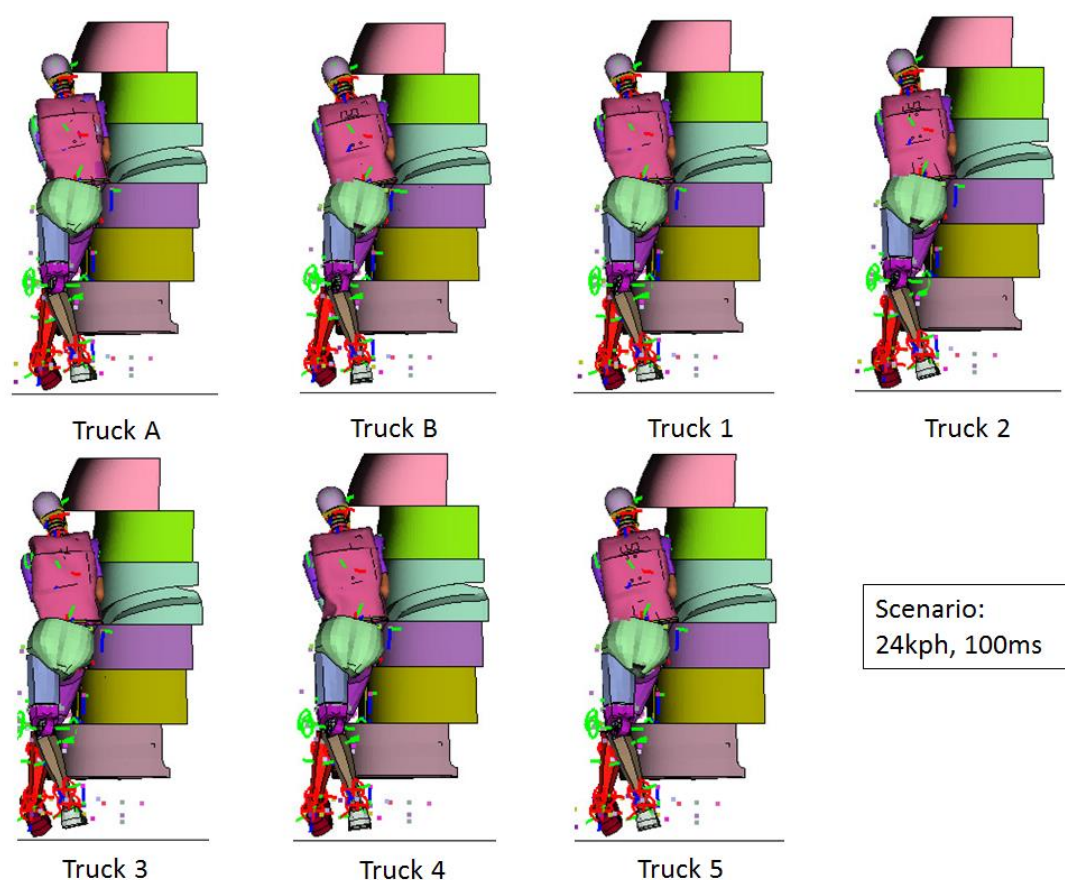


Figure 9.15 24kph collisions at 100ms.

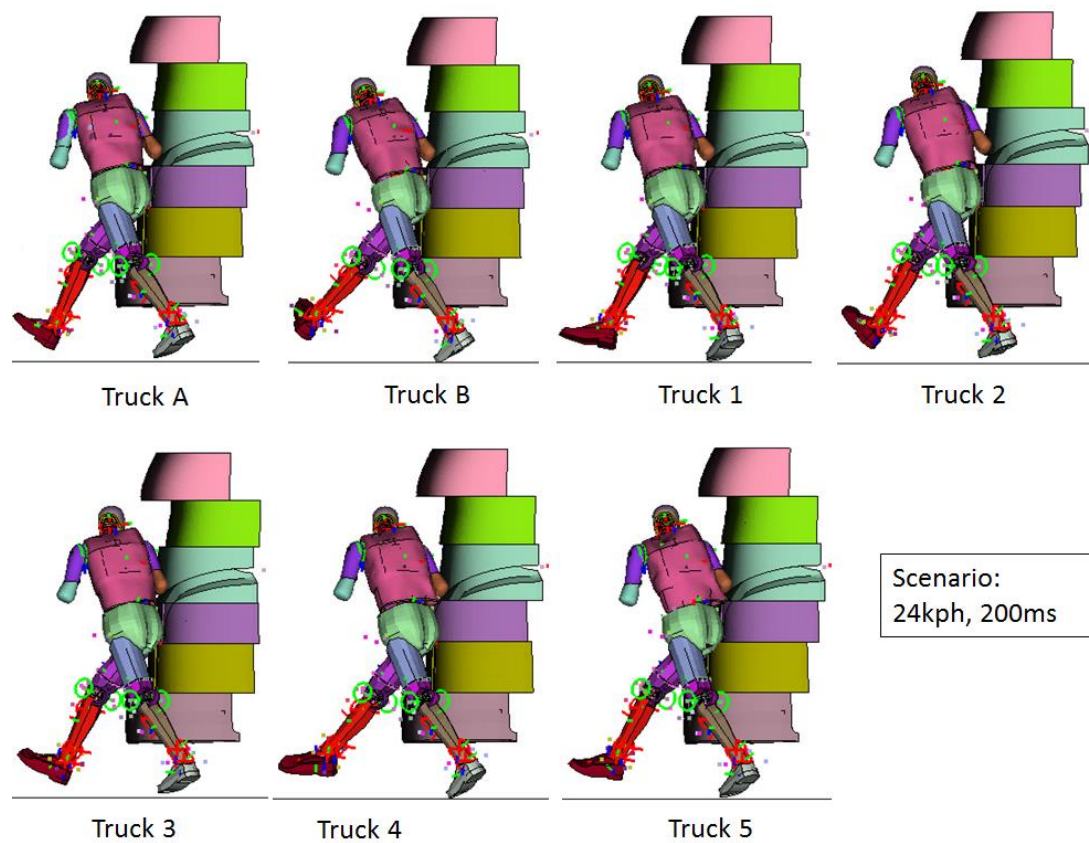


Figure 9.16 24kph collisions at 200ms.

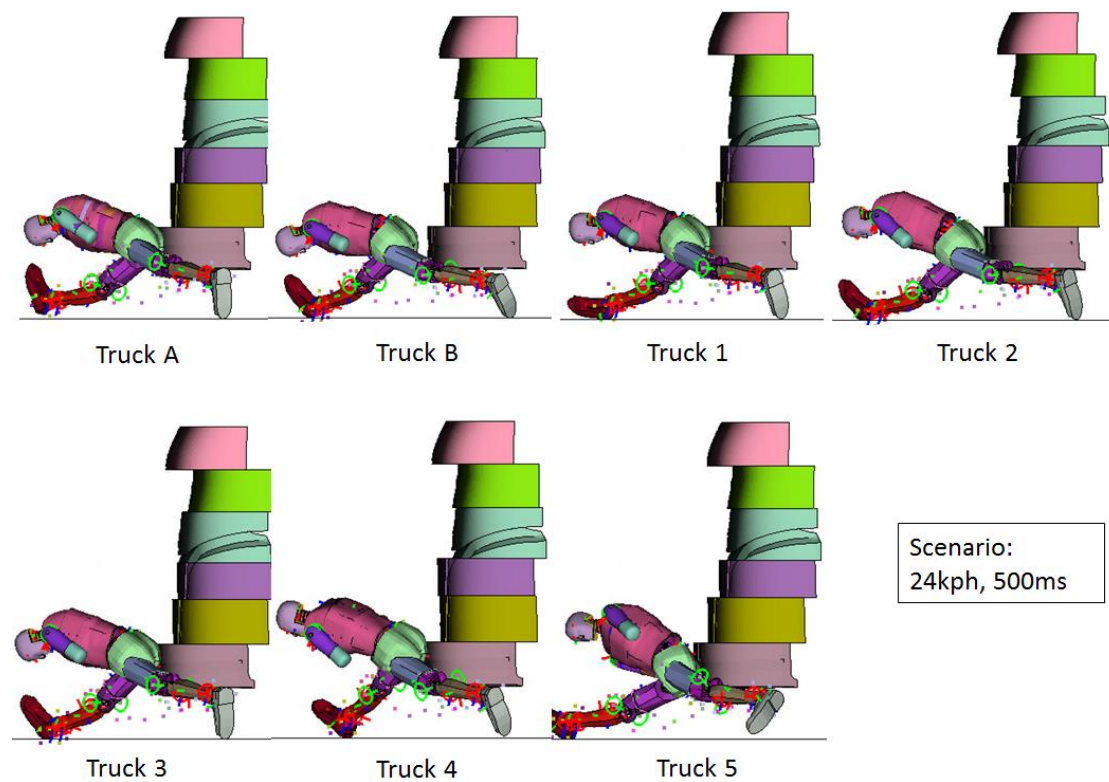


Figure 9.17 24kph collisions at 500ms.

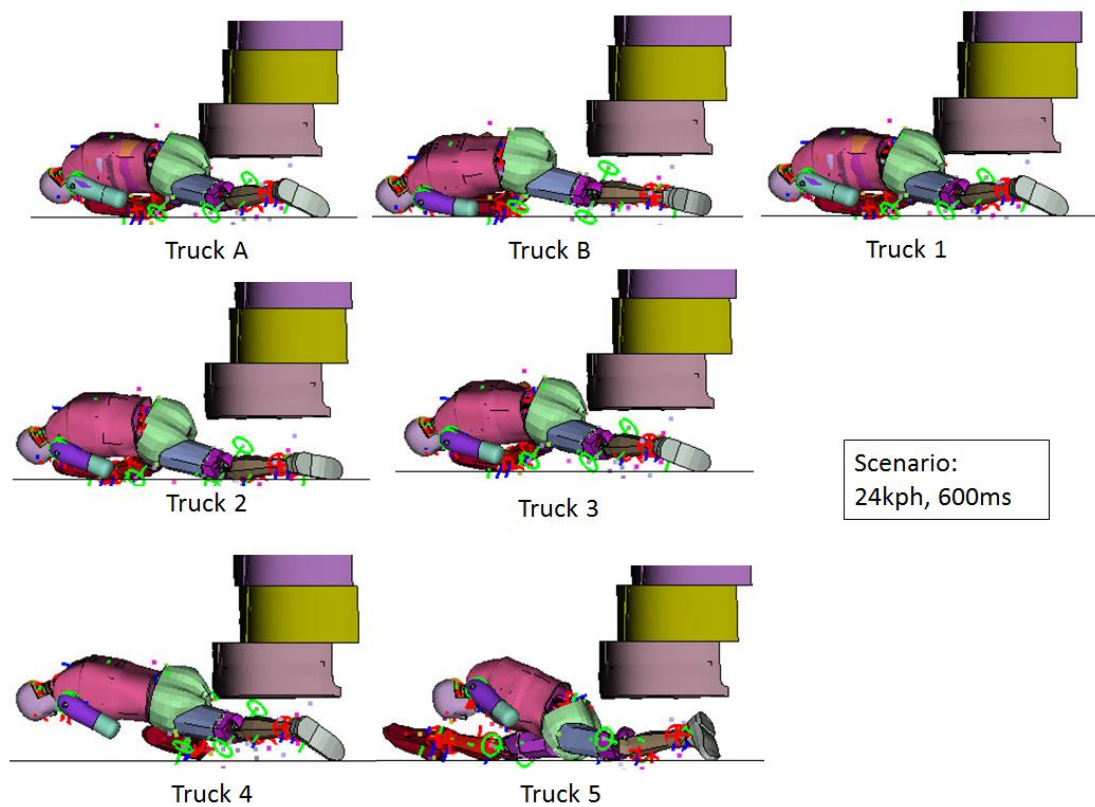


Figure 9.18 24kph collisions at 600ms.

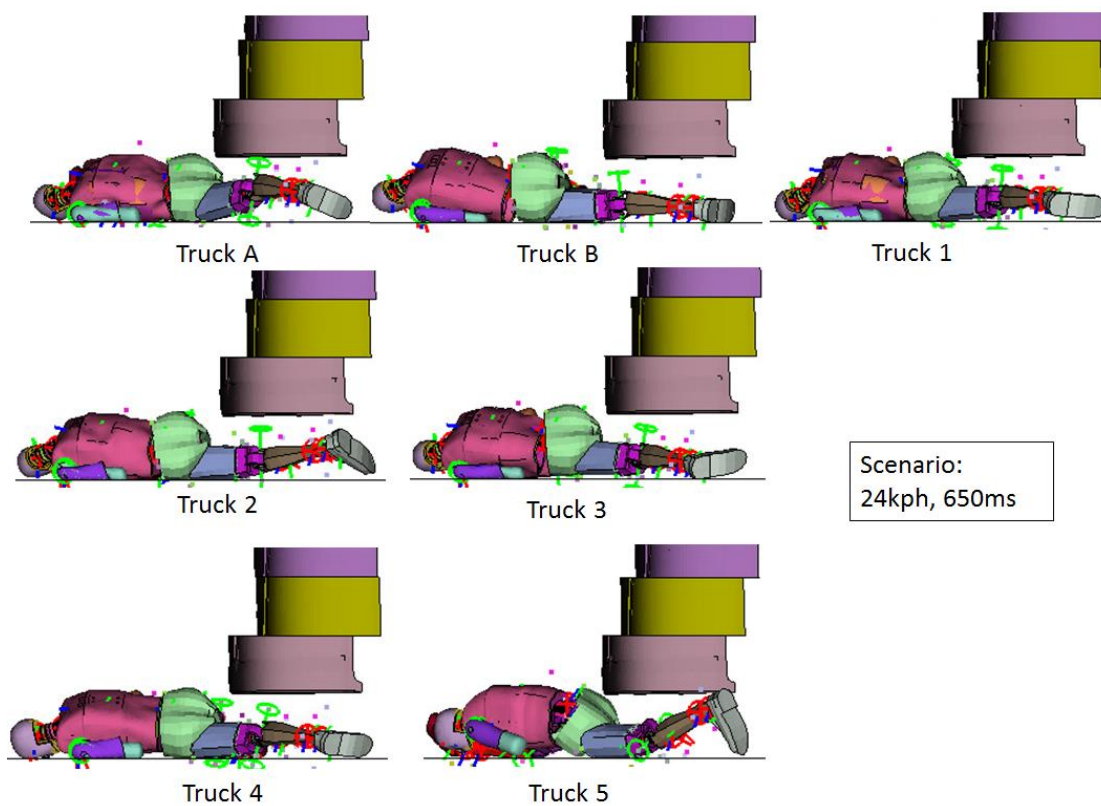


Figure 9.19 24kph collisions at 650ms.

40kph collisions

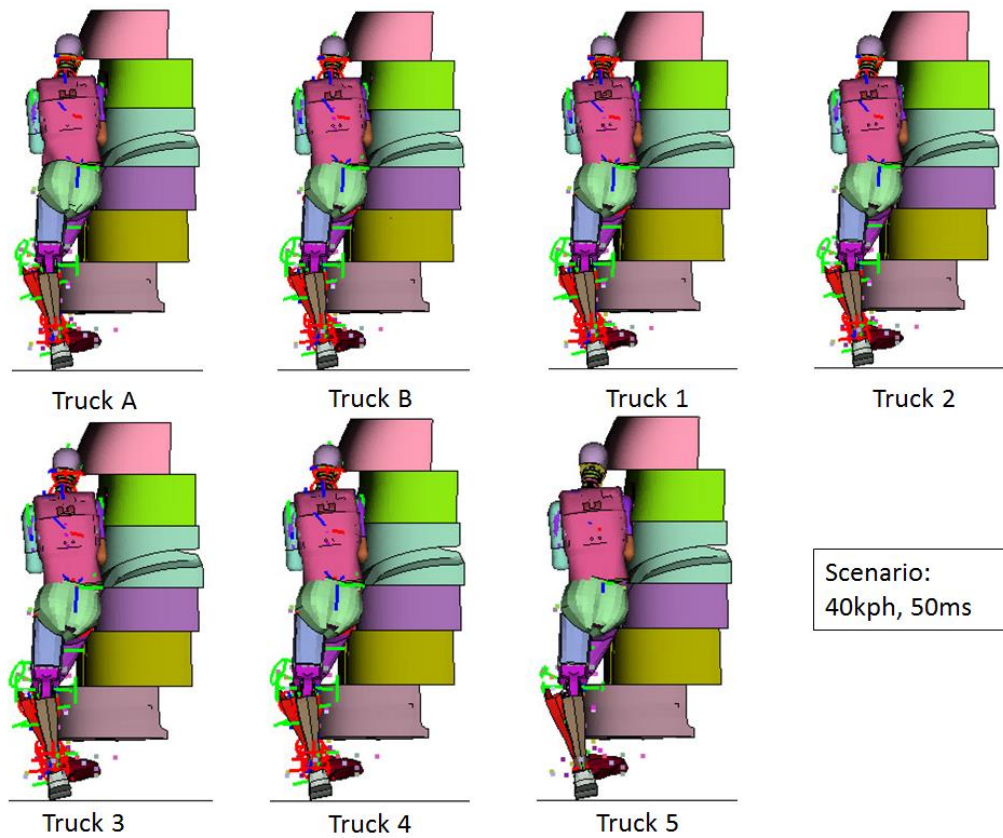


Figure 9.20 40kph collisions at 50ms.

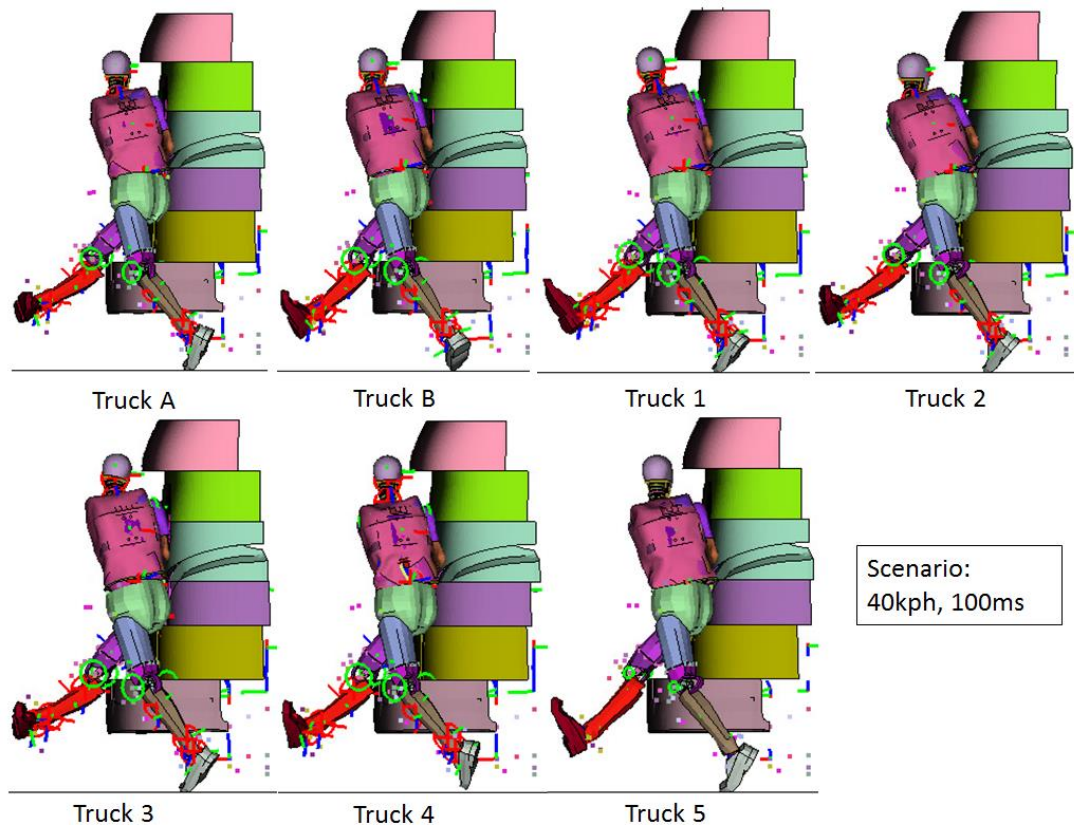


Figure 9.21 40kph collisions at 100ms.

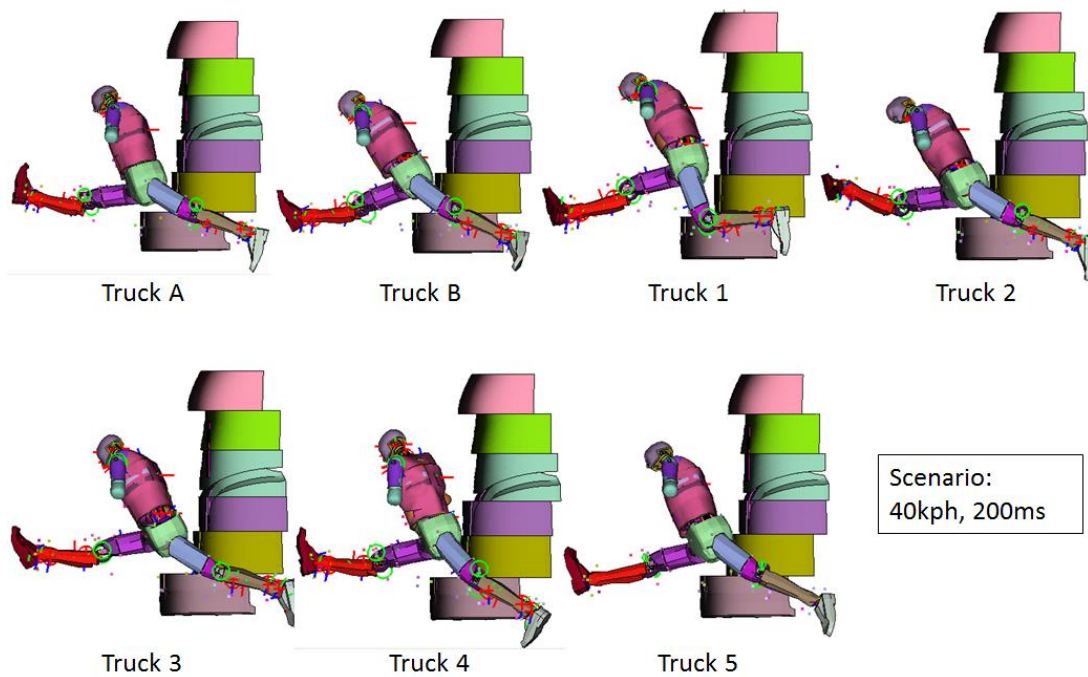


Figure 9.22 40kph collisions at 200ms.

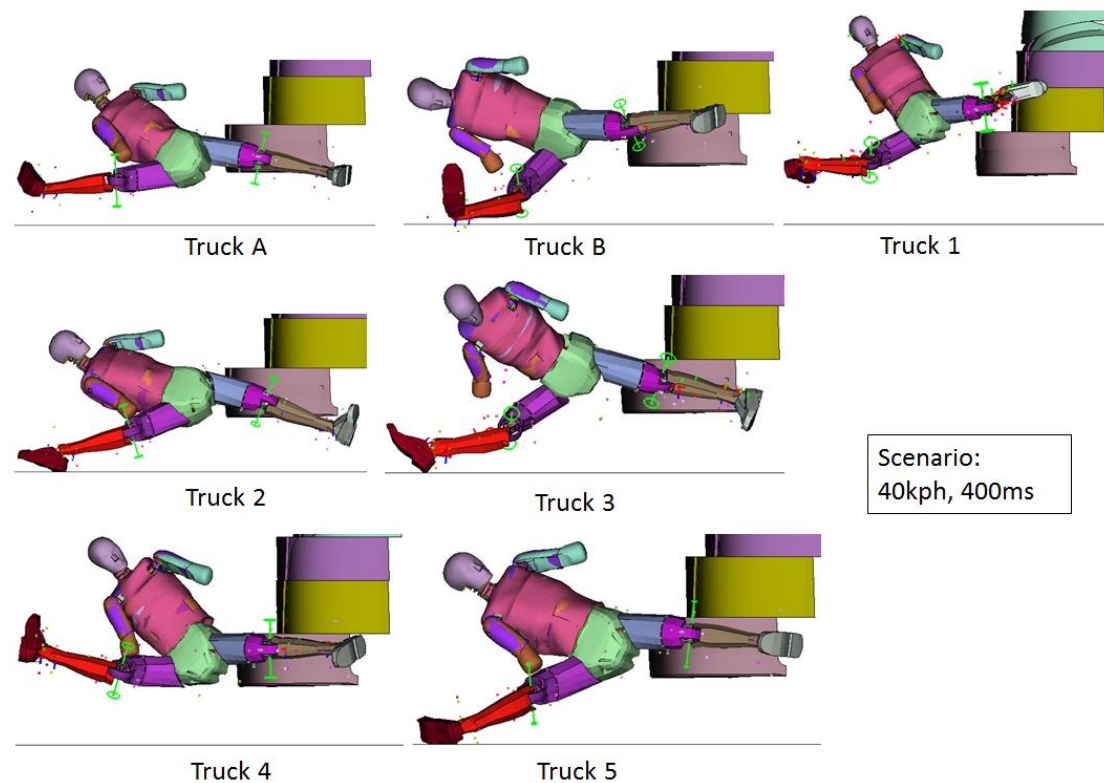


Figure 9.23 40kph collisions at 400ms.

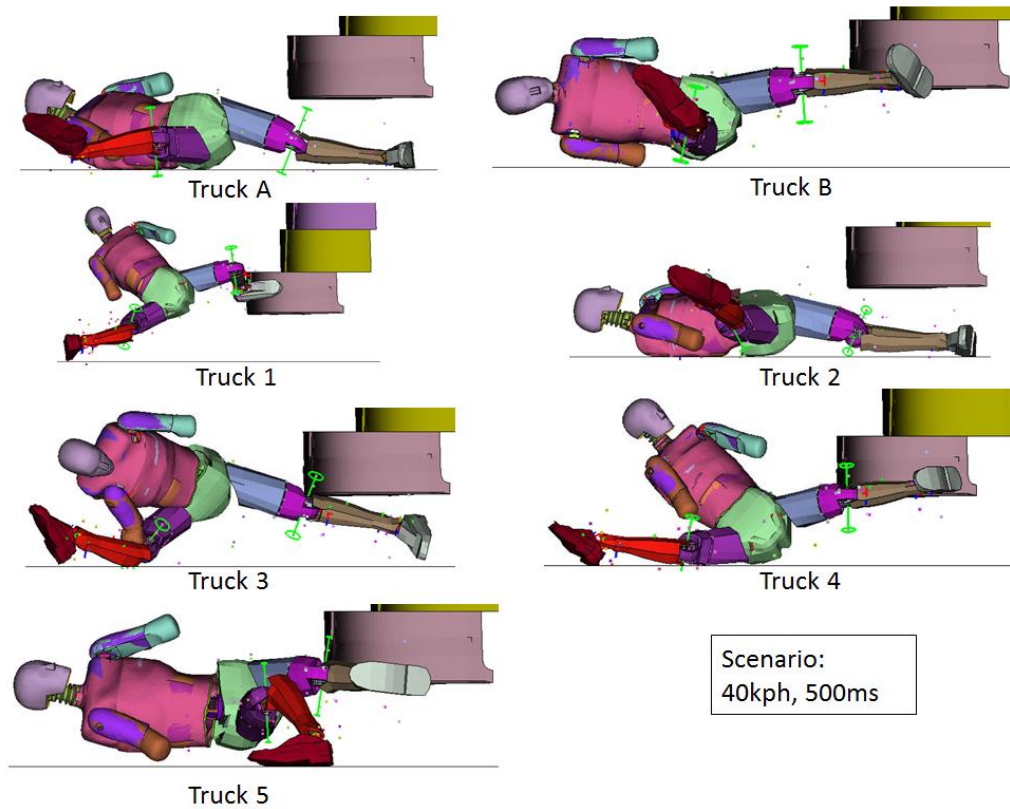


Figure 9.24 40kph collisions at 500ms.

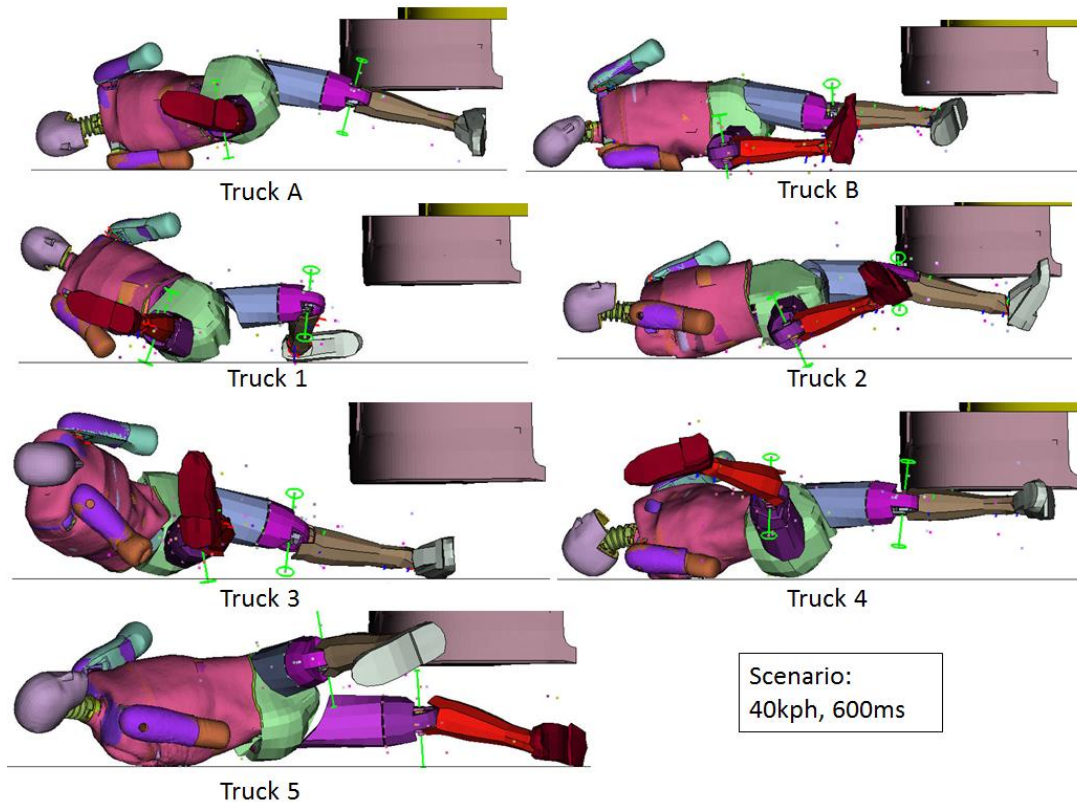


Figure 9.25 40kph collisions at 100ms.